21GW Roadmap Wake Study

Final Report

2025

Abstract

In summary, a high-fidelity atmospheric model was used to calculate the production numbers of the Dutch 21 GW Roadmap. A large number of wind farm scenarios was considered. The present study contributes to a better understanding of cluster wake effects and the relation between installed capacity and energy production.

The Dutch Roadmap for offshore wind energy aims for an installed capacity of around 21 GW in 2032. With the gradual buildout of the Roadmap wind farms, wake effects may become more and more important. The increased capacity of future wind farms may lead to larger internal wake losses. And as the number of wind farms increases, also external wake effects (i.e. wakes from one or multiple wind farms hampering the production of a downstream wind farm) may increase.

In order to reduce the uncertainty in the expected annual energy production and to offer insights in the potential impact of wake effects, Whiffle performed an extensive modeling study with its turbine resolving large-eddy simulation model for varying North Sea wind energy scenarios. The selected set of scenarios represents a wide range of wind farm configurations, which is relevant as the specifications of future wind farms are yet unknown.

A first set of simulation scenarios includes the gradual build out of the 21 GW Roadmap in five incremental steps. In addition, a suite of sensitivity scenarios was run with, for instance, a different turbine type (20 MW turbines instead of the default 15 MW) and leaving out all wind farms of neighboring countries.

The simulation domain has a horizontal extent of 307 x 384 km with a horizontal grid spacing of 120 m (2560 x 3200 grid cells). For the initial and full build out phase of the 21 GW Roadmap a full-year simulation has been performed for the period 17 March 2018 to 17 March 2019, a period which is representative for the long term North Sea wind climate. The remaining scenarios are run for a set of 50 representative days.

The presented production numbers and capacity factors include losses due to internal and external (or farm-to-farm) wake effects and blockage effects. Not included are electrical, power curve hysteresis, curtailment and any other operational losses. Capacity factors are defined as the ratio between the simulated waked production and the installed capacity

The simulated annual energy production of the full buildout scenario of the 21 GW Roadmap is estimated to be 83.7 TWh with an error margin in terms of standard deviation of 5%. This corresponds to a 68% confidence interval of 79.5 to 87.3 TWh. These numbers are based on modeled production numbers that have been corrected for model bias, sampling errors, and long-term representativeness. The corresponding capacity factor of the 21 GW Roadmap is 46%. Average aerodynamic losses (i.e. the sum of internal and external wake losses and blockage effects) with respect to the gross energy production is 21.7%.

The simulations of the incremental build out phases of the 21 GW Roadmap show significant farm-to-farm wake effects. The impact for any particular wind farm depends on the presence and location of neighboring wind farms. Leaving out all wind farms of neighboring countries leads to an overall production increases of 2.1%. For wind farms that are directly bordering non-Dutch wind farms differences are larger. Wind farms for which the default 15 MW turbines were replaced by 20 MW turbines, while leaving the installed capacity the same, showed an increase in production between 0.7 to 1.8%. The scenarios considering overplanting show a significant increase in production, be it at the cost of a reduced capacity factor. However, when the wind farm production is maximized (for instance, because of the transport capacity of offshore substations) to the original wind farm rated power, the increase in production is much less.

To facilitate the accessibility of the simulation results, a web-based GIS Viewer has been developed, which can be found at https://21gw.whiffle.cloud. The GIS Viewer allows for a straightforward and visual inspection of power production and capacity factors of the different scenarios per wind farm.

Version	Date	Author	Reviewed by
1	10 March 2025	P. Baas	R. Verzijlbergh, P. van Dorp
2	22 April 2025	P. Baas	R. Verzijlbergh, P. van Dorp
3	18 May 2025	P. Baas	R. Verzijlbergh
4	6 June 2025	P. Baas	P. van Dorp

Whiffle, Molengraaffsingel 8, 2629 JD Delft, the Netherlands.

Contents

1 Introduction

As part of the transition to renewable energy sources, the installed capacity of offshore wind energy in the North Sea will grow significantly in the next decades. However, the anticipated large-scale roll-out of offshore wind energy may lead to an increased importance of wind farm wake effects, which could result in lower than anticipated electricity production. A better understanding of wake effects can provide valuable opportunities for governments and developers in their planning and decision-making processes.

The Dutch Offshore Wind Energy Roadmap aims for an installed capacity of around 21 GW in 2032 (Netherlands Enterprise Agency, 2024). It is important to better understand the relation between installed capacity and the expected annual energy production (AEP). To that end, the Netherlands Enterprise Agency on behalf of the Ministry of Climate and Green Growth granted Whiffle an extensive modeling study to the energy production and wake effects of the operational and planned wind farms of the 21 GW Roadmap.

The aim of the study is to reduce the uncertainty in the expected AEP and to offer insights in the potential impact of cluster wake effects (i.e. the wake effects from one or multiple wind farms to others). Therefore, a suite of scenarios with incremental buildout steps of the planned offshore wind farms have been performed. In addition, several sensitivity simulations have been carried out. These include scenarios that consider the impact of turbine type, overplanting, layout, and the presence of wind farms of neighboring countries. The selected set of scenarios represents a wide range of wind farm configurations, which is relevant as the specifications of future wind farms are yet unknown.

Simulations were done with Whiffle's large-eddy simulation (LES) model. Whiffle's LES is a fast and robust, commercial high-resolution weather model that has been extensively validated and is used by many developers of offshore and onshore wind farms. The model setup and configuration were taken similar as used in Whiffle (2024), who performed an extensive validation of the model using LiDAR and in-site wind measurements for many locations in the North Sea.

The present report describes the results of the modeling study. The methodology is explained in Sect. 2. This involves the construction of the wind farm scenario's, motivation for the simulated time periods, and details about the model. The Results are presented in Sect. 3. For each scenario and wind farms the production numbers will be discussed. Insight in the wake effects over the Dutch part of the North Sea will be presented. Applied corrections to the raw model output and an assessment of the error margin are discussed in Sect. 4. The conclusions are summarized in Sect. 5.

2 Methodology

2.1 Scenario simulation strategy

To study the annual energy production[1] and (cluster) wake losses of the 21 GW Roadmap, a comprehensive set of offshore wind farm scenarios has been simulated with Whiffle LES.

A first set of simulation scenarios includes the gradual buildout of the 21 GW Roadmap in five incremental steps. This set of scenarios starts with an initial buildout scenario, labeled Scenario 1, which includes all wind farms operational in 2024 plus Hollandse Kust West (HKW, here including sites VI and VII). The included operational wind farms are Luchterduinen, Gemini, Borssele I&II, Borssele III&IV, Hollandse Kust Noord (HKN), and Hollandse Kust Zuid (HKZ). The offshore wind farms Princess Amalia Windpark (PAWP) and Offshore Windpark Egmond aan Zee (OWEZ) are left out of the simulations, as they are expected to be decommissioned in the next decade. In Scenario 2 the IJmuiden Ver Alpha (IJVer-Alpha) and IJmuiden Ver Beta (IJVer-Beta) wind farms are added. Scenario 3 adds IJmuiden Ver Gamma (IJVer-Gamma) and Nederwiek I. Nederwiek II&III are added in Scenario 4. Scenario 5, which is considered the full buildout scenario also includes Doordewind and Ten noorden van de Waddeneilanden (TNW). The gradual buildout of the 21 GW Roadmap follows the time line of the tendering of the subsequent wind farms as outlined in Netherlands Enterprise Agency (2024). Figure 2.1 provides a map of the incremental Roadmap scenarios. The scenarios are summarized in Table 2.1. The *Gross* scenario includes all turbines of all other scenarios combined. As such, by selecting the corresponding turbines from the *Gross* scenario, for each of the other scenarios the gross production can be determined. The specific implementation of the wind farms in the model is discussed in Sect. 2.4.

A constant set of wind farms of neighboring counties is included in all five incremental Roadmap scenarios. It represents the expected situation in the year 2032 and closely follows the KEC 5.0 scenario of offshore wind farms (KEC 5.0, 2024). The final realization of future wind farms may be subject to changes in location, capacity, and/or turbine types. For more details on the location of the included wind farms see Sect. 2.4.

For Scenarios 1 and 5 (initial and full buildout) a full-year simulation has been performed covering the period 17 March 2018 to 17 March 2019. This specific consecutive 365-day period has been carefully selected from 20 years of ERA5 reanalysis data (Hersbach et al., 2020). It is chosen such that is representative for the long-term North Sea wind climate. The selection procedure is explained in Sect 2.5.1. Despite known deficiencies (e.g. Gandoin and Garza (2024)), the ERA5 dataset is generally known for its high quality, also compared to other reanalysis datasets, when it comes to (long-term) correlation with observations (Gualtieri, 2022; Jourdier, 2020; Olauson, 2018; Ramon et al., 2019). In a comparison with LiDAR data from several locations in the North Sea (LichtEiland Goeree, Europlatform, and K13), TNO (2024) conclude that ERA5 is suitable as long term reference data in order to establish long term wind resource for these locations.

The intermediate scenarios (Scenarios 2 to 4) have been run for a set of 50 days, sampled from the full-year scenario run, that form a good representation of the wind climate. This selection method is explained in more detail in Sect. 2.5.2.

[1] Formally, no energy is produced. Wind turbines convert kinetic energy from the flow into mechanical energy, which, in turn, is converted into electricity.

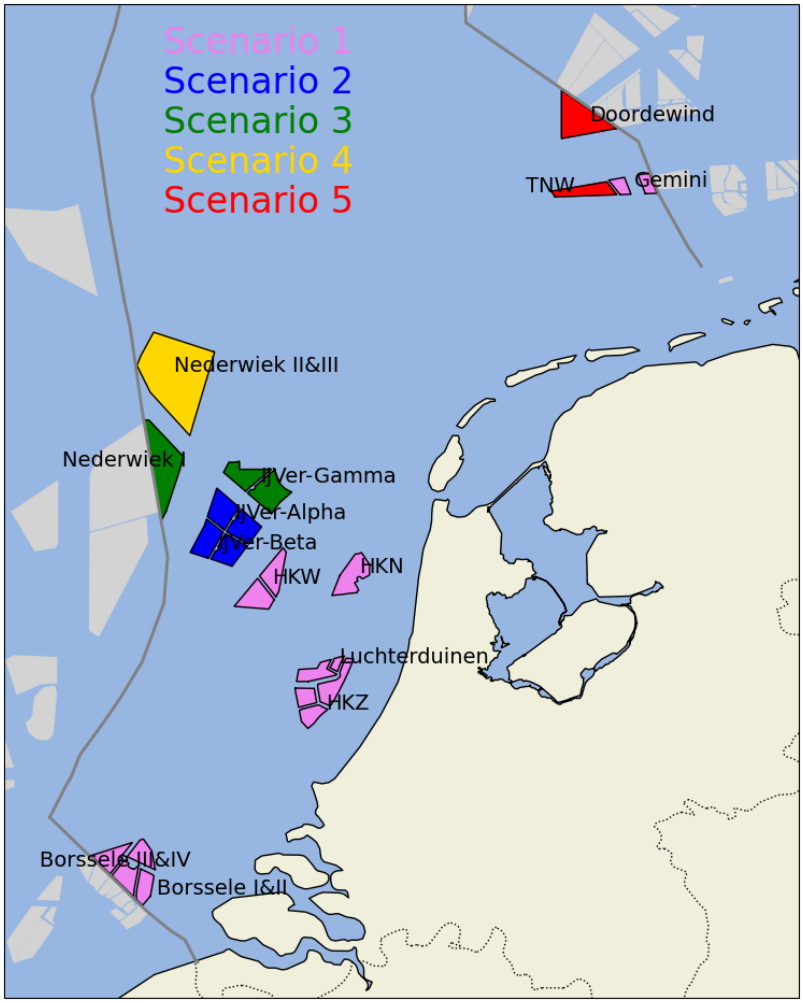

Figure 2.1. Overview of the incremental buildout scenarios. Wind farms of neighboring countries that are included in the simulations are indicated in grey (the same for all scenarios).

Scenario name	Scenario name short	Number of days	Number of turbines	Installed capacity [GW]
Scenario 1 (Initial buildout, operational + HKW)	*Sc*1	365	674	6.02
Scenario 2 (*Sc*1 + IJVer-Alpha and Beta)	*Sc*2	50	942	10.04
Scenario 3 (*Sc*2 + IJVer-Gamma and Nederwiek I)	*Sc*3	50	1210	14.06
Scenario 4 (*Sc*3 + Nederwiek II&III)	*Sc*4	50	1477	18.06
Scenario 5 (Full buildout, *Sc*4 + Doordewind and TNW)	*Sc*5	365	1664	20.87
No wind farms of neighboring countries	*NoFor*	50	1664	20.87
20 MW turbines instead of 15 MW	20*MW*	50	1389	20.82
5% Overplanting	5%*Ovp*	50	1715	21.63
15% Overplanting	15%*Ovp*	50	1827	23.31
Optimized layout	*Layout*	50	1664	20.87
Gross production	*Gross*	50	All	All

Table 2.1. Overview of simulated scenarios. Columns indicate the scenario name, the abbreviation that is used in the remainder of this report, the number of simulated days, the number included turbines, and the installed capacity. The indicated number of turbines and the installed capacity refer to the 21 GW (Dutch) Roadmap wind farms only. The *Gross* scenario includes all turbines of all other scenarios.

A second set of simulation scenarios consists of variations of the full buildout scenario (Scenario 5). The sensitivity simulations are listed in Table 2.1.

For the sensitivity scenarios the configuration of all wind farms of the 21 GW Roadmap that were *operational* in 2024 has been unchanged; the configurations of the *planned* wind farms of the 21 GW Roadmap has been modified. Here, the planned wind farms include HKW, IJVer-Alpa, IJVer-Beta, IJVer-Gamma, Nederwiek I, Nederwiek II&III, Doordewind and TNW.

With the scenario without wind farms of neighboring countries ($NoFor$) the impact of German, United Kingdom (UK), Belgian and Danish wind farms on the 21 GW Roadmap wind farms can be assessed.

In the $20MW$ scenario the default 15 MW turbines of the planned wind farms are replaced by 20 MW turbines, while leaving the installed capacity unchanged. Thus the number of turbines per wind farm decreases which may impact the production and wake effects.

The impact of overplanting is explored with two scenarios. Both 5% ($5\%Ovp$) and 15% ($15\%Ovp$) extra installed capacity is considered.

Finally, a simulation with so-called thrust-free turbines has been performed ($Gross$). The turbines in this scenario do produce power but their thrust is set to zero. As such, they do not produce any wakes and their power production can be considered as gross production. The gross production is the production of a wind farm based on free-stream conditions only, i.e. without considering losses due to wakes or operational losses. Comparison with the waked production numbers provides valuable information on the total aerodynamic losses (i.e. the sum of internal and external wake losses and blockage losses). The wind speed from this simulation represents free-stream conditions.

Just like the intermediate Roadmap scenarios, all sensitivity simulations are simulated for 50 representative days.

The chosen scenario simulation strategy, consisting of two full-year simulations and a large number of 50 representative day simulations, balances the accuracy of a high-fidelity approach on the one hand with a comprehensive set of scenarios on the other hand.

2.2 Model description

2.2.1 Whiffle LES

Whiffle LES, is a large eddy simulation (LES) model that performs its core routines on Graphics Processing Units (GPUs). As such, it overcomes the computation barrier that has been traditionally associated with LES models (Schalkwijk et al., 2015). By numerically integrating the filtered conservation equations of mass, momentum, temperature, and moisture, LES is able to capture the essential aspects of wind farm flow dynamics in a physically sound way.

The origin of Whiffle LES lies in code that is commonly referred to as DALES: Dutch Atmospheric Large Eddy Simulation (Heus et al., 2010). The basic LES equations of Whiffle LES are summarized in Baas et al. (2023). In parallel to the implementation on GPUs, a coupling to a large-scale weather model was realized. Together, these developments paved the way for real weather simulation and forecasting using LES. This important milestone laid the foundation for practical application of LES for various applications, such as accurate wind and solar forecasts.

While most LES codes apply periodic (lateral) boundary conditions, Whiffle LES uses prescribed boundary conditions. A nested domain configuration (1-way nesting) is applied, where the model state of the outer domains is prescribed at the boundaries of the inner domains.

For the present study, boundary conditions from ECMWF's ERA5 reanalysis dataset have been applied (Hersbach et al., 2020). To bridge the gap between the coarse ERA5 grid (~30 km) and the fine LES grid (120 m) of the inner domain, an additional mesoscale simulation is used with a resolution of 3 km. The mesoscale simulation is nested in ERA5, while the boundary conditions of the smaller LES domain are extracted from the mesoscale simulation. For the mesoscale domain, the same model formulation is used as for the inner LES domain, apart from the turbulence, which is not resolved but completely parameterized following Holtslag and Boville (1993).

2.2.2 Lower-boundary conditions

As a lower-boundary condition, Whiffle LES uses a modified version of the Tile ECMWF Scheme for Surface Exchanges over Land (TESSEL) model (ECMWF, 2017). Over water, a Charnock relation (Charnock, 1955) is applied with a Charnock constant, α, of 0.025.

2.2.3 Wind turbine parametrization

Whiffle LES uses an actuator disk parametrization as described by Meyers and Meneveau (2010). This parametrization only needs information about the power curve, thrust curve, rotor diameter, and hub height. The parametrization calculates the drag forces (using the thrust curve) and rotational forces (using the power curve) based on local wind speed, taking the actual induction into account. Individual yaw control based on the local wind direction is applied to the turbines.

For reliable simulation results the manufacturer's power curves must be transformed to disk-based power curves (for instance to account for the effect of turbine induction). These disk-based power curves are obtained by means of a separate simulation.

All turbines are also included in the mesoscale domain. In the mesoscale domain, the same parametrization is used as is used for the LES (model parameters describing the distribution of the turbine forces over the grid are optimized for the respective grid configurations). With this approach wind farm wakes from remote wind farms are being propagated into the inner LES domain. The implementation ensures that also on the coarse mesoscale domain grid, the correct amount of momentum is extracted from the flow.

2.3 Simulation domain

The present study applies exactly the same model setup as utilized in validation phase of this study (Whiffle, 2024). The LES domain has a size of 307.2 x 384 x 5 km. The central coordinate is 52.965N, 4.55E. The size of the LES domain is determined by the locations of the wind farms of the 21 GW roadmap. The domain is chosen such, that each of these wind farms is a least 25 km away from the domain edges (see Sect. 2.4.2 for the treatment of turbines of non-Dutch wind farms near the edge of the LES domain).

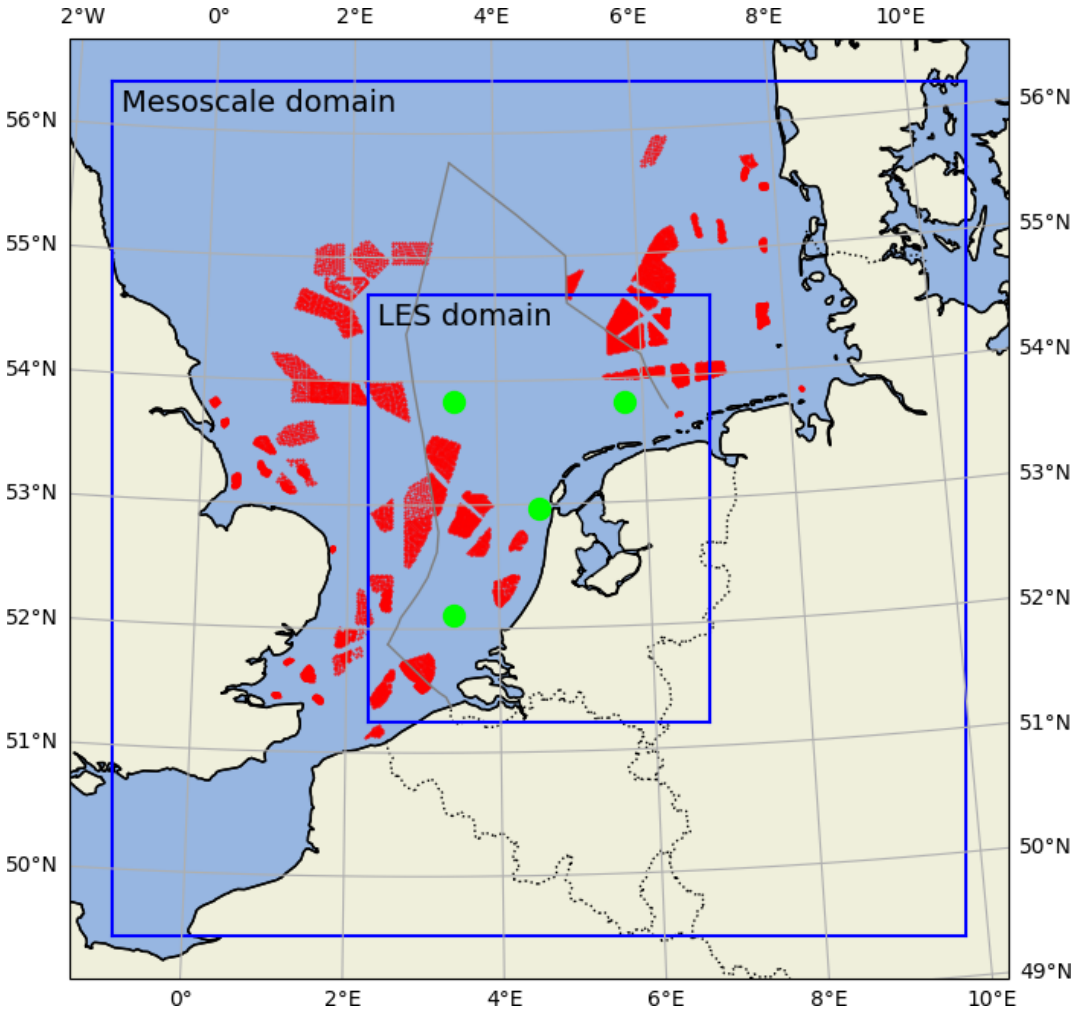

Figure 2.2. Mesoscale and LES domain configuration. Wind farm included in the full buildout scenario are indicated in red. Green dots indicate locations from which ERA5 data has been used to select a representative year.

A horizontal grid-spacing of 120 m is applied. In the lowest part of the domain the vertical grid-spacing is 30 m. Above 320 m, grid-stretching is applied to reduce the number of vertical levels. In the innermost domain (containing 2560 x 3200 x 64 cells) the LES equations are solved. Case and time specific inflow turbulence is generated by means of a concurrent (periodic) LES simulation.

The LES domain is nested in a mesoscale domain with a size of 768 x 768 x 10 km. The horizontal grid spacing is 3000 m. The lowest model level is 20 m. Above the lowest model grid stretching is applied. The mesoscale domain contains 256 x 256 x 64 grid cells and receives its lateral boundary conditions from ERA5. The settings

of the simulation domains are summarized in Table 2.2. Figure 2.2 shows the spatial extent of both the outer (mesoscale) domain and the inner (LES) domain.

In order to include seasonal effects, model simulations have been carried out for a period of one year. Long-term representativeness and the selection procedure for the simulation year are further discussed in Sect. 2.5.1. The simulation year is split into 365 single-day runs. For each day, a 6 h spin-up period is applied for the mesoscale simulation. For the LES domain a 3 h spin-up period was applied.

	Mesoscale domain	LES domain
Δx	3000 m	120 m
Δy	3000 m	120 m
Δz	40	30
L_x	768.0 km	307.2 km
L_y	768.0 km	384.0 km
L_z	10000 m	5000 m
N_x	256	2560
N_y	256	3200
N_z	64	64

Table 2.2. Domain settings indicating grid spacing (Δ), spatial extent (L), and the number of grid points (N) in three directions (x, y, and z).

2.4 Wind farms and turbine types

2.4.1 The 21 GW Roadmap wind farms

Currently operational wind farms (except wind farms PAWP and OWEZ) are included in all simulated scenarios. Turbine locations were obtained from OpenStreetMap.

Wind farm	Lat, Lon	Turbine type	Number of turbines	Capacity [MW]	Capacity density [MW/km^2]	Rotor diameter [m]	Hub-height [m]	Power curve source indicator
Luchterduinen	52.41, 4.16	V112-3.0MW	43	129	8.1	112	81	1
Gemini	54.04, 5.96	SWT-4.0-130	150	600	8.9	130	89	1
Borssele I&II	51.69, 3.07	SG 8.0-167DD	94	752	5.9	167	109	2
Borssele III&IV	51.71, 2.93	V164-9.5MW	79	750	5.1	164	109	2
HKN	52.71, 4.26	SG 11.0-200 DD	69	759	6.0	200	125	3
HKZ	52.31, 4.05	SG 11.0-200 DD	139	1529	5.9	200	125	3
HKW	52.71, 4.26	Reference-15.0MW	100	1500	8.0	236	150	4
IJVer-Alpha	52.82, 3.49	Reference-15.0MW	134	2010	10.7	236	150	4
IJVer-Beta	52.91, 3.58	Reference-15.0MW	134	2010	10.3	236	150	4
IJVer-Gamma	53.03, 3.72	Reference-15.0MW	134	2010	9.0	236	150	4
Nederwiek I	53.10, 3.18	Reference-15.0MW	134	2010	7.4	236	150	4
Nederwiek II&III	53.41, 3.26	Reference-15.0MW	267	4005	5.9	236	150	4
Doordewind	54.27, 5.65	Reference-15.0MW	134	2010	10.0	236	150	4
TNW	54.02, 5.68	Reference-15.0MW	53	795	9.2	236	150	4
Total			1664	20869	7.5			

Table 2.3. List of wind farms and their properties that are included in the 21 GW Roadmap simulations. The respective columns indicate the name of the wind farm, the central latitude and longitude, the applied turbine type, the number of turbines, the installed capacity, the installed capacity density, the rotor diameter, the hub height, and an indicator of the source of the utilized power curve (1: power and thrust curves obtained from the WindPRO database, 2: power curves obtained from https://www.thewindpower.net/, 3: scaled V164-8.0MW for which power and thrust curve were obtained from Desmond et al. (2016), 4: scaled existing turbine).

The planned wind farms of the 21 GW Roadmap have been implemented following the most recent site

boundaries provided by RVO (as indicated in Fig. 2.1). Table 2.3 provides an overview of the 21 GW Roadmap wind farms. For each wind farm, the required number of turbines were evenly distributed within the wind farm boundaries using an iterative maximum repulsion method (for more information see Stratum et al. (2022)). As an example, Fig. 2.3 shows layouts for the Nederwiek II&III wind farms as generated by this method for different scenarios.

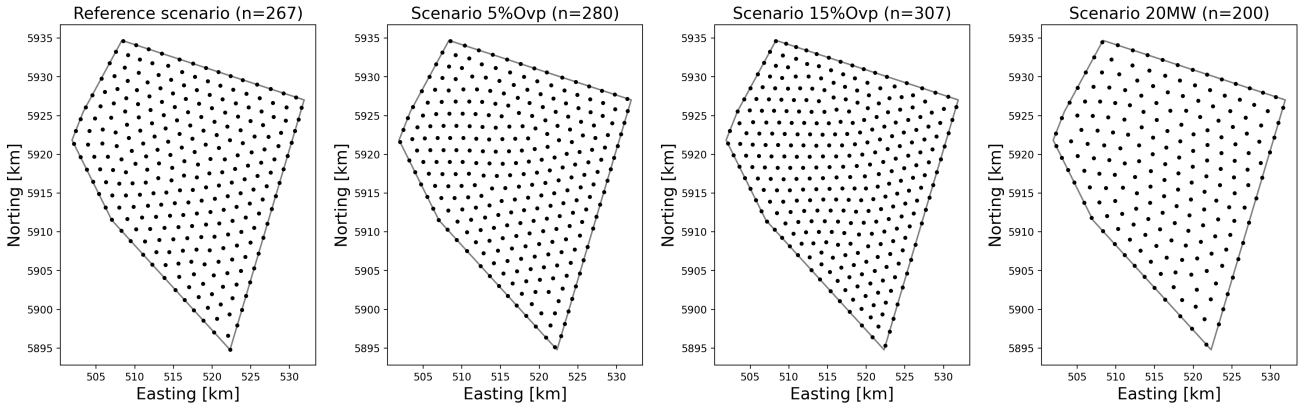

Figure 2.3. Example of layouts of the Nederwiek II&III wind farm for different scenarios as generated by the maximum repulsion method. From left to right: the default scenario, the $5\%Ovp$ scenario, the $15\%Ovp$ scenario, and the $20MW$ scenario. The number of included turbines is indicated in the titles.

For the sensitivity scenarios, the configuration of the planned 21 GW Roadmap wind farms was modified. For the $20MW$ scenario the reference 15 MW turbine was replaced by a 20 MW turbine, leaving the installed capacity of these wind farms the same. For the 20 MW turbine the power and thrust coefficients (i.e. the c_p and c_t values) of the reference 15 MW turbine were used. The rotor diameter was increased to 272.5 m to match the desired rated power of 20 MW. Table 2.4 summarizes the 21 GW Roadmap configuration of the $20MW$ scenario.

Wind farm	Lat, Lon	Turbine type	Number of turbines	Capacity $[MW]$	Capacity density $[MW/km^2]$	Rotor diameter $[m]$	Hub-height $[m]$
HKW	52.71, 4.26	Scaled-20.0MW	75	1500	8.0	272.5	169
IJVer-Alpha	52.82 ,3.49	Scaled-20.0MW	100	2000	10.6	272.5	169
IJVer-Beta	52.91, 3.58	Scaled-20.0MW	100	2000	10.2	272.5	169
IJVer-Gamma	53.03, 3.72	Scaled-20.0MW	100	2000	8.9	272.5	169
Nederwiek I	53.10, 3.18	Scaled-20.0MW	100	2000	7.3	272.5	169
Nederwiek II&III	53.41, 3.26	Scaled-20.0MW	200	4000	5.9	272.5	169
Doordewind	54.27, 5.65	Scaled-20.0MW	100	2000	10.0	272.5	169
TNW	54.02, 5.68	Scaled-20.0MW	40	800	9.2	272.5	169

Table 2.4. Configuration of planned 21 GW Roadmap wind farms in the $20MW$ scenario. The respective columns indicate the name of the wind farm, the central latitude and longitude, the applied turbine type, the number of turbines, the installed capacity, the installed capacity density, the rotor diameter, and the hub height.

For the two overplanting scenarios, $5\%Ovp$ and $15\%Ovp$, the installed capacity of the planned wind farms is increased by 5 and 15%, respectively. For each of the modified wind farms the number of turbines and installed capacities is summarized in Table 2.5. For these scenario the reference 15 MW turbine has been utilized.

Although applying fully optimized layouts is out of the scope of the present study the *layout* scenario explores the impact of replacing the reference layouts, constructed using the maximum repulsion algorithm, by more realistic layouts. For this, the rationale of the so-called boundary-grid method is applied (e.g. Stanley and Ning (2019)). In this method, first a large number of the required turbines is placed along the wind farm boundary. The remaining turbines are placed in the interior of the wind farm in a grid that is oriented towards the dominant wind direction. Spacing in the along-wind direction is increased with respect to the direction perpendicular to the dominant wind

direction. As an example, Fig. 2.4 shows the reference (maximum repulsion) and boundary-grid layout of the Nederwiek II&III wind farm.

Wind farm	Lat, Lon	$5\%Ovp$ Number of turbines	$5\%Ovp$ Capacity $[MW]$	$5\%Ovp$ Capacity density $[MW/km^2]$	$15\%Ovp$ Number of turbines	$15\%Ovp$ Capacity $[MW]$	$15\%Ovp$ Capacity density $[MW/km^2]$
HKW	52.71, 4.26	105	1575	8.4	115	1725	9.1
IJVer-Alpha	52.82, 3.49	140	2100	11.2	154	2310	12.3
IJVer-Beta	52.91, 3.58	140	2100	10.7	154	2310	11.7
IJVer-Gamma	53.03, 3.72	140	2100	9.4	154	2310	10.3
Nederwiek I	53.10, 3.18	140	2100	7.7	154	2310	8.5
Nederwiek II&III	53.41, 3.26	280	4200	6.2	307	4605	6.8
Doordewind	54.27, 5.65	140	2100	10.5	154	2310	11.5
TNW	54.02, 5.68	56	840	9.7	61	915	10.6

Table 2.5. Configuration of planned 21 GW Roadmap wind farms in the $5\%Ovp$ and $15\%Ovp$ overplanting scenarios. For each wind farm, the number of included turbines, the installed capacity, and the installed capacity density is indicated for both scenarios.

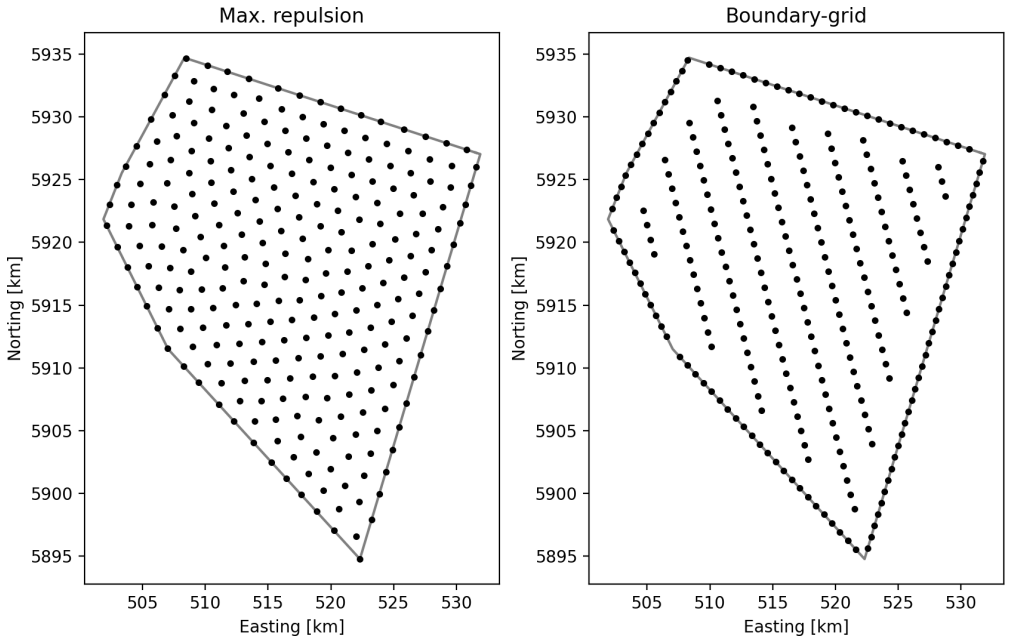

Figure 2.4. Example of applied layout methodologies for the Nederwiek II&III wind farm. Left: maximum repulsion (default), right: boundary-grid.

2.4.2 Wind farms of neighboring countries

A fixed set of wind farms of neighboring countries (i.e. non-Dutch) has been included in all model simulation (except for the *NoFor* scenario). In connection with the timeline of the 21 GW Roadmap, all non-Dutch wind farms that will most likely be operational in the year 2032 have been included. The applied scenario closely follows the KEC 5.0 scenario of offshore wind farms (KEC 5.0, 2024).

For wind farms that are already operational, turbine locations were obtained from OpenStreetMap. For planned foreign wind farms for which no turbine locations were available, a layout was created by distributing the required number of turbines over the wind farm site using the maximum repulsion algorithm. Site boundaries were taken

from the KEC 5.0 scenario database (as well as the wind farm installed capacities and the turbine rated power). An overview of the included wind farms, including their turbine properties, is given in Appendix A. In Fig. 2.2 the locations of the wind farms are indicated in red. The mesoscale domain contains all turbines. For the LES domain a buffer zone of 2.5 km is applied, meaning that it contains all turbines that are located more than 2.5 km away from its edges. As such, wind farms of neighboring countries that are crossing the boundaries of the domain are only partly present in the LES (as indicated in Table A.1).

2.4.3 Turbine properties

A turbine power curves specifies how much energy a turbine produces as a function of the wind speed. A thrust curve specifies how much thrust the turbine exerts on the flow, which also depends on the wind speed. Each turbine type has its own specific power and thrust curve. Power and thrust curves for the present study were obtained from a variety of sources. Whenever available, data from the WindPRO turbine dataset has been used. For remaining turbines, power curves were obtained from `https://www.thewindpower.net/`. Also power curve data provided in Grothe et al. (2022) and Desmond et al. (2016) were used. For turbine types for which only power curve data were available, thrust coefficients have been estimated by utilizing the relation between power and thrust coefficients from turbines for which both were known.

The 21 GW Roadmap wind farms are modeled using a 15 MW wind turbine, which is a modified and scaled version of an existing turbine of comparable rated power. Power and thrust curves are given in Fig. 2.5. In the following, this turbine is referred to as 'Reference-15.0MW'.

Properties of remaining (future) turbines for which no power and thrust curves are available are estimated using the power and thrust coefficients of the Reference-15.0MW turbine, while modifying the rotor diameter to obtain the desired rated power. The hub heights are adjusted accordingly. This involves the 20 MW turbines of the $20MW$ scenario, but also several turbine types of planned wind farms of neighboring countries. For illustration, power curves of the scaled 20.0 MW turbine are included in Fig. 2.5.

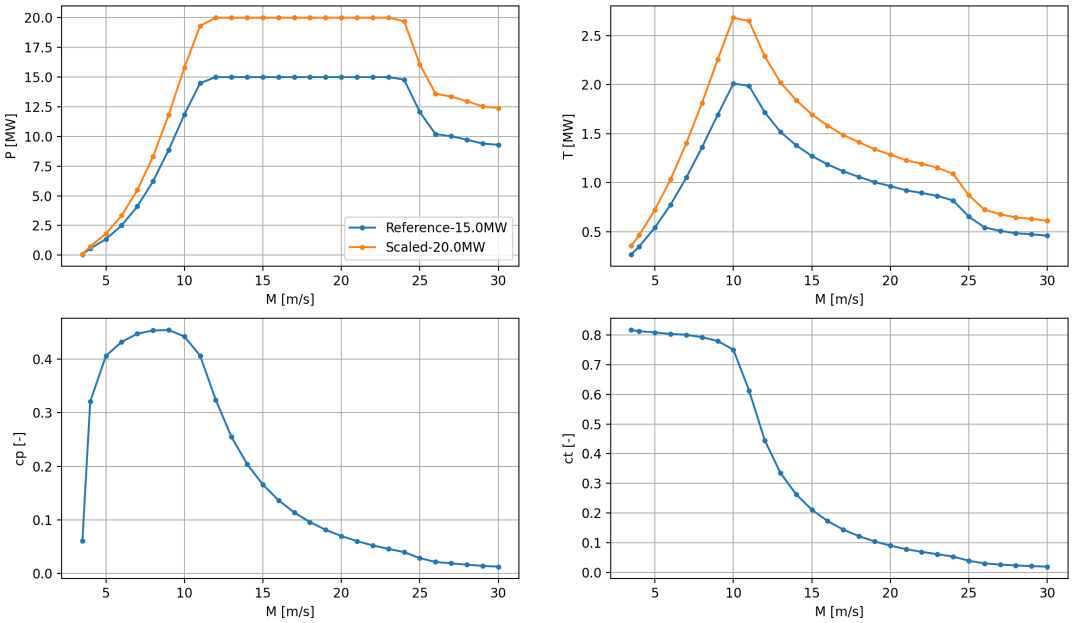

Figure 2.5. Power and thrust curves for the Reference-15.0MW turbine. Also curves for the Scaled-20.0MW turbine are presented.

2.5 Selection of simulation periods

For two scenarios (i.e. Scenario 1 and Scenario 5) a full-year simulation has been performed. The simulated period is 17 March 2018 to 17 March 2019. This specific 365-day period has been carefully selected from 20 years of ERA5 reanalysis data to be as much long-term representative as possible. The selection procedure is discussed in Sect. 2.5.1. In order to balance computational costs with a wide range of simulation scenarios, the remaining scenarios have been simulated for a representative set of 50 days. The selection of the set of 50 days is discussed in Sect. 2.5.2.

2.5.1 Selection of representative year

As a starting point for selecting a representative year, ERA5 100-m wind speed and direction hourly time series were downloaded for the 20-year period May 2004 to May 2024 for four locations in the simulation domain. These reference points are indicated with green dots in Fig. 2.2. The combined distributions of wind speed and direction of the four locations form the long-term reference.

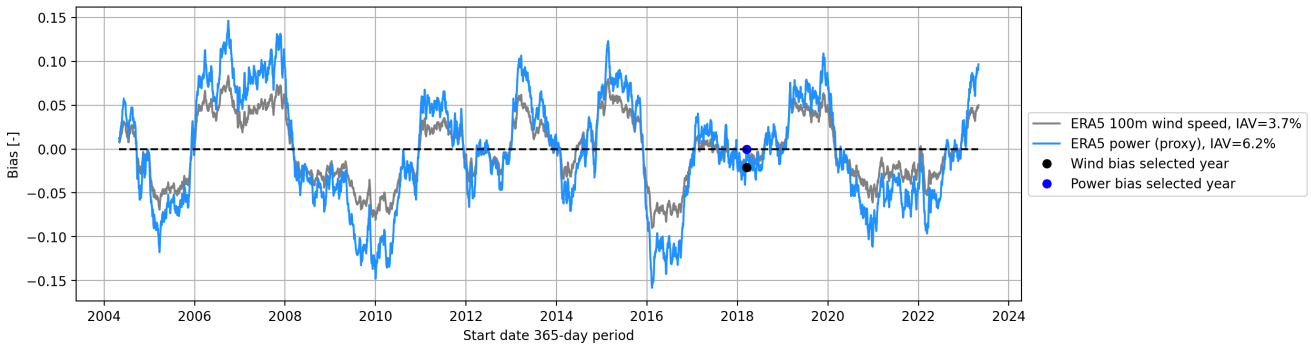

Figure 2.6. ERA5 wind speed and power biases for consecutive 365-day periods between May 2004 and May 2024. Values for the selected simulation year are indicated with separate symbols. IAV indicates interannual variability.

For determining the optimal 365-day period we did not restrict ourselves to calender years (1 January to 31 December). Instead, we examined all possible consecutive 365-day periods within the considered 20-year period by shifting the starting date of the 1-year period forward one day at a time (19 times 365 possibilities).

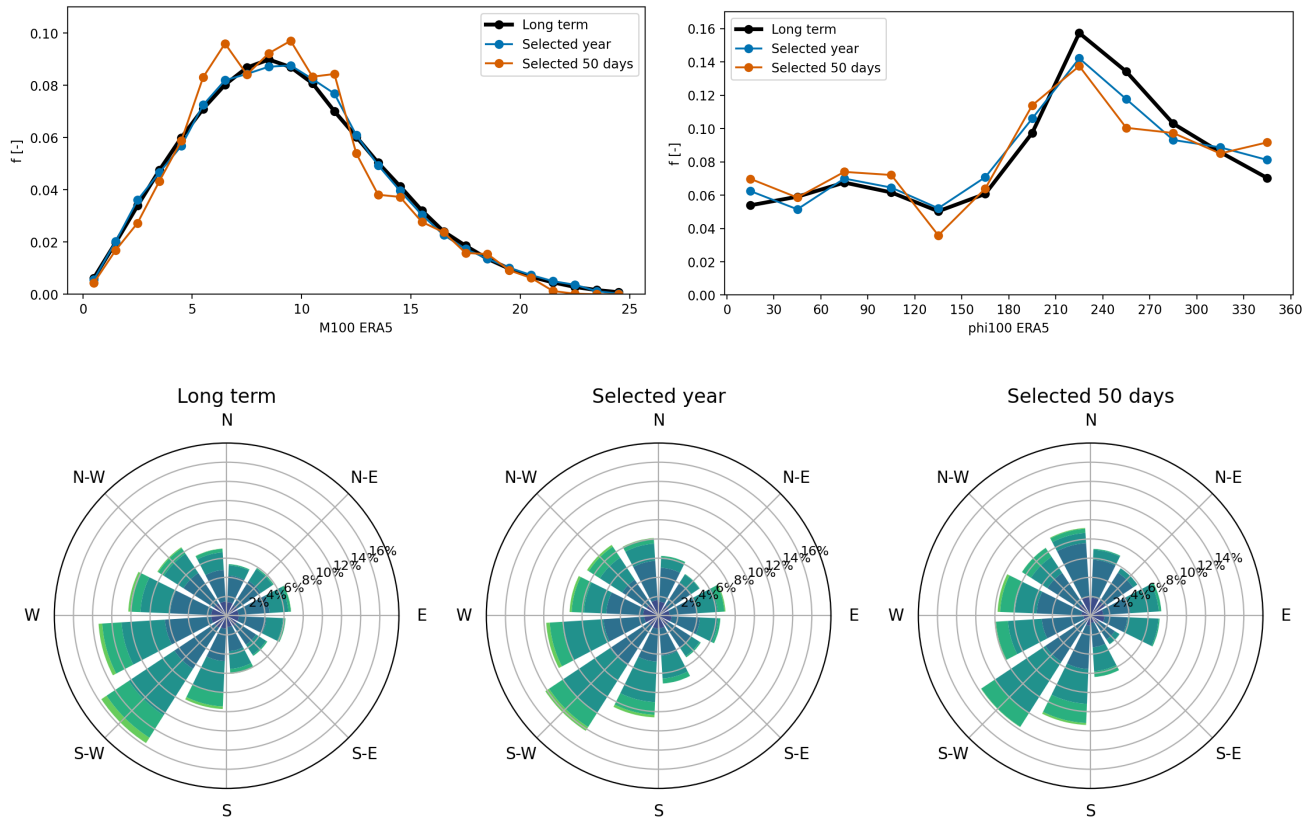

Figure 2.7. Top: ERA5 100-m wind speed and direction distributions for both the long-term and the selected year (17 March 2018 to 17 March 2019). For completeness, the distributions for the representative set of 50 days are given as well (see Sect. 2.5.2). Bottom: ERA5 100-m wind roses for the long-term period, the selected year, and the selected set of 50 days.

For all those consecutive 365-day periods the wind speed bias with respect to the full 20 year period was determined. Also, the ERA5 wind speed time series was converted to a power output. For this, the ERA5 wind speed was fed into an effective wind farm power curve that was derived from a year long LES simulation of a 4 GW wind farm (Scenario 1 of Baas et al. (2023)). This wind farm power curve was obtained by determining the mean

'waked' power (i.e. the simulated aggregated production of the 4 GW wind farm) for 0.5-m/s bins of the free-stream wind speed. The resulting ERA5-based power time series should not be used in an absolute sense. In a relative sense it can be used to determine a power bias for each of the consecutive 365-day periods with respect to the long-term reference period.

As an illustration, Fig. 2.6 shows the ERA5 wind speed and power bias for all considered 365-day periods. Significant interannual variability (IAV), with the IAV defined as the standard deviation divided by the mean value. Due to the non-linearity of power production and wind speed, the relative variations in power production are larger than in wind speed. For wind speed, the dataset considered here has an IAV of 3.7%, in close agreement with values reported for the Dutch EEZ by DNV GL (2016) and Ronda et al. (2017). With 6.2% the IAV of power production is considerably larger.

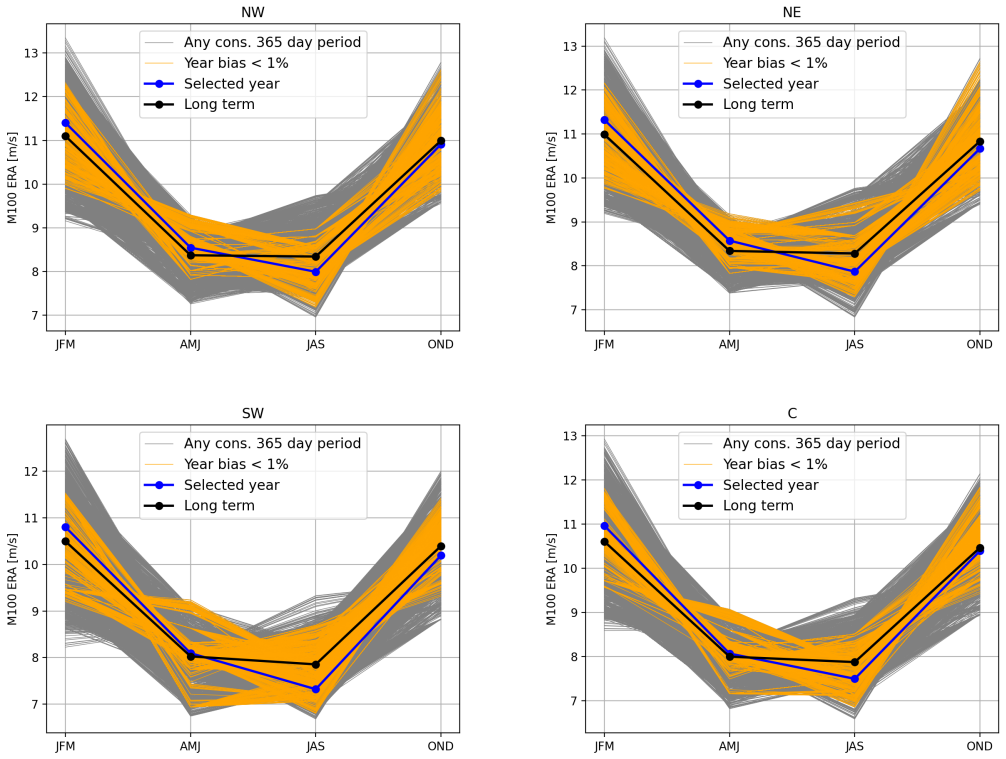

Figure 2.8. Seasonal variation of the ERA5 100m wind speed. Grey lines indicate any consecutive 365-day period, orange lines indicate 365-day periods with a mean wind speed bias <1%. The bold black line represents the long-term mean, the bold blue line the selected year. The titles 'NW', 'NE', 'SW', and 'C' refer to the four ERA5 reference locations in Fig. 2.2.

In addition, for all 365-day periods the correspondence with the long-term distributions of wind speed and direction was determined. For this, we use we use the Perkins skill score (PSS, Perkins et al. (2007)), which is defined as

$$\mathrm{PSS} = \sum_{1}^{n} \min(h_n^{\mathrm{short}}, h_n^{\mathrm{long}}). \tag{2.1}$$

Here n is the number of bins that are considered, h_n^{short} is the normalized frequency of values in a given bin of the short term data and h_n^{long} is the normalized frequency of the corresponding bin of the long-term distribution. For two perfectly overlapping distribution the PSS is equal to 1, for two distributions without any overlap the PSS is equal to 0. For wind speed, a bin-width of 1 m/s was applied. For wind direction, a bin-width of 30 degrees was applied.

In summary, for each consecutive 365-day period the above procedure provided four metrics regarding long-term representativeness: 1) bias in the mean wind speed, 2) bias in the power production, 3) correspondence in the wind speed distribution and, 4) correspondence in wind direction distribution.

A preselection was made of all 365-day periods with both a wind speed and power bias of less than 1% compared to the long-term period. From this subset, the 365-day periods with the highest combined Perkins scores for wind speed and direction were selected. After visual comparison of wind speed and direction distributions, together with wind roses, the period of 17 March 2018 to 17 March 2019 was chosen as the optimal simulation period.

Figure 2.7 presents ERA5 100 m wind speed and direction distributions for the selected year and the long-term reference. Corresponding wind roses are given, as well. For comparison, the distributions and wind rose of the representative set of 50 days, discussed in the next Section, are also included.

As an additional check, the seasonal cycle of the wind speed was inspected. Figure 2.8 shows that for all four reference the selected year follow the long-term pattern satisfactory well.

2.5.2 Selection of 50 representative days

The 50 representative days are chosen such, that they resemble the characteristics of the full selected year as close as possible. Therefore, they have been selected using wind and power output from the full-year LES simulations only. In particular, the selection is based on

1. time series of the aggregated power production of the 21 GW Roadmap wind farms of both Scenario 1 (initial buildout) and Scenario 5 (full buildout).

2. time series of the 150-m wind speed from the Scenario 1 simulation for the four reference locations indicated in Fig. 2.2.

The selection of the 50 days is based on random draws of 50 days from the selected full-year period. For each random draw, biases of wind speed and power production (for $Sc1$ and $Sc5$) are calculated with respect to the full-year period. Also, the correspondence of the distributions of wind speed, wind direction, and stability are determined by means of the PSS (2.1).

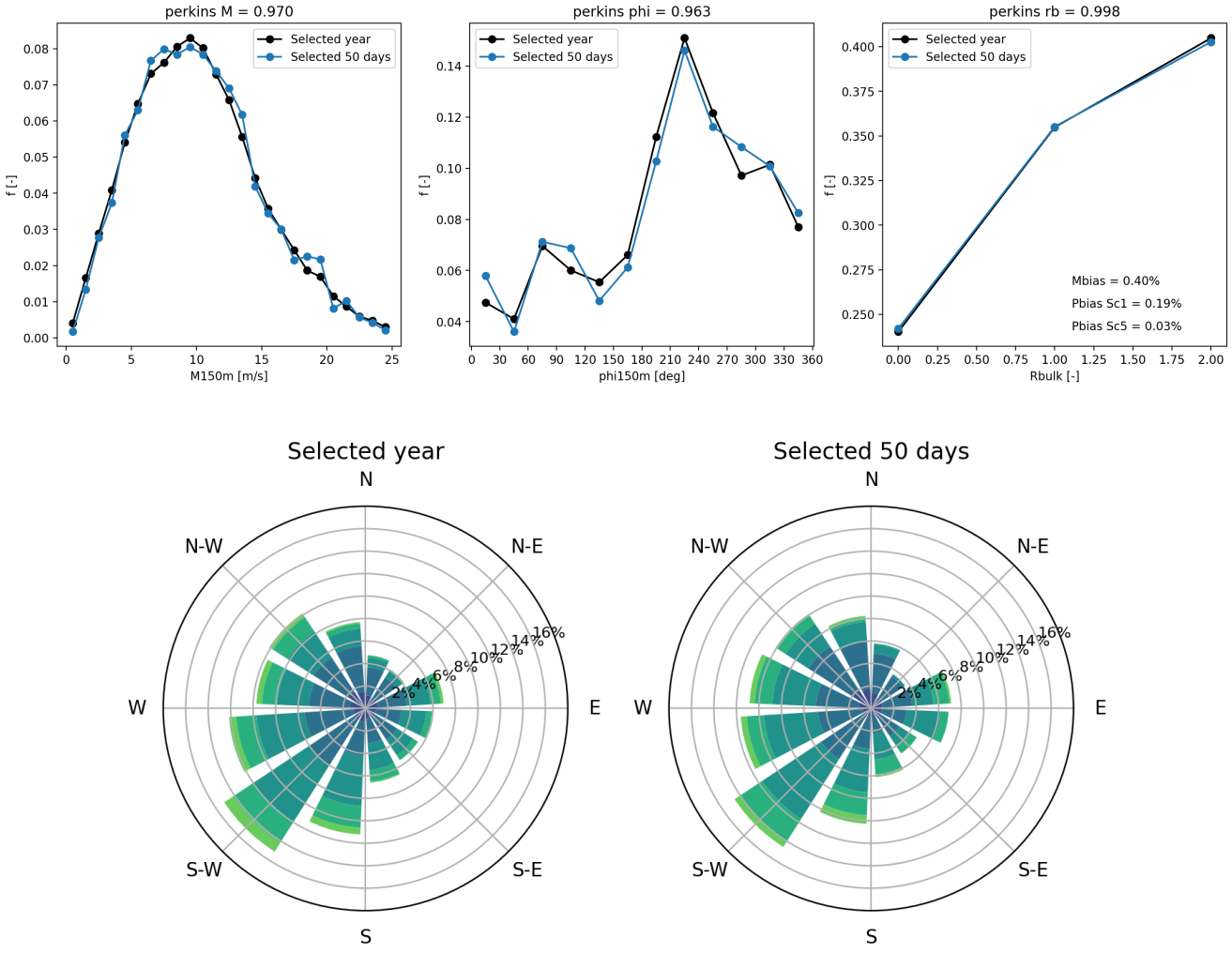

Figure 2.9. Distributions of wind speed, wind direction, and stability for the selected year and the selected set of 50 representative days (top). Windroses for the selected year and the selected set of 50 representative days (bottom). Underlying data is taken from the full-year LES simulations.

To characterize stability the bulk Richardson number

$$Ri_b = g/\bar{\theta}\ \frac{(z_1 - z_0)(\theta_{z_1} - \theta_{z_0})}{(u_{z_1} - u_{z_0})^2 + (v_{z_1} - v_{z_0})^2}, \tag{2.2}$$

is taken over the height interval 45 (z_0) to 255 m (z_1), which roughly corresponds to the vertical rotor footprint of a 15 MW wind turbine. Here g is the acceleration due to gravity, θ is the potential temperature, u is the eastward component of the wind, and v is the northward component of the wind. Three classes of Ri_b are used, each approximately containing one third of the data: $-\infty < Ri_b \leq 0$, $0 < Ri_b \leq 0.5$, and $0.5 < Ri_b \leq \infty$, roughly corresponding to unstable, weakly stable, and very stable conditions, respectively. The Ri_b is a robust and commonly used parameter to distinguish between stability regimes (e.g. Baas et al. (2023); Cantero et al. (2022); Holtslag et al. (2014)). Specific values of Ri_b and, as such, any applied threshold values, may depend on the considered height interval (e.g. Bardal et al. (2018); Hooijdonk et al. (2015)).

From 1 million random drawing of 50 days, the 10 best samples were stored as a preselection. That is to say, the 10 samples with highest average PSS for the three variables considered and with a wind and power bias (for both scenarios) of less than 1%. In total, this procedure was carried out 10 times, resulting in 100 preselected 50-day samples with low wind and power biases and, at least, a reasonable distribution of wind speed, direction and stability.

From the 100 preselected samples a final 50-day sample was chosen by expert judgment after inspecting biases, distributions, and wind roses. Figure 2.9 shows distribution of wind speed, wind direction and stability for the selected set of 50 representative days. Also wind roses for the full year and the 50 selected days are included. The characteristics of the subset of 50 representative days closely resemble those of the selected full-year period. For comparison, the wind speed and direction distributions and the wind rose of the selected 50 days based on the ERA5 100 wind are included in Fig. 2.7. The difference in the distributions of the ERA5 data is slightly larger than in Fig. 2.9. This is because no ERA5 data was involved in the selection of the 50 days.

3 Results

This Section describes the results of the modeling study.

To start with, Sect. 3.1 presents spatial fields of the wind speed at 150 m height are presented for different wind directions for the initial and full buildout scenarios of the 21 GW Roadmap. Next, simulated production numbers will be presented in subsequent levels of details, starting with aggregated production numbers per scenario (Sect. 3.2). Section 3.3 discusses production numbers per wind farm and the differences between scenarios. Section 3.4 analyzes directional wake effects by comparing simulated wind and power data from the initial and full buildout scenarios. Characteristics per wind farm are summarized in Sec. 3.5. To put the presented results into perspective, a brief comparison with other modeling studies is made in Sect. 3.7.

Depending on the application, production numbers are given in as a time-average value (units W or MW) or as integrated annual energy production (units TWh). Production numbers are also expressed as a capacity factor. The capacity factor is defined as the production divided by the installed (or the maximum theoretically possible) production.

The presented production numbers include losses due to wake and blockage effects. Not included are electrical, hysteresis, curtailment and other operational losses. Raw model production numbers have been corrected for model bias, sampling errors, and long-term representativeness. The different elements included in the correction factor and their associated error margins are extensively discussed in Sect. 4.

3.1 Spatial patterns in the annual mean 150 m wind speed

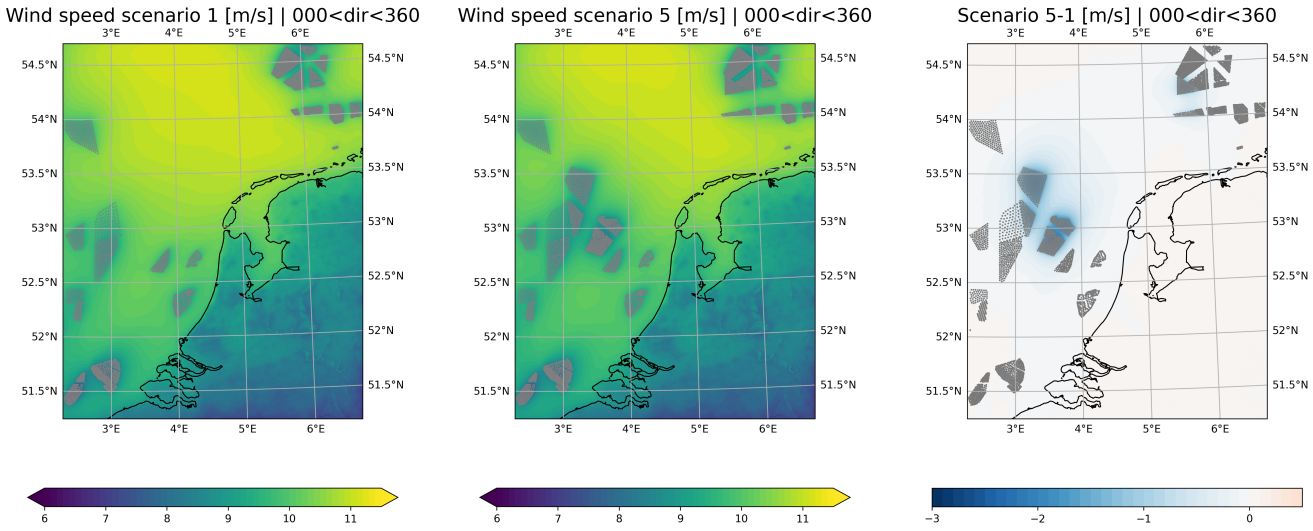

Figure 3.1. Annual, omnidirectional mean wind speed at 150 m for $Sc1$ and $Sc5$, as well as the difference between the two scenarios.

From the full year simulation of the initial ($Sc1$) and full ($Sc5$) buildout scenarios of the 21 GW Roadmap averaged maps of the 150 m wind speed have been made.

Figure 3.1 shows the yearly averaged, omnidirectional wind field for both scenarios. Also the difference between the two is shown. The largest differences are seen for an extended area around the IJVer cluster plus surrounding wind farms, which together cover a large part of the 21 GW Roadmap. Here (in particular in the area of IJVer-Alpha and Beta) the additional wake effect of the full buildout of the 21 GW Roadmap maximizes at 2.5 m/s. In an extended area of roughly 70 by 100 km the difference between the two simulations is 0.5 m/s or more. Also note the significant wake effects that are related to the extensive wind farm cluster in the German Bight. As these are included in both scenarios, the wakes are not visible in the difference plot, but the mean wind fields show a clear impact.

As wind farm wakes are a directional phenomenon, omnidirectional velocity deficits convey only part of the story as wakes tend to average out over the different wind directions. Therefore, Figs. 3.2 and 3.3 show the mean wind fields at 150 m for two selected 30-degree (domain-averaged) wind direction bins. Strong wake effects are visible, where significant velocity deficits extend tens of kilometers downstream of the main wind farm clusters (for reference, half a degree of latitude equals approximately 50 km). At some locations a slight acceleration of the flow is visible in the full buildout scenario (reflected in positive values in the right-hand panels of Figs. 3.2 and 3.3), in particular along the edges of the largest wind farm clusters. This is a manifestation of the blockage effect: the wind speed decreases already upstream of the wind farms, while a speed-up of the flow can occur along the sides (e.g. Baas et al. (2023); Meijer et al. (2024)).

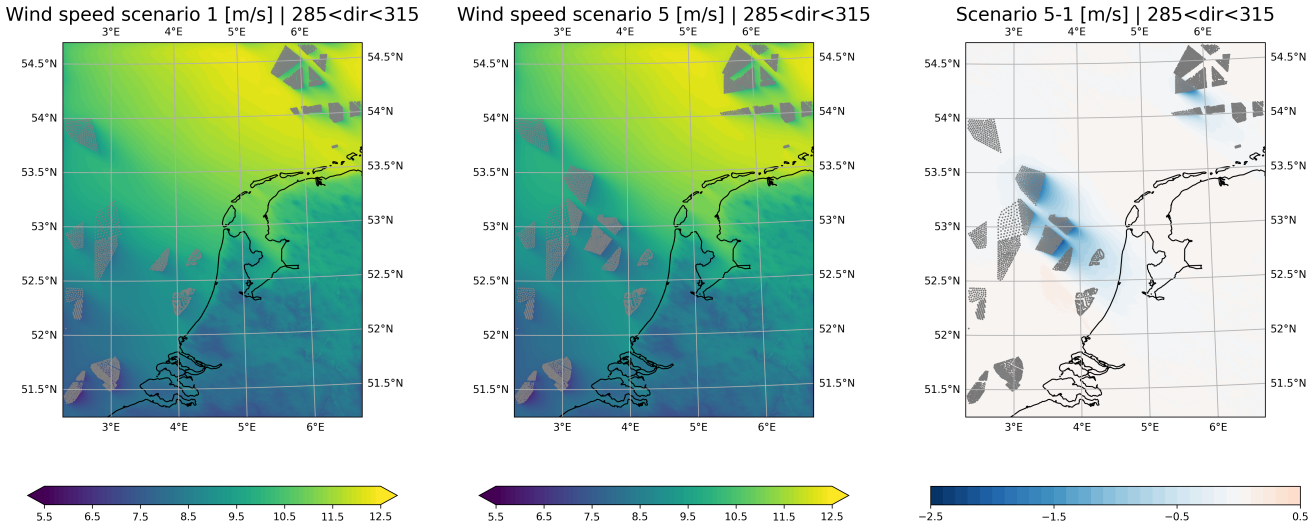

Figure 3.2. Annual mean wind speed at 150 m for *Sc*1 and *Sc*5, as well as the difference between the two scenarios. Only cases with a mean wind direction between 285 and 315 degrees are included.

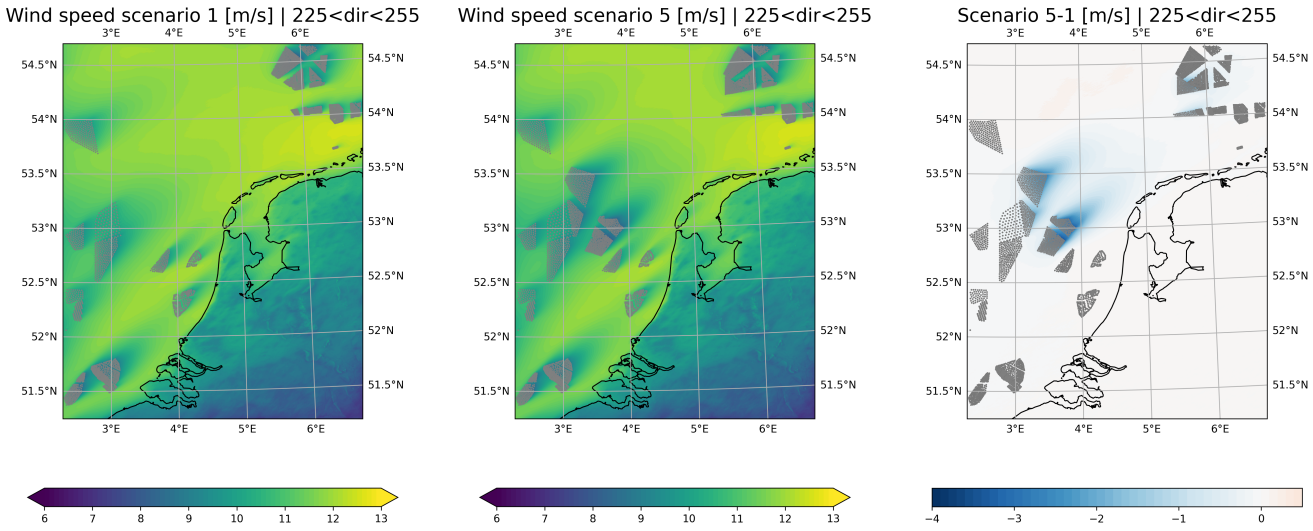

Figure 3.3. Annual mean wind speed at 150 m for *Sc*1 and *Sc*5, as well as the difference between the two scenarios. Only cases with a mean wind direction between 225 and 255 degrees are included.

3.2 Aggregated production numbers

To start with, this Section presented simulated aggregated Annual Energy Production (AEP) per scenario. The AEP (units TWh) is calculated by multiplying the mean production (in units W) by the numbers of hours in a year (24 x 365 = 8760 h).

Figure 3.4 presents the production numbers per scenario. The corresponding capacity factors are shown in Fig. 3.5. Exact numbers are summarized in Table 3.1, which also includes the installed (or rated) capacity for each scenario. The presented data reflect corrected production numbers. Correction methods are discussed in Sect. 4.

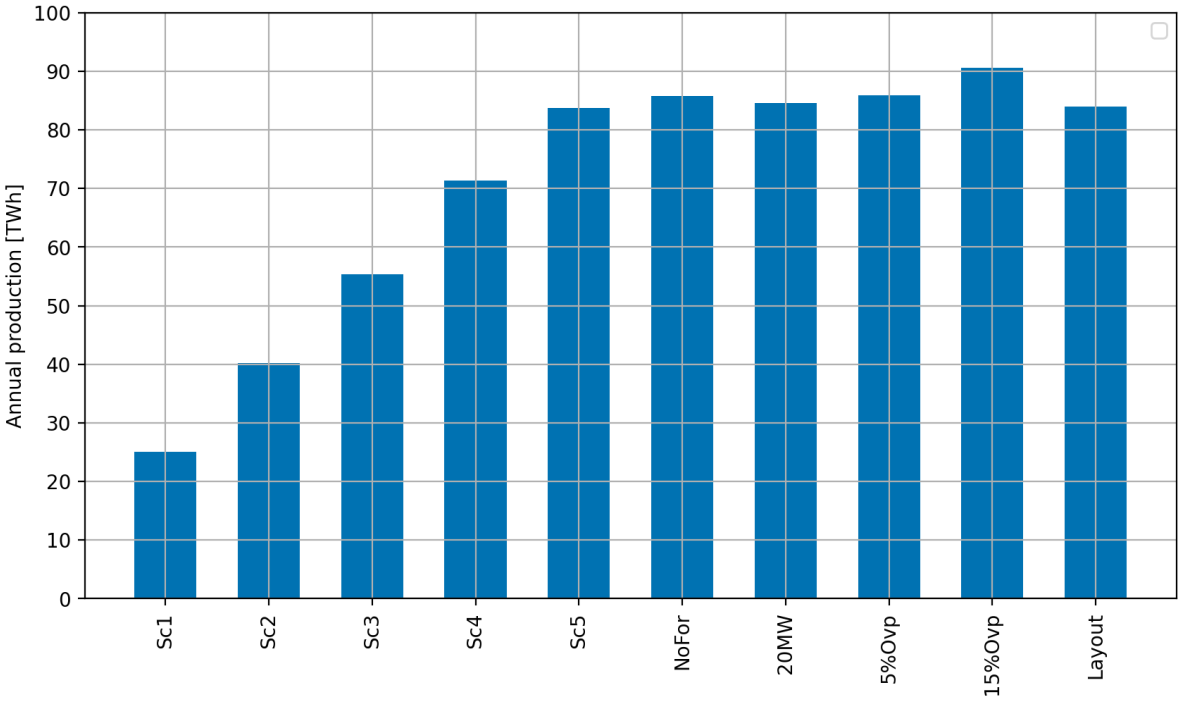

Figure 3.4. Aggregated production numbers (in TWh) per scenario.

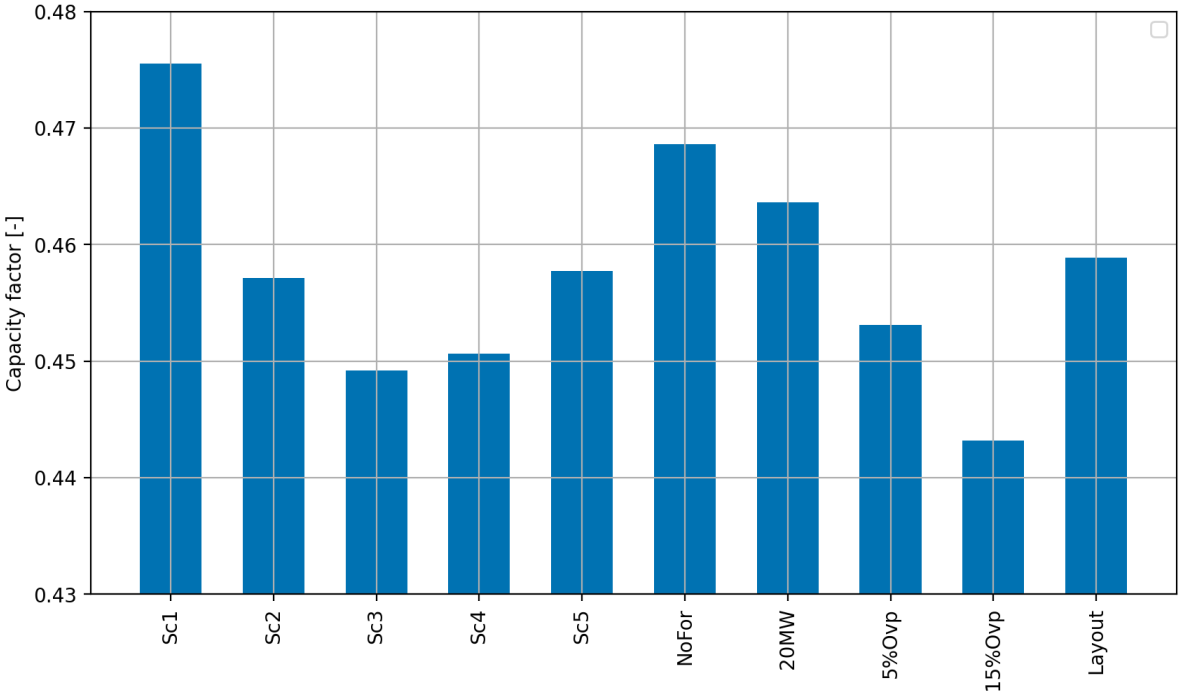

Figure 3.5. Capacity factor per scenario.

The incremental buildout of the 21 GW Roadmap is reflected in a gradual increase in the AEP when going from $Sc1$ to $Sc5$. The best-estimate of the AEP for $Sc5$, the full buildout scenario, is 83.7 TWh. As motivated in Sect. 4, the error margin in terms of standard deviation associated with the production numbers is 5%.

The subsequent addition of the various wind farms lead to a slight reduction of the capacity factor, for $Sc5$ the capacity factor is increased again. This is caused by the relatively large capacity factors of the Doordewind and TNW wind farms (see Sect 3.3).

Without considering the Gross scenario, the capacity factors of the scenarios varies by 3 percent points. Compared to $Sc5$, the capacity factors of the $NoFor$ and $20MW$ scenarios is slightly increased. Leaving out all foreign wind farms increases the overall AEP by 2.3%. For the overplanting scenarios the capacity factor is a bit lower than for the reference $Sc5$, but production is increased (2.5 and 8.1% for 5 and 15% overplanting, respectively). The smallest impact is found for the $Layout$ scenario.

Production in the $Gross$ scenario is 27.8% higher than in $Sc5$ (Table 3.1). Expressed differently, this means that the actual, or waked production of $Sc5$ is 21.7% lower than the gross production. This 21.7% indicates the so-called total aerodynamic losses, which is defined as the sum of all internal and external wake and blockage losses.

Scenario	Inst. Cap. [GW]	Corr. Prod [TWh] (w.r.t Sc5)	Corr c.f. [-] (w.r.t Sc5)
$Sc1$	6.02	25.08 (-70.0%)	0.476 (3.9%)
$Sc2$	10.04	40.20 (-52.0%)	0.457 (-0.1%)
$Sc3$	14.06	55.32 (-33.9%)	0.449 (-1.9%)
$Sc4$	18.07	71.31 (-14.8%)	0.451 (-1.6%)
$Sc5$	20.87	83.68 (0.0%)	0.458 (0.0%)
$NoFor$	20.87	85.68 (2.4%)	0.469 (2.4%)
$20MW$	20.82	84.56 (1.0%)	0.464 (1.3%)
$5\%Ovp$	21.64	85.87 (2.6%)	0.453 (-1.0%)
$15\%Ovp$	23.32	90.52 (8.2%)	0.443 (-3.2%)
$Layout$	20.87	83.89 (0.2%)	0.459 (0.2%)
$Gross$	20.87	106.97 (27.8%)	0.585 (27.8%)

Table 3.1. Overview of AEP numbers for each scenario. Columns indicate the scenario names, installed capacities, production numbers, and capacity factors, respectively. In brackets, the differences with respect to $Sc5$ are given.

3.3 Production numbers per wind farm per scenario

In this subsection the simulated annual production per wind farm is presented for each scenario. Data are compared to the production of the full buildout scenario ($Sc5$). Also a comparison to the gross (or free-stream) production is made. The presented numbers in this section refer to *corrected* model output.

As a starting point, Fig. 3.6 shows the mean annual production per scenario for each wind farm of the 21 GW Roadmap. Differences are mainly governed by the installed capacity of the wind farms. The underlying data are shown in Table B.1.

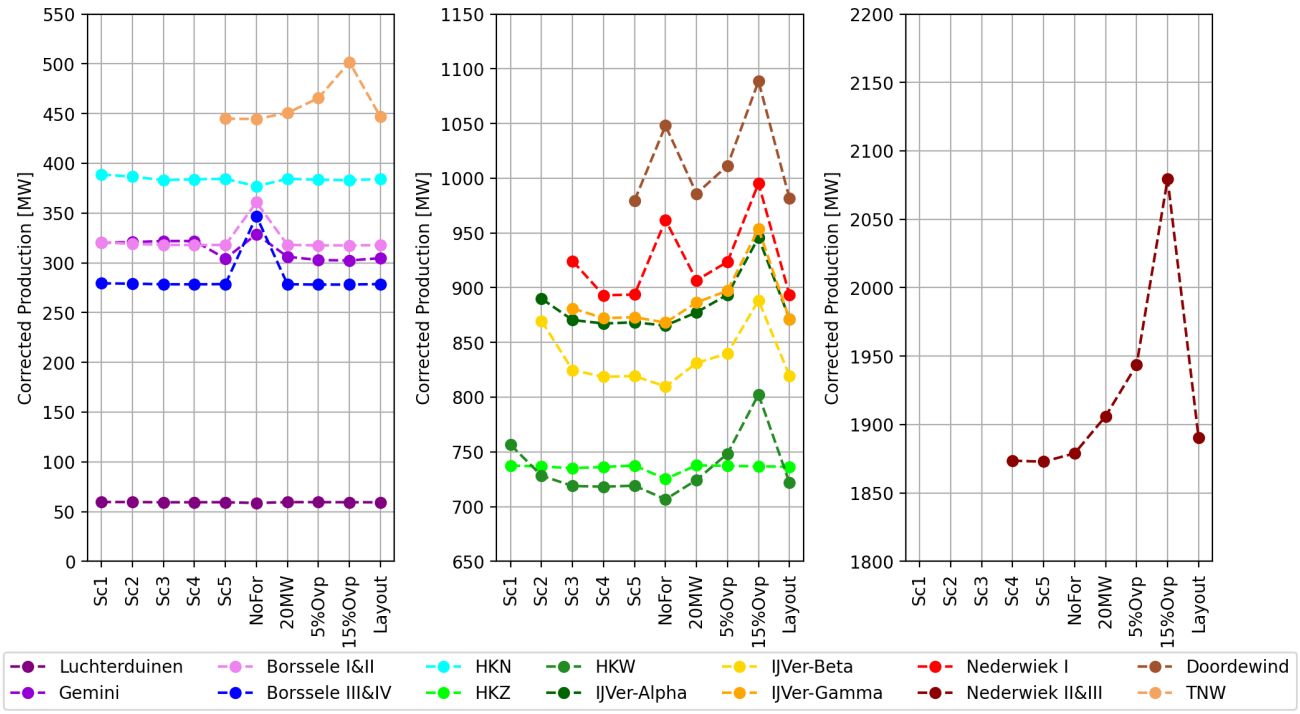

Figure 3.6. Mean annual production (in MW) per scenario for each wind farm. Underlying data are presented in Table B.1.

Considering the production with respect to the full buildout scenario, $Sc5$ (Fig. 3.7) or the capacity factor (Fig. 3.8) provides a more detailed view on the differences between the scenarios. For completeness, the numbers presented in these Figures are given in Tables B.2 and B.3.

Incremental buildout scenarios

Significant differences between the wind farms exist. Figure 3.7 shows that the impact of gradual roll-out of the 21 GW Roadmap on the currently operational wind farms (Luchterduinen, Gemini, Borssele, HKN, HKZ) is relatively small. The addition of IJVer-Alpha and IJVer-Beta in $Sc2$ has a significant impact on the production of HKW. Adding IJVer-Gamma and Nederwiek I ($Sc3$) mainly impacts IJVer-Beta, and, to a lesser extent, IJVer-Alpha. The addition of Nederwiek II&III in $Sc4$ is mostly confined to Nederwiek I. The production of Gemini is only significantly changed in $Sc5$, with the addition of TNW and Doordewind. From $Sc1$ to $Sc4$ the production of Gemini increases by a few tenth of a percent. Inspection of the production data per day reveals that most of this difference is realized in a limited number of days. No systematic wake and/or blockage effect that is causing this subtle increase could be determined.

At the same time, Fig. 3.8 shows that large differences exist in the capacity factors of the various wind farms. Factors that influence the capacity factor are the distance to neighboring non-Dutch wind farms (e.g. the Borssele wind farms) and the distance to other 21 GW Roadmap wind farms (e.g. IJVer-Beta). Also, in the North Sea the wind speed gradually increases from South to North (Geyer et al. (2012)). This explains the relatively high capacity factors of Gemini and Doordewind (resulting in an increased overall capacity factor of $Sc5$ compared to $Sc4$, see Sect. 3.5).

Studies in literature indicate that the capacity factor strongly depends on the installed capacity density (Sect. 3.7). Comparison of Fig. 3.8 with the corresponding capacity densities given in Table 2.3 suggests that on the level of individual wind farms other factors like the vicinity to and size of neighboring wind farms is of larger importance.

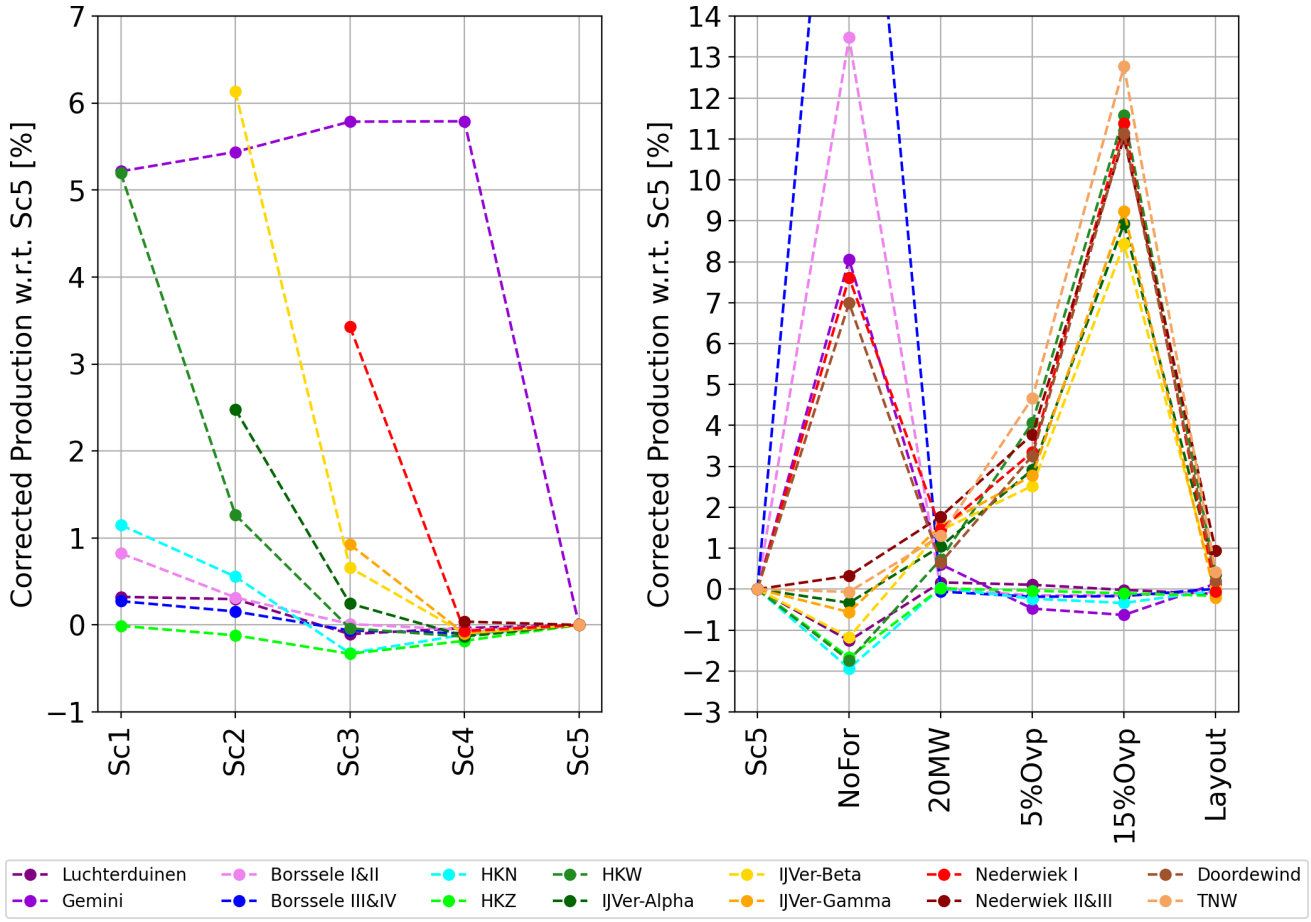

Figure 3.7. Production increase/decrease (in %) per scenario for each wind farm with respect to the production of *Sc*5. Underlying data are presented in Table B.2. The outlier value for Borssele III&IV, the *NoFor* scenario, with a value of 24.5%, is excluded from the Figure for clarity reasons. The left panel presents data for the incremental buildout scenarios, the right panel for the sensitivity scenarios.

Sensitivity scenarios

Figures 3.7 and 3.8 also provide a more detailed view on the impact sensitivity scenarios on the various wind farms. Leaving out the wind farms of neighboring countries mainly impacts the production of the Borssele, Nederwiek I, TNW, and Doordewind wind farms. These are all wind farms that are directly bordered by non-Dutch wind farms. For the Borssele wind farms the impact is largest as the neighboring Belgium wind farms are located upstream of the dominant wind direction.

Interestingly, some other wind farms that are further away from the borders of the Dutch EEZ, show a slight decrease in production when the wind farms of neighboring countries are left out. This is seen, for instance, for HKN, HKZ, HKW, and Luchterduinen. This mainly occurs for northerly to northeasterly directions. No clear pattern is visible in the directionally averaged wind speed maps. The results suggest that for the mentioned wind farms the presence of the massive German cluster in the north may for specific cases lead to a small increase of the wind speed. The same can be argued for the wind farms of the IJVer cluster, that also show reduced production numbers in the *NoFor* scenario. For these wind farms the reduction for north(easterly) directions more than compensates for the increase in production that results from leaving out the smaller and less dense UK wind farms. In Sect. 3.4 this feature is discussed in more detail.

For the sensitivity scenarios $20MW$, $5\%Ovp$, $15\%Ovp$, and *Layout* the configurations of the planned wind farms of the 21 GW Roadmap have been modified (including HKW) as explained in Sect. 2.1. For the already operational wind farms no changes have been made.

Replacing the default 15 MW turbines by a reduced number of 20 MW turbines, while leaving the installed capacity the same, increases the production of the concerning wind farms by 0.7 to 1.7%. This is mainly the result of reduced wake effects and not so much of the increase in hub height (from 150 to 169 m): the increase in actual (waked) production is absent in the corresponding gross production numbers (see Table B.4). The limited impact of the change in hub height may be explained by the relatively low wind shear in offshore conditions.

The two scenarios with overplanting show a significant increase in production. In the $5\%Ovp$ scenario (5% overplanting) the production of the concerning wind farms increases between 2.5 and 5%. For scenario $15\%ovp$

(15%) overplanting an increase between 8 and 12.5% is simulated. As the increase in production is lower than the applied overplanting the capacity factors of the concerning wind farms is reduced.

In practice, the results for the overplanting scenarios are likely to be too optimistic as the energy that can be delivered to the electricity grid is limited by the original rated capacity of the wind farms (theoretically, the surplus could be locally stored in, for instance, hydrogen). For both overplanting scenarios, Table 3.2 provides an overview of production for the cases were no capping is applied (default as presented in other parts of this study) and where the production is limited to the original rated capacity of the wind farms. When a capping of the production is applied the increase with respect to *Sc5* is much less than when no capping is applied. This indicates that the additional production in case of the overplanting scenarios mainly occurs in the regime of rated production. In practice, turbine curtailment to prevent the wind farm production from exceeding the rated production, could lead to a reduction of wake effects. However, as in rated conditions wake effects quickly become less important and because only a small part of a wind farms would need to be curtailed, this effect is considered insignificant.

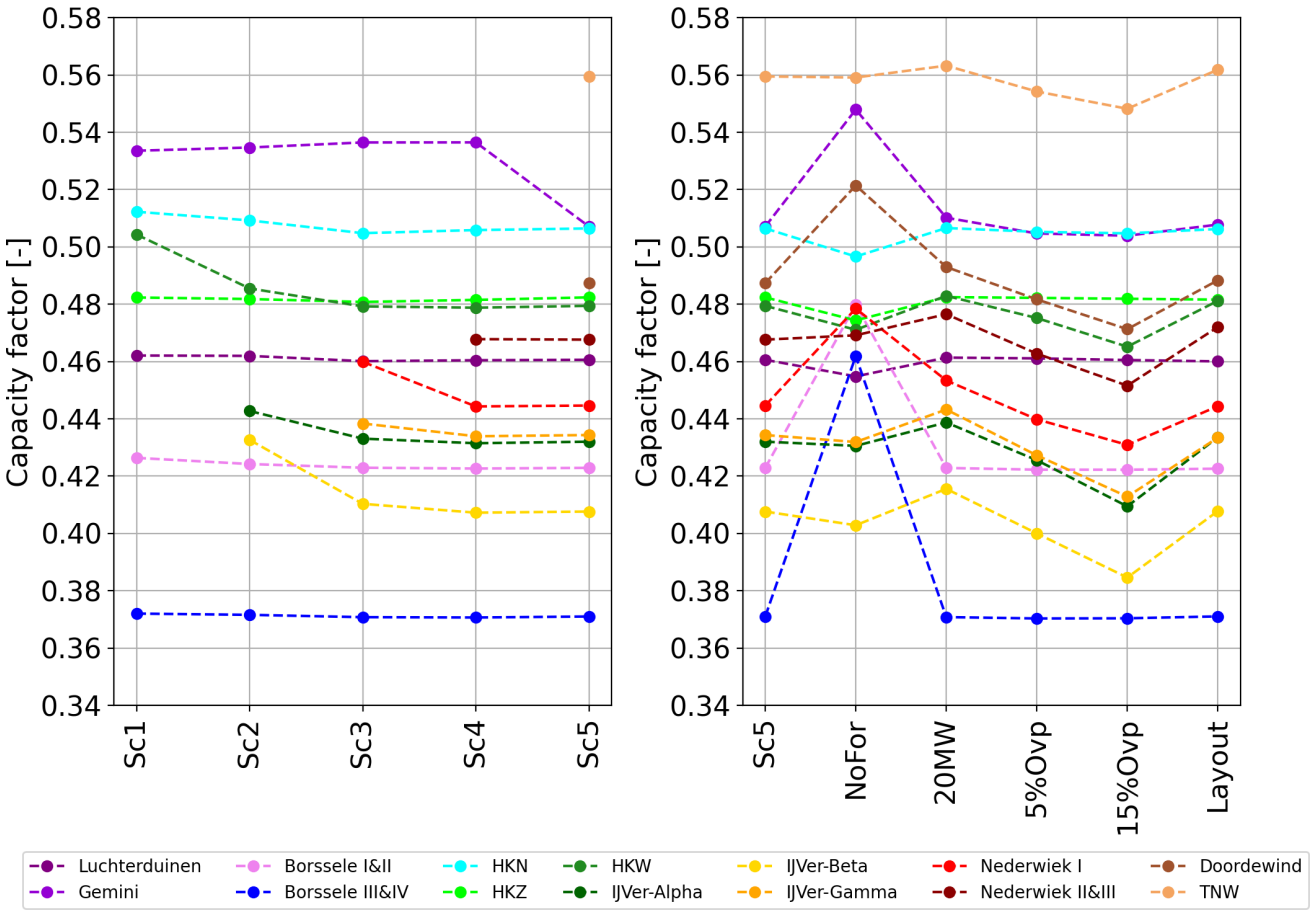

Figure 3.8. Capacity factor per scenario for each wind farm. Underlying data are presented in Table B.3. The left panel presents data for the incremental buildout scenarios, the right panel for the sensitivity scenarios.

Optimizing the layouts has a small impact on the production. For some wind farms the selected layout leads to a small reduction of the production. For all wind farms, the difference with *Sc5* (the reference scenario) is less than 1%. In the present study, a simplified optimization routine has been applied (e.g. effects of wind farm wakes were not taken into account). With more sophisticated optimization algorithms larger effects could be obtained.

The *Gross* scenario provides gross production numbers per wind farm for each scenario (see Table B.4). Combining those with the actual ('waked') production numbers yields the total aerodynamic losses (i.e. the sum of all internal and external waken and blockage losses). Those are presented for each wind farm and scenario in Fig. 3.9 (corresponding numbers are given in Table B.5). Differences between wind farms are large. Relatively isolated wind farms like HKN, HKZ have losses in the order of 15%, while the denser and more clustered wind farms of IJmuiden Ver have losses of around 30%. Losses of this magnitude are higher than those reported by Baas et al. (2023) for a 4 GW wind farm in the North Sea. However, the results presented in their study are not long-term representative, applied wind farm configurations and turbine types were different, and a previous version of the LES model using periodic boundary conditions was used. As discussed in Sect. 4.6, the present configuration of the model reproduces observed wind farm production numbers and internal wake losses reasonably well. The tendencies visible in Fig. 3.9 are consistent with the results discussed above (e.g. the increase in losses for HKW in

Wind farm	5% Overplanting Inst. Cap. $[MW/km^2]$	5% Overplanting No Capping $[TWh]$ (w.r.t Sc5)	5% Overplanting Capped $[TWh]$ (w.r.t Sc5)	15% Overplanting Inst. Cap. $[MW/km^2]$	15% Overplanting No Capping $[TWh]$ (w.r.t Sc5)	15% Overplanting Capped $[TWh]$ (w.r.t Sc5)
Luchterduinen	8.1	0.52 (0.1%)	0.52 (0.1%)	8.1	0.52 (-0.0%)	0.52 (-0.0%)
Gemini	8.9	2.65 (-0.5%)	2.65 (-0.5%)	8.9	2.65 (-0.6%)	2.65 (-0.6%)
Borssele I&II	5.9	2.78 (-0.1%)	2.78 (-0.1%)	5.9	2.78 (-0.2%)	2.78 (-0.2%)
Borssele III&IV	5.1	2.44 (-0.2%)	2.44 (-0.2%)	5.1	2.44 (-0.2%)	2.44 (-0.2%)
HKN	6.0	3.36 (-0.2%)	3.36 (-0.2%)	6.0	3.36 (-0.3%)	3.36 (-0.3%)
HKZ	5.9	6.46 (-0.0%)	6.46 (-0.0%)	5.9	6.45 (-0.1%)	6.45 (-0.1%)
HKW	8.4	6.56 (4.1%)	6.40 (1.6%)	9.1	7.03 (11.6%)	6.54 (3.8%)
IJVer-Alpha	11.2	7.83 (2.9%)	7.68 (1.0%)	12.3	8.29 (8.9%)	7.77 (2.2%)
IJVer-Beta	10.7	7.36 (2.5%)	7.21 (0.4%)	11.7	7.78 (8.4%)	7.27 (1.3%)
IJVer-Gamma	9.4	7.86 (2.8%)	7.70 (0.7%)	10.3	8.35 (9.2%)	7.82 (2.2%)
Nederwiek I	7.7	8.09 (3.3%)	7.93 (1.2%)	8.5	8.72 (11.4%)	8.12 (3.7%)
Nederwiek II&III	6.2	17.03 (3.8%)	16.63 (1.4%)	6.8	18.22 (11.0%)	16.96 (3.4%)
Doordewind	10.5	8.86 (3.3%)	8.67 (1.0%)	11.5	9.54 (11.1%)	8.86 (3.3%)
TNW	9.7	4.08 (4.7%)	3.96 (1.5%)	10.6	4.39 (12.8%)	4.05 (4.0%)
Total	7.8	85.87 (2.6%)	84.38 (0.84%)	8.4	90.52 (8.2%)	85.60 (2.3%)

Table 3.2. AEP numbers per wind farm for the 5 and 15% overplanting scenarios in TWh. Besides the values without capping, values for which production is capped to the original rated production of the wind farm are given. Values in brackets indicate the difference with $Sc5$ (in %).

$Sc2$ compared to $Sc1$, the reduced losses for the Borssele wind farms for the $NoFor$ scenario).

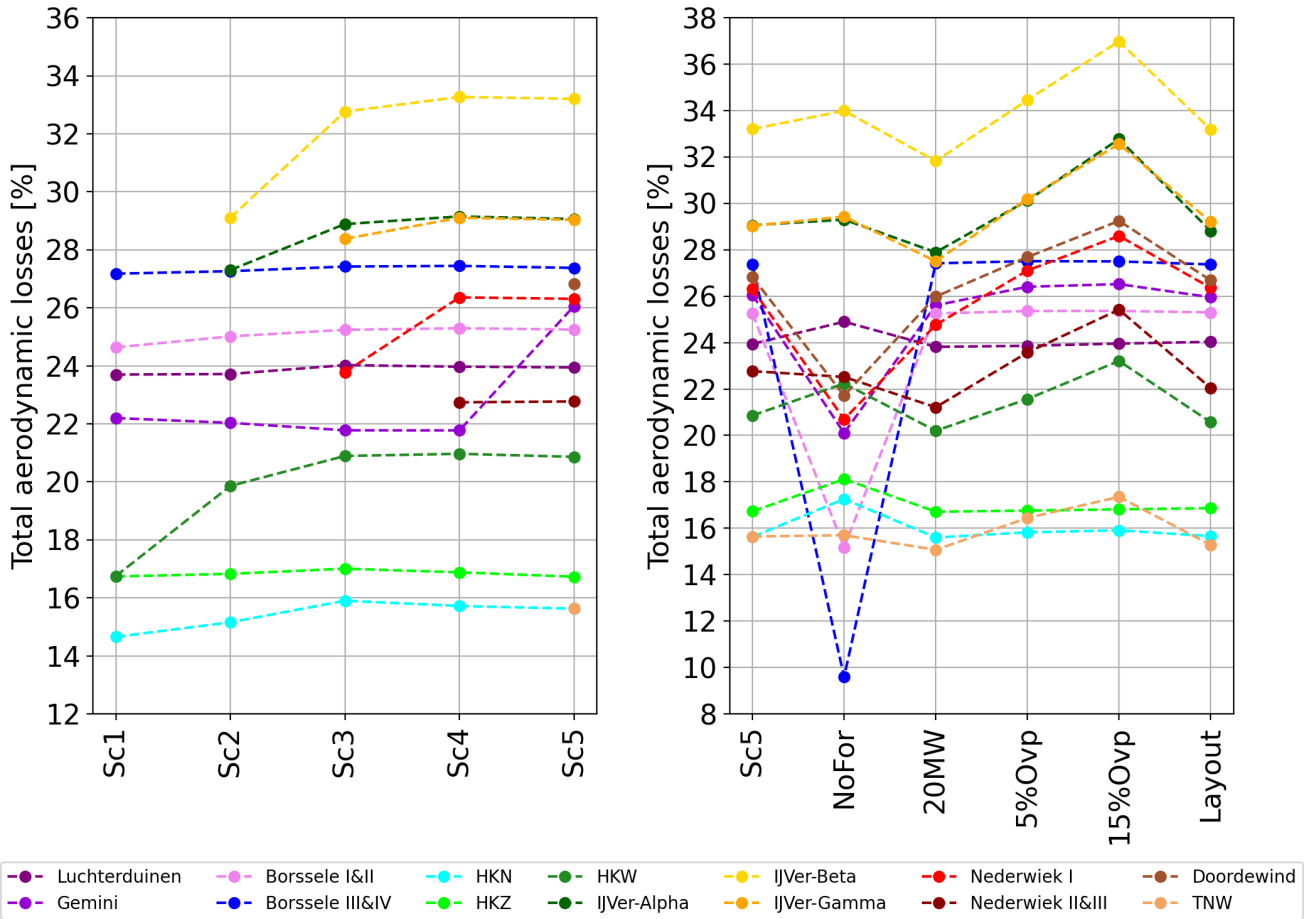

Figure 3.9. Total aerodynamic losses (in %) per scenario for each wind farm. Underlying data are presented in Table B.5. The left panel presents data for the incremental buildout scenarios, the right panel for the sensitivity scenarios.

3.4 Wake effects as a function of wind direction

Full buildout scenario versus the initial buildout scenario

In this Section wake effects are discussed as a function of wind direction. Only results from the two full-year simulations are compared (the full buildout scenario, $Sc5$, and the initial buildout scenario. $Sc1$). As the analysis presented here is based on time series, raw (non-corrected) model output is used.

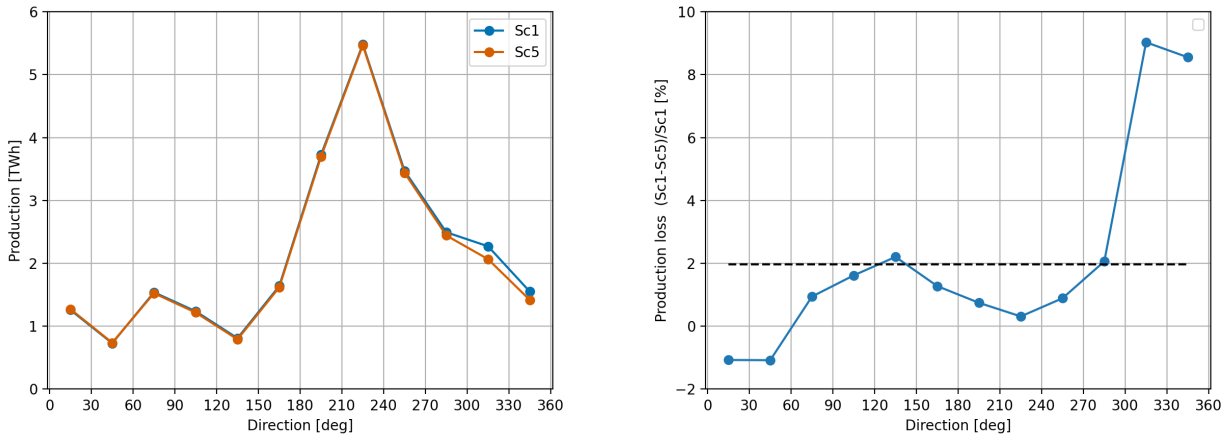

Figure 3.10. Left: Simulated production as a function of wind direction. Numbers for $Sc5$ only include the wind farms are present in $Sc1$. Right: Directional loss of production in $Sc5$ with respect to $Sc1$. The dashed line indicates the omnidirectional value.

As a starting point, Fig. 3.10 presents the production of $Sc1$ and $Sc5$ as a function of wind direction (30°bins). To facilitate a comparison between the two scenarios, numbers for $Sc5$ only include the wind farms that are present in $Sc1$. Consistent with the wind climate (Fig. 2.5.1) production is largest for southwesterly directions (50% of the production is realized for directions between 180°and 270°). Differences between the two scenarios are shown in the right-hand panel of Fig. 3.10. This reflects the direction-dependent wake effects of the full buildout of the 21 GW Roadmap ($Sc5$) on the wind farms of the initial buildout ($Sc1$). How this is distributed over the concerning wind farms is discussed in the next paragraph, but it is clear that for northwesterly directions the impact is largest with an overall decrease in production of 8 to 9%. For northeasterly direction the addition of more wind farms leads to a small (order 1%) increase in the production of the $Sc1$ wind farms.

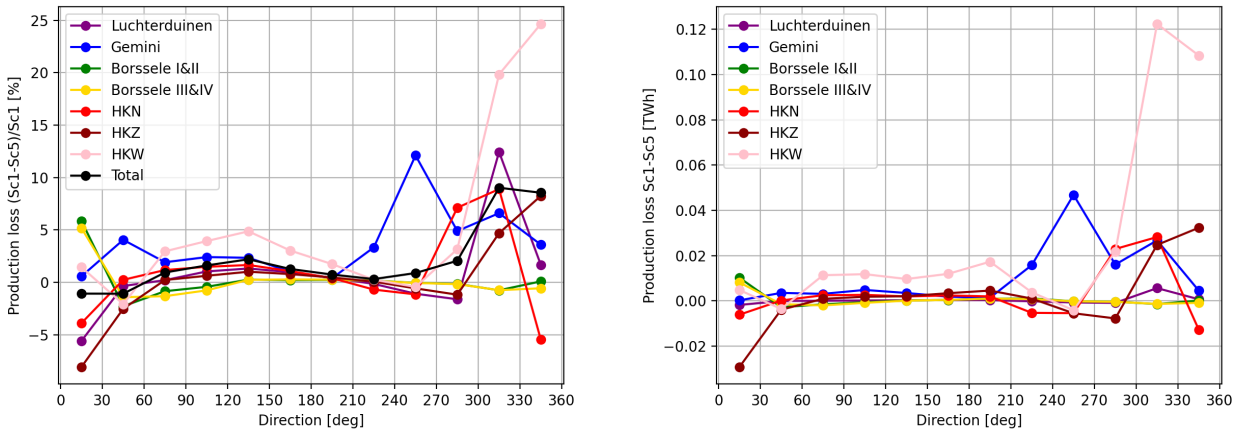

Figure 3.11. Directional loss of production in $Sc5$ with respect to $Sc1$ for individual wind farms in % (left) and as absolute values (right).

Figure 3.11 shows how the production losses are distributed over the individual wind farms. For northwesterly directions, the majority of losses is related to HKW. For this direction sector, production of this wind farm is 20 to 25% lower in $Sc5$ compared to $Sc1$. This significant reduction is related to wakes extending downstream from

the IJVer cluster, as an be seen in Fig. 3.2. For easterly directions the production of HKW is reduced by several percents as a result of the blockage effect induced by IJVer. Wake effects from IJVer also impact the production of HKN, HKZ, and Luchterduinen for northwesterly winds (mainly wind directions between 300°and 330°) and the Borssele wind farms for northeasterly (wind direction between 0°and 30°) winds. For the same direction sector, speed-up effects along the IJVer cluster have a beneficial effect on the production of HKZ, HKN, and Luchterduinen. The production of Gemini is impacted by the addition of TNW (12% for the sector between 240°and 270°) and Doordewind (6% for the sector between 300°and 330°). The production loss of Gemini between 30°and 60°is related to blockage effects from TNW.

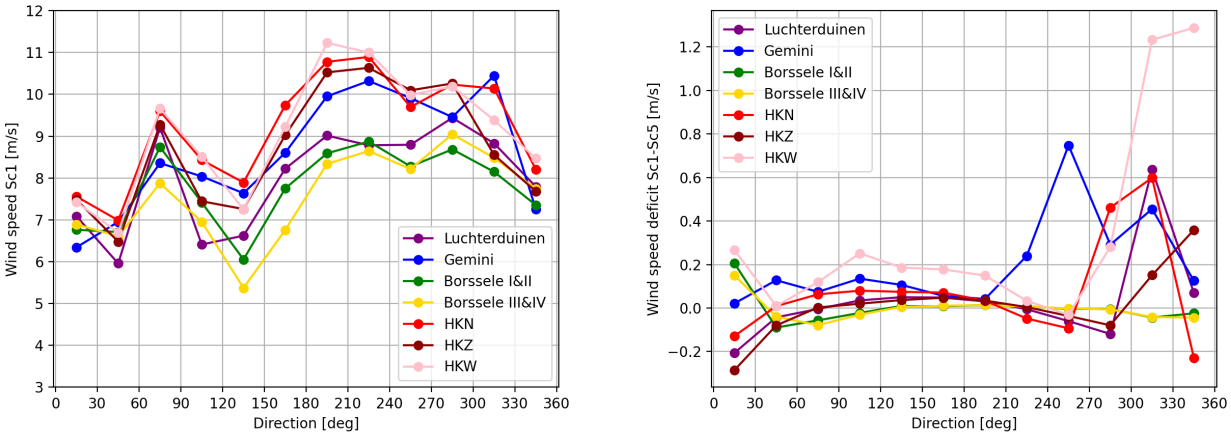

Figure 3.12. Mean wind speed $Sc1$ (left) and the difference ($Sc5$-$Sc1$) in mean wind speed (right) for the individual wind farms as function of wind direction.

To better understand the production losses discussed in the previous paragraph we inspect the corresponding wind speed deficits. To start with, the left-hand panel of Fig. 3.12 shows the mean wind speed per wind farm as modeled in $Sc1$ as a function of wind direction. Values mostly are in the range where small differences have direct impact on the production (steep part of the power curve). The right-hand panel of Fig. 3.12 shows the difference in simulated wind speed between $Sc1$ and $Sc5$ as a function of wind direction. This velocity deficit can be related to the production losses presented in Fig. 3.11. For instance, the 25% decrease in production for HKW in the 330°to 360°sector corresponds to a mean wind speed deficit of 1.24 m/s, with the mean wind speed in $Sc1$ being 8.5 m/s. Patterns in the production deficit closely match the pattern in the wind speed deficit.

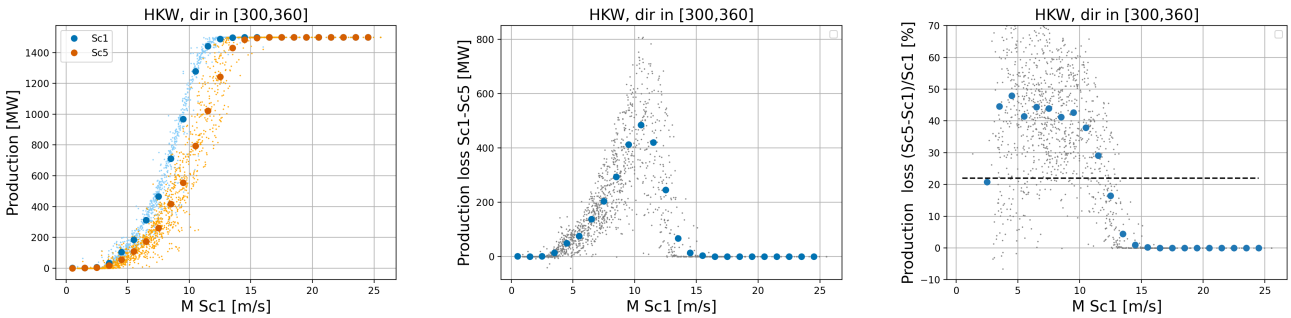

Figure 3.13. Left: Simulated production of HKW of $Sc1$ and $Sc5$ for wind directions between 300°and 360°as function of the wind farm mean wind speed. Middle: corresponding production differences $Sc1$ - $Sc5$ in MW. Right: Production differences relative to the $Sc1$ production (dashed horizontal line indicates the mean value). Large markers indicate mean values for 1-m/s wind speed bins, small markers represent individual 1 h time records.

As shown above, when considering the differences between $Sc5$ and $Sc1$ the largest wake effects are found for HKW, in particular for wind directions between 300°and 360°. Here, as an illustration, we explore these specific situations into more detail (this 60°direction sector includes 16% of the data points). For the two scenarios, Fig. 3.13 shows the simulated production of HKW as a function of the mean wind wind farm wind speed from $Sc1$ (left panel). For a given $Sc1$ wind speed, the production of $Sc5$ is lower than for $Sc1$ as a result of wake effects from the upstream wind farms. The middle panel of Fig. 3.13 shows the difference between the two scenario in an absolute

sense (in MW). These production losses due to wake effects from added wind farms occur mainly for a narrow wind speed range of 7 to 13 m/s. For lower wind speed, production is low anyway, while for higher wind speeds the wind farm operates at rated power despite the presence of a large upstream wind farm cluster. Corresponding relative losses are given in the right-hand panel of Fig. 3.13. For above-rated conditions the additional losses are zero. For lower wind speeds they are rather constant with a value of roughly 40%. In line with Fig. 3.11, the resulting overall additional losses of $Sc5$ compared to $Sc1$ amount to 21.9% for the considered 60°direction sector.

Leaving out the non-Dutch wind farms

As discussed in Sect. 3.3, the simulation results indicate that the production of HKN, HKZ, HKW, and Luchterduinen *decreases* when all non-Dutch wind farms are left out. Also for the wind farms of the IJVer cluster this is the case, which is remarkable given the relatively close proximity of the UK wind farms. Here, we provide more detailed results to better understand this specific result. The wind farm of IJver-Alpha is taken as an example.

Figure 3.14 shows the difference in wind speed between $NoFor$ and $Sc5$ for IJVer-Alpha as a function of wind direction. As expected, for westerly winds leaving out the non-Dutch (UK) wind farms leads to an increase in wind speed compared to $Sc5$. For (north)easterly direction, however, leaving out the non-Dutch wind farms leads to reduced wind speeds compared to $Sc5$. Overall, the wind speed in IJVer-Alpha is slightly reduced in the $NoFor$ scenario compared to $Sc5$ consistent with the reduction in power production as seen in Fig. 3.7.

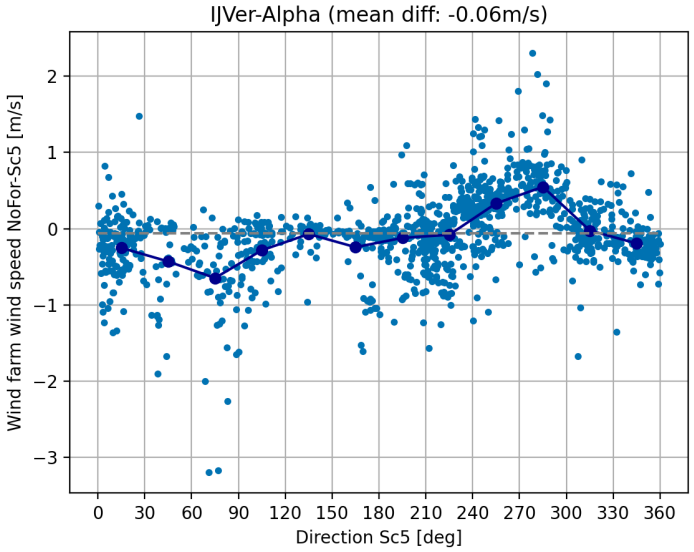

Figure 3.14. Wind speed difference between $NoFor$ and $Sc5$ as a function of wind direction for IJVer-Alpha (average values over all turbines of the wind farm). Data points indicate individual hourly time records. The solid blue line indicates the 30-degree mean values, the grey dashed line the omni-directional mean value.

Figure 3.15 shows the mean 150 m wind speed for the $NoFor$ and $Sc5$ for easterly directions, as well as the difference between the two scenarios. In particular the extensive cluster of German wind farms in the north has a significant impact on the flow with local wind speed differences of up to 5 m/s. For these easterly winds, leaving out all German wind farms leads to a reduction of the wind speed over the Southern North Sea. In other words, the simulation results suggest that including the German wind farm cluster leads to an increase in wind speed in large parts of the Dutch North Sea. This is a large-scale manifestation of the global blockage effect: the wind farm cluster acts like a huge obstacle in the flow with accelerations occurring along the sides. An assessment of the magnitude of this effect as present in the model simulations is not straightforward as an installed capacity of 30 to 35 GW of wind energy on a limited surface area as anticipated in the German Bight is unprecedented.

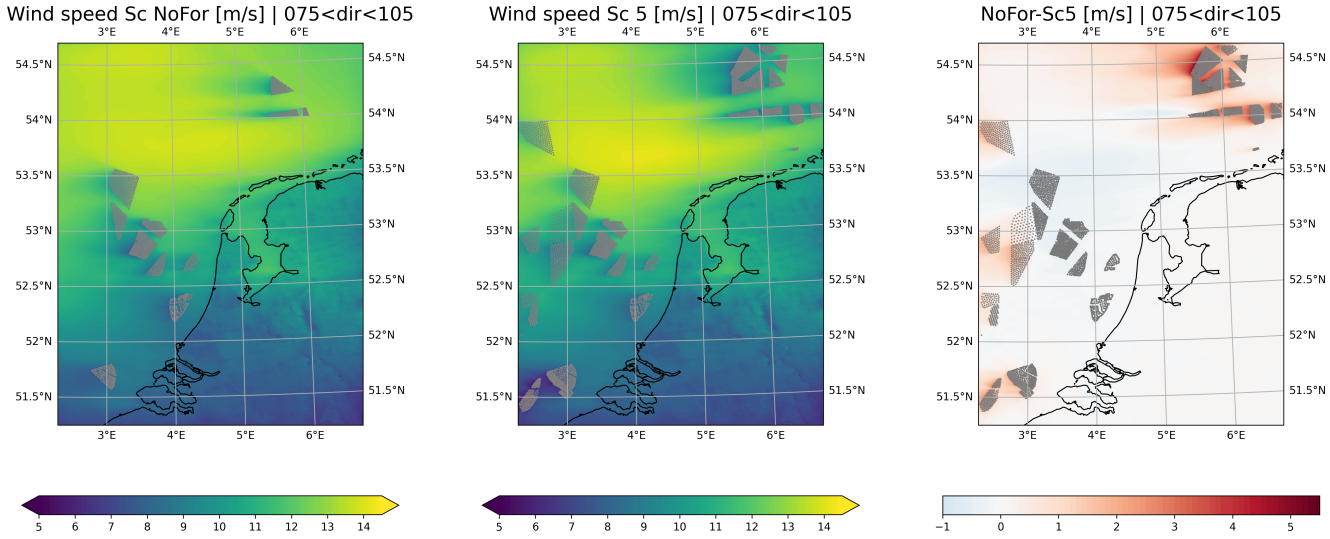

Figure 3.15. Mean wind speed at 150 m for *NoFor* and *Sc*5, as well as the difference between the two scenarios. Only cases with a mean wind direction between 75 and 105 degrees are included.

3.5 Summary of main findings for each wind farm

In this Section, the characteristics for each wind farm are summarized. Specific features are illustrated with directional composite maps of velocity difference. Each of those figures covers a limited area of 100 by 100 km centered on the wind farm of interest. Without pretending to be complete, the overview presented here provides insights in how differences in power production are related to differences in the wind field.

Luchterduinen

The wind farm is surrounded by HKN and relatively far away from planned 21 GW Roadmap wind farms and from wind farms of neighboring countries. Production differences between the scenarios are small and generally within 1%. For NW directions production is reduced due to the addition of the IJVer wind farms in *Sc*2 and *Sc*3 (Fig. 3.16, see also Fig. 3.11).

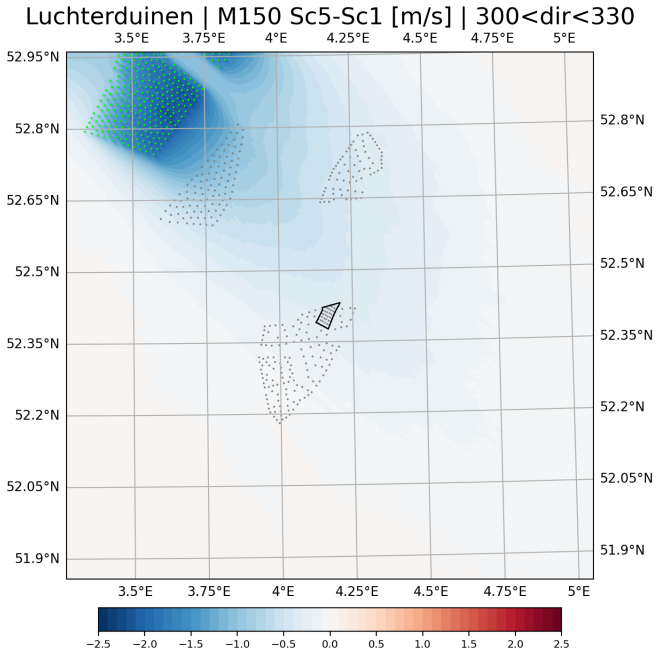

Figure 3.16. Wind speed difference *Sc*5-*Sc*1 for NW directions for the Luchterduinen area. Turbines included in both scenarios are indicated in grey. Turbines included in *Sc*5 only are indicated in green.

Gemini

The major impact is seen in the step from $Sc5$ with the addition of TNW and Doordewind. The addition of TNW reduces the production for WSW directions by 12% (Fig. 3.11). For NW directions the Gemini area is impacted by wakes from Doordewind (Fig. 3.17). For NE directions the Gemini production is also reduced in $Sc5$. This is likely due to blockage effect of TNW. The sensitivity scenarios have little impact, except for the $NoFor$ scenario. In this scenario the impact of the bordering Borkum Riffgrund 3 wind farm is visible for easterly directions. For northerly directions wake effects downstream of the large cluster of German wind farms impacts the production.

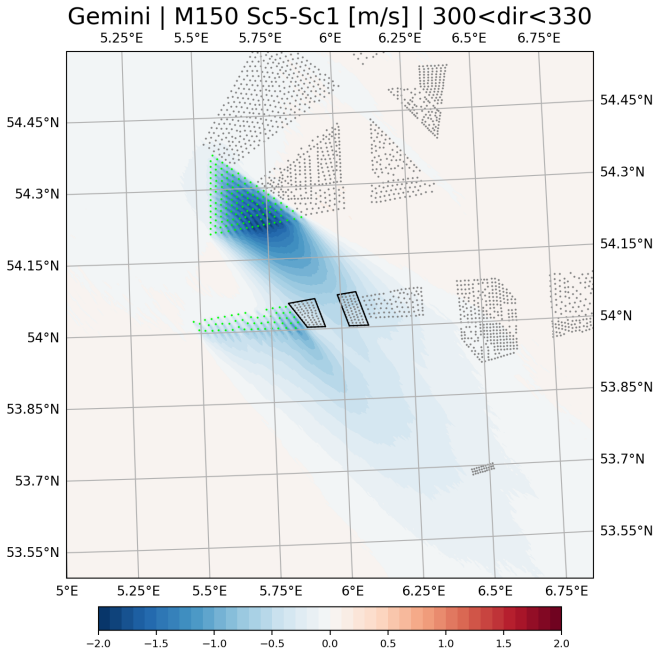

Figure 3.17. Wind speed difference $Sc5$-$Sc1$ for NW directions for the Gemini area. Turbines included in both scenarios are indicated in grey. Turbines included in $Sc5$ only are indicated in green.

Borssele I&II

The incremental buildout of the Roadmap leads to a small reduction in production due to wakes for northerly directions. Not surprisingly, leaving out the Belgian wind farms increases the wind speed and production considerably for almost a 180°wide sector (Fig. 3.18).

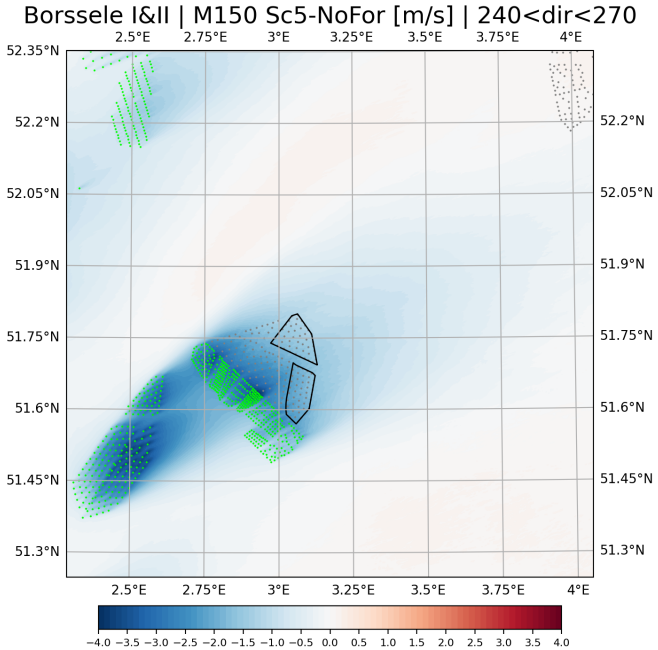

Figure 3.18. Wind speed difference $Sc5$-$NoFor$ for SW directions for the Borssele area. Turbines included in both scenarios are indicated in grey. Turbines included in $Sc5$ only are indicated in green.

Borssele III&IV

Patterns for Borssele III&IV are generally the same as for Borssele I&II. Only the impact of leaving out the wind farms of neighboring countries is even larger. For NNE directions the mean wake of the IJVer cluster is mostly recovered (Fig. 3.19). Impact on production will be more pronounced for specific conditions. The northeasterly section of Fig. 3.19 shows speed up effects along the sides of the IJVer cluster.

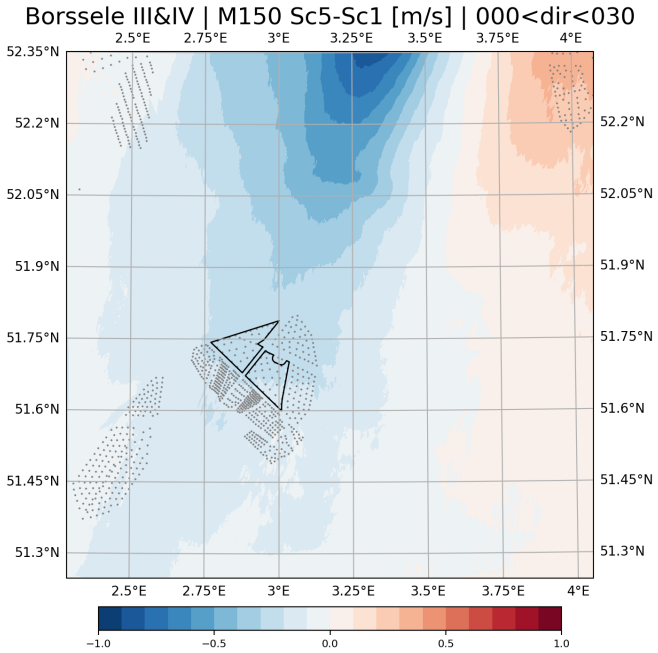

Figure 3.19. Wind speed difference $Sc5$-$Sc1$ for NNE directions for the Borssele area. Turbines included in both scenarios are indicated in grey. Turbines included in $Sc5$ only are indicated in green.

HKN

The impact of the roll-out of the 21 GW Roadmap is small, except for NW directions where production is reduced due to the buildout of the IJVer cluster. A comparison of $Sc1$ with free stream conditions for southerly winds shows reduced wind speed due to the upstream presence of HKZ (Fig. 3.20).

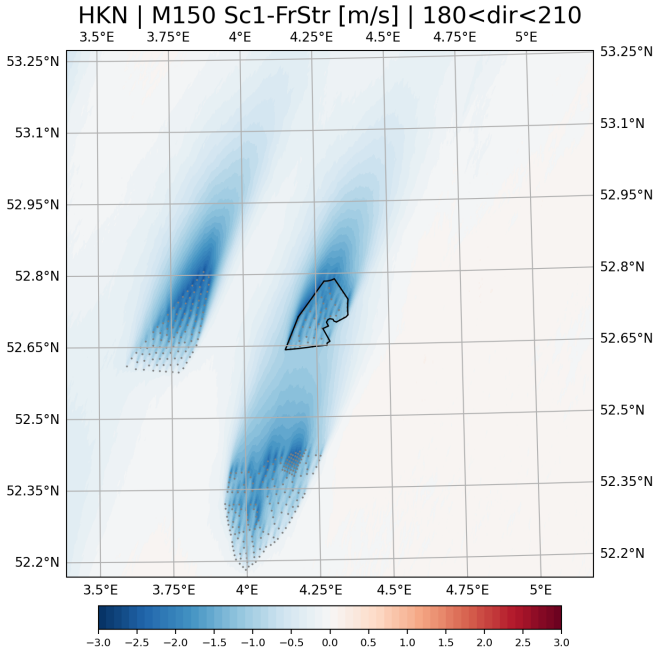

Figure 3.20. Wind speed difference between $Sc1$ and free-stream conditions for SSW directions for the HKN area. Turbines included in $Sc1$ are indicated in grey.

HKZ

The impact of the roll-out of the 21 GW Roadmap on HKZ is comparable to HKN. Here, the main impact of the subsequent addition of wind farms is mostly seen for NNW directions (between 330 and 360°). For NNE directions the production of HKZ is increased due to speed up effects along the sides of the IJVer cluster (Fig. 3.21). The same holds for HKN and Luchterduinen, see also Fig. 3.11.

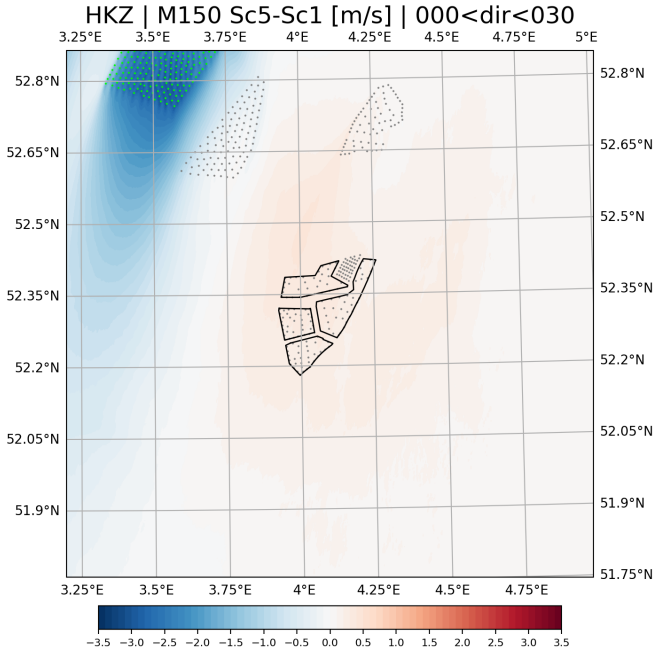

Figure 3.21. Wind speed difference $Sc5$-$Sc1$ for NNE directions for the HKZ area. Turbines included in both scenarios are indicated in grey. Turbines included in $Sc5$ only are indicated in green.

HKW

The addition of the IJVer cluster has a significant impact on the production of HKW. The omnidirectional production decrease is around 5% (Fig. 3.7). However, the production deficit occurs mainly for NW directions. For this sector, the deficit amount 20 to 25% (Fig. 3.11). Figure 3.22 shows that large differences exist over the wind farm: wake effects are strongest in the northern part, while, for the considered direction sector, they are negligible for the most southwesterly turbines. Along the southern edge of the IJVer cluster a significant acceleration of the flow is visible that, for the considered direction section, is just passing the southern tip of HKW.

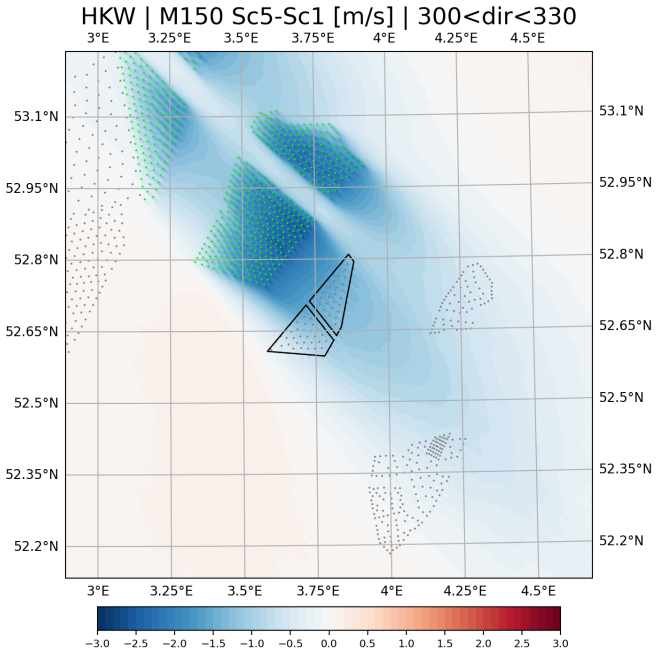

Figure 3.22. Wind speed difference $Sc5$-$Sc1$ for NW directions for the HKW area. Turbines included in both scenarios are indicated in grey. Turbines included in $Sc5$ only are indicated in green.

IJVer-Alpha

The addition of IJVer-Gamma and Nederwiek I (in $Sc3$) has a clear impact on the production of IJVer-Alpha. The same holds for the addition of Nederwiek II&III in $Sc4$. Compared to $Sc5$, wake effects in the $15\%Ovp$ scenario are stronger, as shown in Fig. 3.23 for WSW directions. This is also seen for other wind farms with overplanting like HKW and the Nederwiek wind farms.

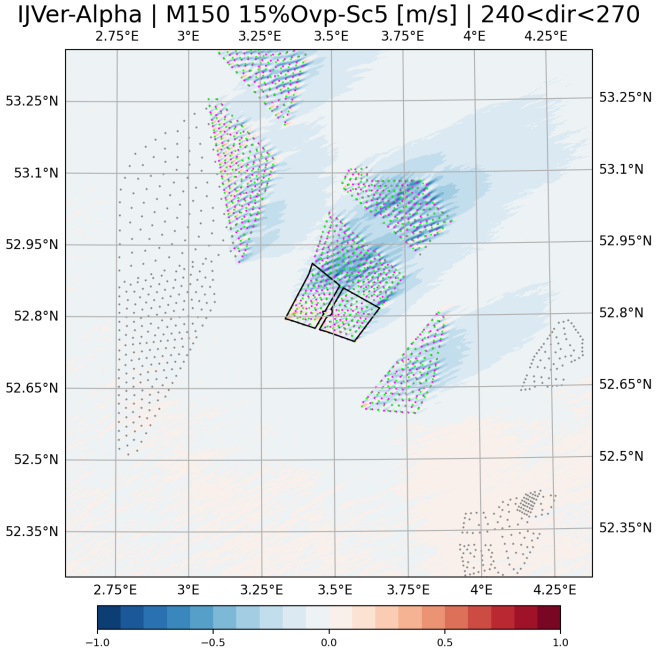

Figure 3.23. Wind speed difference $15\%Ovp$-$Sc5$ for WSW directions for the IJVer-Alpha area. Turbines included in both scenarios are indicated in grey. Turbines included in $Sc5$ / $15\%Ovp$ only are indicated in green / magenta.

IJVer-Beta

Patterns for IJVer-Beta are comparable to IJVer-Alpha. Generally, losses for IJVer-Beta are bit larger because this wind farm is bordered by upstream wind farms at two opposite sites (IJVer-Alpha in the southwest, IJVer-Gamma in the northeast). The strongest wake effects (with respect to free-stream conditions) of the 21 GW Roadmap occur in this region (Fig. 3.24).

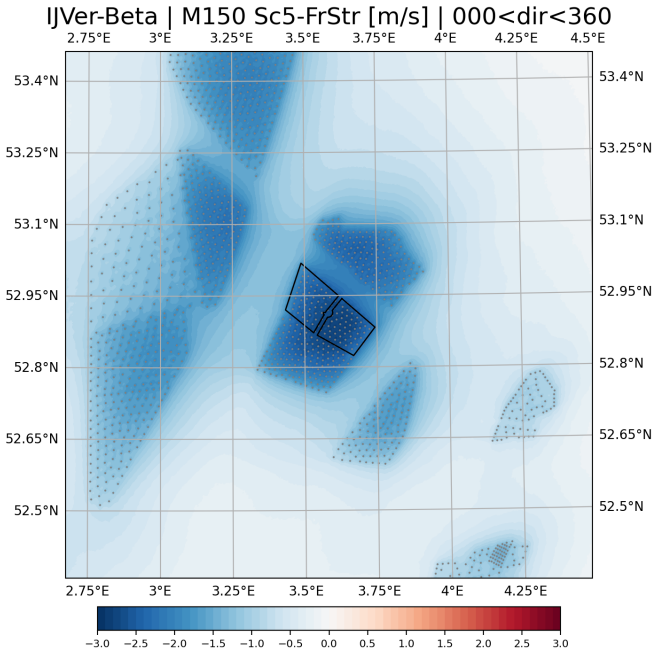

Figure 3.24. Wind speed difference between $Sc5$ and free-stream conditions (omnidirectional) for the IJVer-Beta area. Turbines included in $Sc5$ are indicated in grey.

IJVer-Gamma

The addition of Nederwiek II&III leads to reduced production for NW directions. Interestingly, for NNE directions flow acceleration along the edges of Nederwiek II&III has a positive impact on the IJVer-Gamma production. For SW direction the $20MW$ scenario shows weaker downstream wakes then in the default $Sc5$. This phenomenon is also present for the wind farms surrounding IJVer-Gamma (Fig. 3.25).

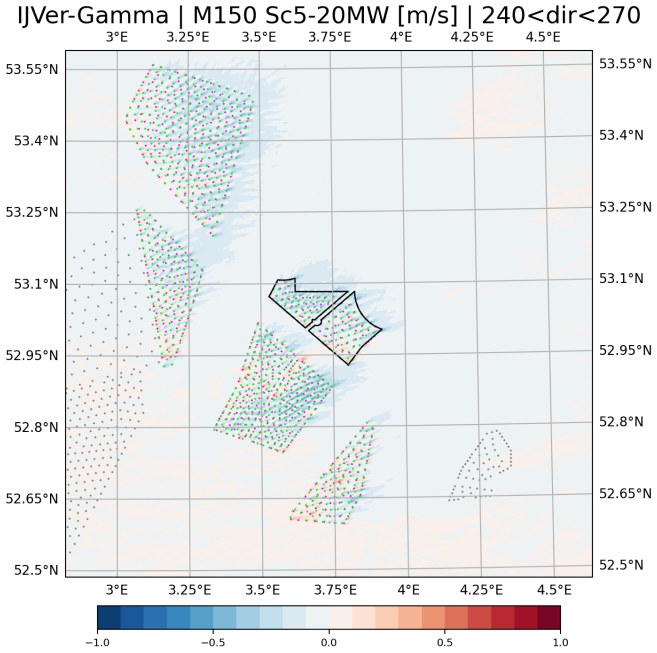

Figure 3.25. Wind speed difference between $20MW$ and $Sc5$ for SW directions for the IJVer-Gamma area. Turbines included in both scenarios are indicated in grey. Turbines included in $Sc5$ / $20MW$ only are indicated in green / magenta.

Nederwiek I

Nederwiek I is included in the same Scenario ($Sc3$) as IJVer-Gamma. For NNE direction the production is almost halved after the addition of Nederwiek II&III in $Sc4$. As a result of the low frequency of occurrence of these northerly winds, and the relatively low wind speeds, the impact on the wind farm's total production is only a few percent. More

important for the production of Nederwiek I are the neighboring UK wind farms. For the unfavorable SW direction these have a negative impact (Fig. 3.26).

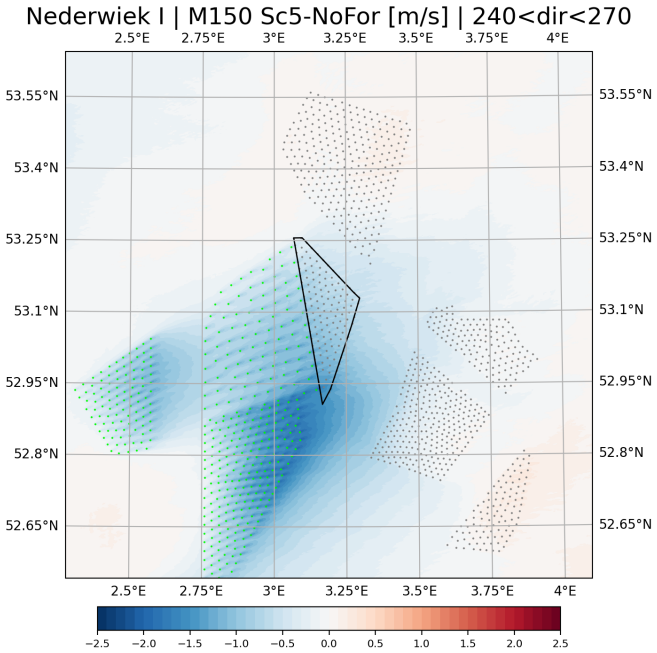

Figure 3.26. Wind speed difference between *Sc*5 and *NoFor* for SW directions for the Nederwiek I area. Turbines included in both scenarios are indicated in grey. Turbines included in *Sc*5 only are indicated in green.

Nederwiek II&III

Nederwiek II&III is located just northwest of the IJVer cluster. As a result, the wind farm's efficiency drops considerably for southeasterly flow compared to more easterly directions. Apart from production losses due to wakes from the Norfolk cluster, also the Hornsea 3 wind farm has an impact. For WSW direction the boundary-grid layout reduces the internal wake effects compared to the default maximum repulsion layout (Fig. 3.27).

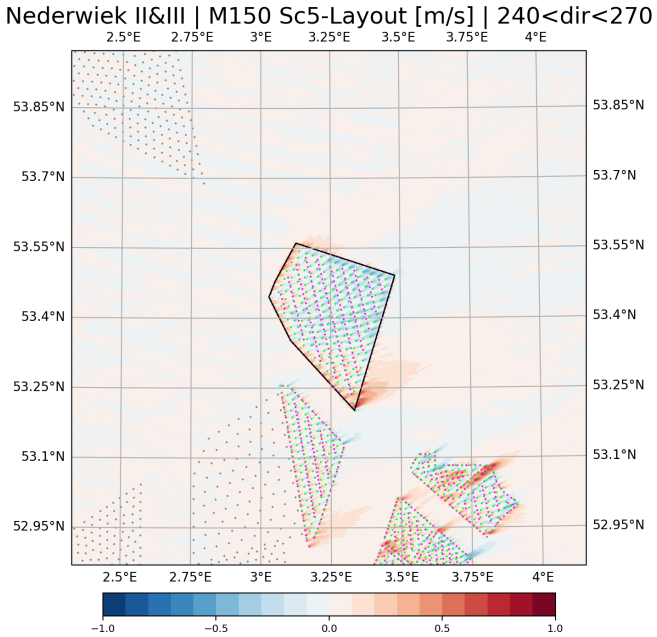

Figure 3.27. Wind speed difference between *Layout* and *Sc*5 for WSW directions for the Nederwiek II&III area. Turbines included in both scenarios are indicated in grey. Turbines included in *Sc*5 / *Layout* only are indicated in green / magenta.

Doordewind

Doordewind is directly neighboring a large German wind farm cluster. For NNE directions its production is

substantially reduced (Fig. 3.28). However, for the predominant SW sector, which also has the strongest winds, Doordewind faces free stream conditions. This makes that the overall losses due to wind farms of neighboring countries are much lower than for the Borssele cluster, where the situation is reversed.

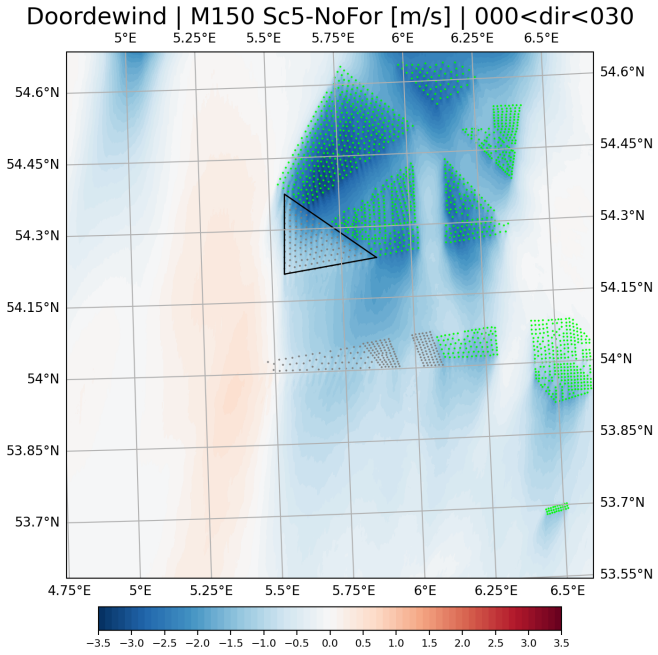

Figure 3.28. Wind speed difference between *Sc*5 and *NoFor* for NNE directions for the Doordewind area. Turbines included in both scenarios are indicated in grey. Turbines included in *Sc*5 only are indicated in green.

TNW

TNW is one of the most efficient wind farms of the 21 GW Roadmap. It faces free stream condition for the dominant wind direction and it has a favorable elongated west-east orientation. Wake effects due to wind farms of neighboring countries are relatively small, as well. For WSW directions the wake of TNW extends over the neighboring Gemini wind farm (Fig. 3.29).

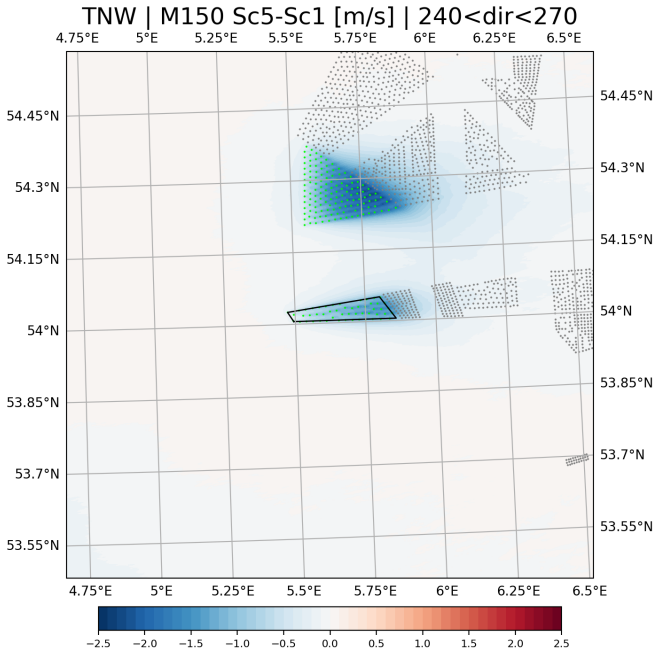

Figure 3.29. Wind speed difference between *Sc*5 and *NoFor* for WSW directions for the TNW area. Turbines included in both scenarios are indicated in grey. Turbines included in *Sc*5 only are indicated in green.

3.6 21 GW Roadmap wake study GIS Viewer

To facilitate the accessibility of the simulation results, a web-based GIS Viewer has been developed, which can be found at https://21gw.whiffle.cloud. The GIS Viewer allows for a straightforward and visual inspection of the capacity factors of the different scenarios per wind farm. As an illustration, Fig. 3.30 shows a screenshot of the Viewer, displaying an overview of simulated capacity factors of the 21 GW Roadmap wind farms in $Sc5$, the full buildout scenario. In a similar way, data from all scenarios can be inspected by selected the desired scenario from the list.

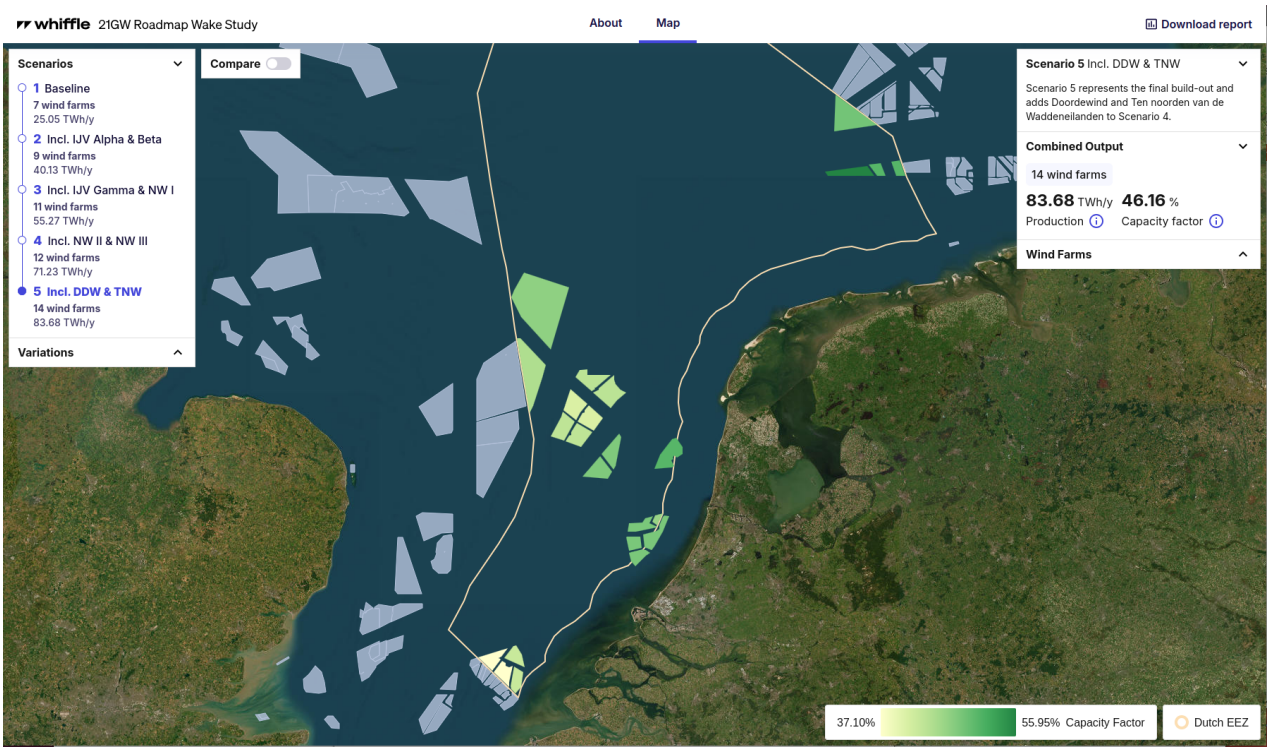

Figure 3.30. Screenshot of the 21 GW Wake Study GIS Viewer, showing capacity factors the 21 GW Roadmap wind farms.

The Viewer allows for a comparison between different scenarios. In that case the coloring of the wind farms indicates the difference in the capacity factors for each wind farm for the two selected scenarios.

Clicking on a wind farm provides additional information as the installed capacity and the applied turbine type. Also the production and capacity factor numbers are shown.

The numbers presented in the Viewer are corresponding one-to-one with the data presented in this report, in particular in Sect. 3.2 and 3.3.

3.7 Comparison with other modeling studies

To put our results into perspective, a comparison is made with capacity factors obtained by other modeling studies that explore the impact of a large-scale roll out of offshore wind energy on the production numbers.

Studying cluster-scale wake losses over the North Sea, Borgers et al. (2024) conclude that the integrated capacity factor strongly depends on the installed capacity density, varying from 51.2% for a 3.5 MW/km^2 capacity density to 38.2% for a 10 MW/km^2 capacity density.

A modeling study on the potential of offshore wind in the German North Sea reports capacity factors ranging from 42% for a capacity density of 5 MW/km^2 to 35% for 10 MW/km^2 (Energiewende, Agora Verkehrswende, Technical University of Denmark and Max-Planck-Institute for Biogeochemistry, 2020).

Assessing the power production of projected wind farm cluster off the US east coast, Pryor et al. (2021) find capacity factors ranging from 45% (at 4 MW/km^2) to 52% (at 2 MW/km^2). For the same region, a separate modeling study by Pryor and Barthelmie (2024) (installed capacity of 37 GW at 4 MW/km^2) reports capacity factors of 42 and 53% depending on the applied wind farm parameterization (either based on Fitch et al. (2012) or Volker et al. (2015)).

Several other modeling studies reporting significant cluster wake and blockage effects over the North Sea (Akhtar et al., 2021; Baas, 2024; Cañadillas et al., 2022; Porchetta et al., 2024; Schneemann et al., 2020).

Although numbers from different studies are not one-to-one comparable due to differences in methodology and wind farm scenarios, the aggregated capacity factor of 46% reported in the present study (with an average installed capacity of 7.5 MW/km^2) is in line with values reported in literature.

4

Corrections and error margin estimation

Several corrections have been applied to the raw model output to account for biases, sampling errors and long-term representativeness. Also, the error margin is assessed. The following corrections / error sources are discussed:

- Bias correction method (Sect. 4.1)
- Uncertainty in the model bias (Sect. 4.2)
- Sampling error in ambient conditions of the 50 representative days with respect to the full year (Sect. 4.3)
- Sampling error in the wake effects of the 50 representative days with respect to the full year (Sect. 4.4)
- Wind farm specific long-term correction (Sect. 4.5)
- Error margin in the wake modeling (Sect. 4.6)

The error margins of the different error sources are expressed as standard deviations, which are combined in Sect. 4.7 (error propagation) to arrive at an overall error margin for the simulated production numbers. Formally, the concept of standard deviations implies an assumption of Gaussianity. As for several error sources the number of samples is limited, this assumption may not be always satisfied. But even then, the present method of combining uncertainties provides a sensible weighing of the different error sources.

The error margins as discussed here apply to the *simulated production numbers*. Production numbers that will be actually realized when the 21 GW Roadmap has been build out are subject to additional uncertainties that are beyond the scope of the present modeling study. These include, for instance, uncertainties in the realization of the planned wind farms, including their exact locations and shapes, the division into separate sites, the layouts, and the turbine types.

According to Sterl et al. (2015) "global warming will not change the wind climate over the Netherlands and the North Sea beyond the large range of natural climate variability that has been experienced in the past". Cheneka et al. (2023) find no significant evidence that climate change will change the wind power capacity factor over the North Sea. Uncertainties in the impact of climate change are therefore ignored in the present study and not part of the error margin estimation.

4.1 Bias correction

A separate model validation study, using the exact similar model settings and simulation domain indicated that a persistent bias exists of around 4% at 150 m height (the hub height of the 15 MW reference wind turbine). This has been documented in a validation report, where model data has been extensively compared to a large collection of in-situ and LiDAR wind measurements (Whiffle, 2024). It was concluded that for the scenario simulations of the 21 GW Roadmap a bias correction would be required.

Based on availability of the LiDAR observations, the simulation period for the validation simulation was 1 April 2023 to 1 April 2024. For the scenario simulations, the period of 17 March 2018 to 17 March 2019 was selected because its long-term representativeness (Sect. 2.5.1).

This section describes the bias correction procedure for the simulated power production of the 21 GW Roadmap wake study scenario simulations as presented in the current report. The wind farm aggregated production numbers

of the scenario simulations are corrected based on the error (i.e. bias) statistics of the 1-year validation simulation. The validation of this assumption and the associated uncertainty for the final production numbers is discussed in Sect. 4.2. Here, the focus is on the bias correction procedure itself.

4.1.1 Annual mean energy production calculation

The LES runs provide wind farm specific time series of wind farm power production, P, and a wind farm wind speed, M, to be defined later. Wind farm power and wind farm wind speed have their probability densities, $f_P(P)$ and $f_M(M)$. The mean power production is the integral of $f_P(P)$ weighted by it's values,

$$\overline{P} = \int f_P(P) P dP. \tag{4.1}$$

Also, a so-called joint probability distribution, $f_{P,M}(P,M)$, can be obtained from the simulated time series of power and wind speed. It describes the frequency of occurrence of *combinations* of power and wind speed.

By definition, the joint probability distribution, $f_{P,M}(P,M)$, can be written as the product of the conditional probability, $f_{P|M}(P|M)$, and the wind speed distribution, $f_M(M)$:

$$f_{P,M}(P,M) = f_{P|M}(P|M) f_M(M). \tag{4.2}$$

The conditional probability describes the distribution of power production *given a certain wind farm wind speed*. When integrating over M, Eq. 4.2 reduces to the probability distribution of P:

$$\int f_{P,M}(P,M) dM = \int f_{P|M}(P|M) f_M(M) dM = f_P(P). \tag{4.3}$$

So, if the conditional probability distribution of power and wind are known together with the probability distribution of wind, the probability distribution of power can be calculated. From this, the mean power production (hence AEP) can be easily calculated from Eq. 4.1. So far, no assumptions have been made. A similar methodology is followed by Postema et al. (2024).

The conditional probability, $f_{P|M}(P|M)$, can be interpreted as the relation between the simulated wind farm power and the wind farm wind speed, i.e. as the simulated wind farm power curve. If the underlying model timeseries is of sufficient length, this simulated wind farm power curve will include any wake effects and varying meteorological conditions in a representative way.

Bias corrected power numbers can be calculated by utilizing a bias corrected distribution of the wind farm wind speed. This is one of the essential assumptions of the present bias correction method.

If we denote the bias-corrected power production and wind farm wind speed distributions with a hat ($\hat{f}_P(P)$ and $\hat{f}_M(M)$), the estimate for the bias-corrected power production distribution takes the form:

$$\hat{f}_P(P) \approx \int f_{P|M}(P|M) \hat{f}_M(M) dM. \tag{4.4}$$

The (corrected) mean power value (typically in MW) can be translated to the annual energy production (AEP, typically in TWh) by multiplying with one year.

The integral quantities presented until here are computed as discrete sums. This means the quantities of interest need to be binned. For wind speed, bins of 0.5 m/s are chosen. As shown by Postema et al. (2024), this value is in the range where the method has low sensitivity to the exact bin-width. For power, the bin-width is set to the wind farm rated power divided by 60 (i.e. for the 600 MW Gemini wind farm the bin-width is 10 MW, for larger wind farms the bin-width in MW is also larger).

4.1.2 Bias statistics of the validation simulation

As a starting point for constructing a bias-corrected wind farm wind speed distribution for the scenario simulations, we take the observed and modeled data from 13 LiDARs on the North Sea from the validation simulation. The LiDARs were operated by RVO and TNO. As shown by Whiffle (2024), differences in model performance between these 13 LiDAR locations are relatively small. For the purpose of the present bias correction procedure we reduce the 13 datasets to one single dataset.

First, for each of the 13 locations, observed and modeled data are vertically interpolated to specified heights above the surface: 60, 80, 100, ..., 220, and 240 m. This 120 m height range centers on the hub height (150 m) of the 15 MW turbine used in the simulations. Figure 4.1 presents the difference of the thus obtained modeled and observed profiles for the 13 locations. Also the average bias profile is indicated. Also a scatterplot of the combined modeled versus observed wind speed for a height of 150 m is included. Red crosses indicate the quantile-quantile relation.

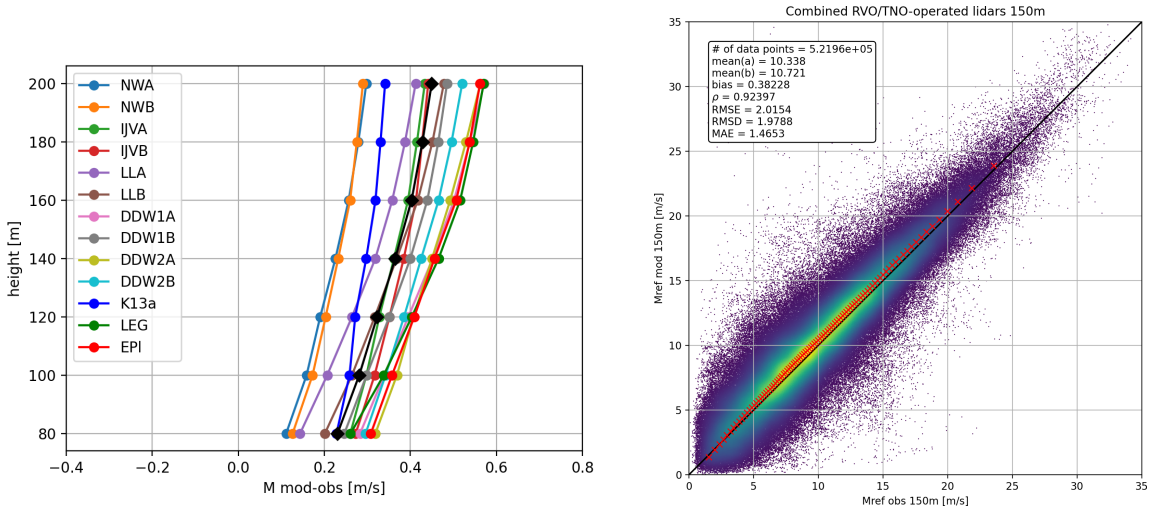

Figure 4.1. Bias profiles for the 13 combined RVO/TNO LiDAR locations with the mean bias profile in black (left). Modeled versus observed 150 m wind speed for the 13 LiDAR locations combined. Red crosses indicate the quantile-quantile relation.

For the bias correction, we use the combined time series of the 13 LiDAR locations interpolated to the wind farm hub height. We will refer to this as the 'reference wind speed', M_{ref}. The sensitivity to the applied definition of M_{ref} to the bias-corrected wind farm power will be discussed is Sect. 4.1.4.

The observed and modeled frequency distributions and cumulative frequency distributions of M_{ref} are given in Fig. 4.2.

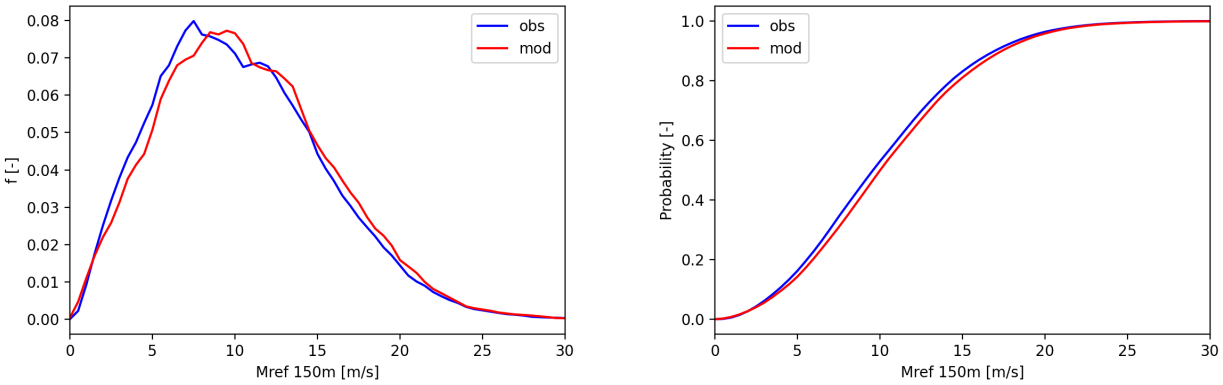

Figure 4.2. Observed and modeled frequency distributions (left) and cumulative frequency distributions of the 150 m M_{ref} (right).

4.1.3 Bias-correcting wind farm power

The present bias correction procedure assumes that the difference between the modeled and observed cumulative distribution functions of M_{ref} (Fig. 4.2) can be used to correct the wind farm wind speeds of the scenario simulations.

To correct the simulated wind farm wind speed distribution of Eq. 4.3 to the bias-corrected equivalent of 4.4, quantile mapping is applied (e.g. Holthuijzen et al. (2021)). Starting point is the time series of the wind farm wind speed of a scenario simulation. For each time step the following steps are performed:

- From the modeled cumulative frequency distribution of M_{ref} the percentile that corresponds to the wind farm wind speed is determined. For the wind farm wind speed, we take the 95^{th} percentile of the wind speed from all individual turbines of the wind farm. This approaches free-stream wind conditions.
- For the thus derived percentile, the wind speed corresponding to this percentile in the observed cumulative distribution of M_{ref} is determined. This wind speed is assumed to be the corrected equivalent of the wind farm wind speed.

Following this procedure for every time record transforms the time series of a wind farm wind speed to a bias corrected time series, where the bias correction is wind-speed dependent through the quantile mapping procedure. The distribution of this corrected time series can be used to determine the bias-corrected wind farm power following Eq. 4.4.

4.1.4 Sensitivity assessment

Next, we discuss the sensitivity of the bias correction method on the final production numbers to specific choices, in particular to the definitions of the reference wind speed and the wind farm wind speed.

By default, the wind farm wind wind speed is defined as the 95^{th} percentile of the wind speed from all individual turbines of the wind farm. As an alternative, we take the *mean* of the wind speed of all turbines.

For the reference wind speed, M_{ref}, we use the combined time series of the 13 LiDAR locations interpolated to the wind farm *hub height*. As an alternative, we consider the mean value of the modeled and observed wind speed profile. The result is a time series of modeled and observed data over the *height interval 60 - 240 m* (roughly representing the vertical footprint of a wind turbine) for each of the 13 locations.

Finally, as an alternative to the quantile mapping (which essentially applies a wind speed-dependent factor), the wind farm wind speed is corrected by a constant factor, namely the mean relative difference between modeled and observed M_{ref} (in the example of the Fig. 4.1 for 150 m height, this factor would be 10.338 / 10.721 = 0.964, a reduction of 3.6%).

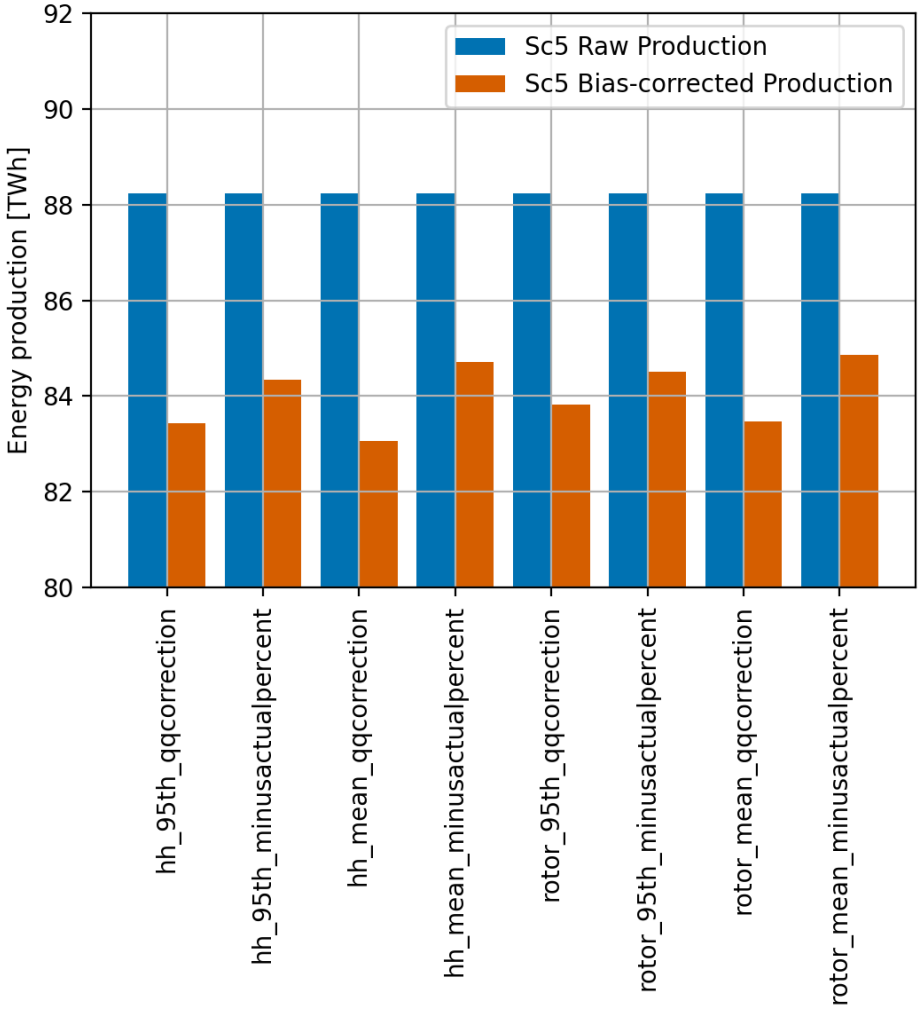

Figure 4.3. Sensitivity of the bias correction method to specific choices made in the process.

Combining the different choices listed above gives eight different ways of applying the bias correction (three times 2). Figure 4.3 shows how the different combinations affect the total energy production of $Sc5$. Depending on the specific choices, the correction on the total energy production varies between 4 and 6 %.

Over all 14 wind farms of the 21 GW Roadmap and all considered variations of the bias correction method the standard deviation on the energy production is 0.8%. In Sect. 4.7.2 this number is included in the estimation of the overall standard deviation of the simulated energy production.

When applying a constant correction factor, the correction tends to be slightly lower than when applying the quantile mapping method. This is, because the model bias (in a relative sense) is not constant over the range of occurring wind speeds, which is taken into account in the quantile mapping method.

For correction of the production numbers we select the quantile mapping method, with the wind farm wind speed defined as the 95^{th} percentile of the wind speed from all individual turbines, and with the reference wind speed, M_{ref} defined at the the wind farm *hub height* (corresponding to the label *hh_95th_qqcorrection* in Fig. 4.3).

Summary

A bias correction method for the scenario simulations is proposed. Corrections are applied per wind farm per scenario. Related to the bias correction method, a standard deviation on the energy production of 0.8% is assigned that will be included in the overall error margin estimation (Sect. 4.7.2).

4.2 Uncertainty in the model bias

While the previous section discussed the bias correction method, also the model bias of wind speed itself comes with an uncertainty. Here, we address this uncertainty in the modeled wind and translate this to an uncertainty in power production.

4.2.1 Site-to-site variation of the bias

The first source of uncertainty is derived from Fig. 4.1. It is taken as the variation of the model bias among the 13 LiDAR locations at a height of 150 m, which, expressed in a standard deviation, amounts to 0.9%.

4.2.2 Uncertainty in the observations

A second source of uncertainty in the model wind speed bias is the uncertainty in the observations. As explained in the previous section the applied bias-correction makes use of the combined signal of 13 LiDAR instruments. Thus we require an estimate of the uncertainty of this combined signal. Given the complexity of this procedure as a whole, we propose to adopt one typical value for the uncertainty of a single lidar system. Then, we estimate the uncertainty of the combined signal as

$$\sigma_{\bar{x}} = \frac{1}{\sqrt{N}}\sigma_x, \tag{4.5}$$

with σ_x indicating the uncertainty of a single LiDAR system, $\sigma_{\bar{x}}$ the uncertainty of the combined signal and N the number of LiDAR signals (in this case 13).

As a typical value for the uncertainty of a single offshore LiDAR system we take a standard deviation of 4%. Following Eq. 4.5, for a combined signal of 13 LiDARs this results in a standard deviation of 1.1%.

The adopted value of 4% for a single lidar is a conservative value following performance verification reports of several LiDARs. For instance, TNO (2019a,b,c) report uncertainties of 2.6-3.3%, 2.9-3.5%, and 2.7-3.2% for the TNO-operated LiDARs of Lichteiland Goeree, Europlatform, and, K13, respectively. Performance verification reports for the RVO-operated LiDARs can be found at `https://offshorewind.rvo.nl`.

4.2.3 Comparison of model bias between the scenario simulations and the validation simulation

The third source of uncertainty is related to the assumption that the bias statistics of the validation simulation can be utilized to correct the results of the scenario simulations. However, as mentioned before, these simulations cover different periods in time. To estimate the uncertainty related to the above assumption, model wind speed biases of the scenario simulation period have been compared to those of the validation simulation.

Therefore, a validation of the scenario simulation was performed with available observations. This validation effort is restricted to observational locations that were operational during both simulation periods. Figure 4.4 shows model biases of the scenario simulation period, specifically $Sc1$, versus those of the validation simulation. Biases for the two simulation periods are positively correlated. Note that absolute numbers may vary significantly due to 1) the sometimes challenging measuring conditions at oil and gas platforms (for instance, for these locations flow obstructions are typically larger than for regular ground-based weather stations) and 2) differences in measuring height (Whiffle, 2024).

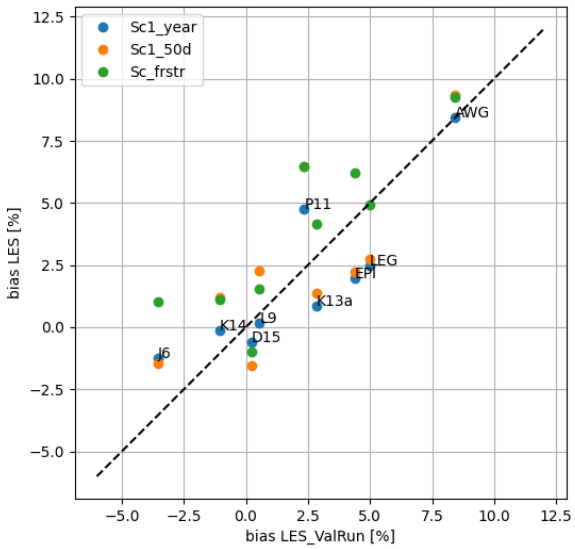

Figure 4.4. Wind speed bias (in %) of the simulation of Scenario 1 (17 March 2018 - 17 March 2019) versus the bias in the validation simulation (1 April 2023 - 1 April 2024) for different measurement locations. Data for the full-year scenario simulation are given (Sc1_year), as well as the selected set of 50 days (Sc1_50d), and the free-stream simulation (Sc_frstr, also 50 days). Measurement locations include the TNO LiDARs Lichteiland Goeree (LEG, 140 m), EuroPlatform (EPl, 141 m) and K13a (141 m), as well as the KNMI measuring stations J6 (76.5 m), K14 (75 m), D15 (62.5 m), L9 (88.3 m), P11 (51.37 m), and AWG (60 m). Values between brackets indicate measuring heights. See Whiffle (2024) for further details of the measurements.

A complicating factor in comparing biases between the validation simulation and the scenario simulation is that the configuration of the wind farms is different. Although $Sc1$ is closest to operational conditions, it contains HKW and a scenario of wind farms of neighboring countries anticipated in the year 2032. So in principle the model bias of $Sc1$ is expected to be lower than for the validation simulation, depending on the observation locations. For reference, the results of the free-stream scenario are added as well, although in this case no wind farms are included at all. Differences of model bias between the full-year and the selected 50 days are generally small.

With all complexities discussed above, Figure 4.4 suggests that the assumption that bias statistics of the validation simulation can be applied for correcting the scenario simulations is reasonable. To account for the uncertainty due to the difference in simulation period we apply a standard deviation calculated from the model biases shown in Fig. 4.4 (i.e. the standard deviation of the difference in bias between the two simulation period over 9 sites and 3 scenario simulation datasets), which is equal to 2.1%.

4.2.4 Aggregation and conversion to impact on power production

The above paragraphs discussed three sources of uncertainty in the model bias: site-to-site variations, uncertainty in the observations, and the uncertainty related to applying biases statistics from one period to another. It is assumed that these error sources are uncorrelated. In that case, the overall standard deviation of the modeled wind speed becomes 2.5%, where the components of the three source have been added according to

$$\sigma_t^2 = \sigma_1^2 + \sigma_2^2 + \sigma_3^2. \tag{4.6}$$

The obtained standard deviation in the modeled wind speed is converted to a standard deviation in modeled power production by applying the bias correction method outlined in Sect. 4.1, where the so-called wind farm wind speed was modified by a constant factor of +1 standard deviation and -1 standard deviation (i.e. the 2.5% as derived above). Averaged over all wind farms and scenarios, the resulting standard deviation in power production then becomes 3.2%. In Sect. 4.7.2 this number is included in the estimation of the overall error margin of the simulated energy production.

Summary

The uncertainty in the simulated wind speed is estimated and transformed into an uncertainty (expressed in a standard deviation) of overall power production of 2.9%. This includes site-to-site variations in the model bias and uncertainty associated with applying the bias statistics of the validation simulation period to those of the scenario

simulations. This will be included in the overall uncertainty estimation (Sect. 4.7.2). No corrections to the mean power have been applied here.

4.3 Sampling error in ambient conditions of the 50 representative days with respect to the full year

For two scenario of the 21 GW Roadmap a full-year simulation was performed. Simulations for the remaining scenarios were done for a carefully selected set of 50 representative days. Although Sect. 2.5.2 indicates that the selected set of 50 days resembles the general wind and power production characteristics over the target area very well, locally representation mismatches occur in the order of several percents in power.

Comparison of production number full-year simulations with 50 representative days

Figure 4.5 shows the ratio of simulated production of the full year over the selected 50 days for each wind farm. Although small differences exist between $Sc1$ and $Sc5$ (see Sect. 4.4) the variations in the year to 50 day mismatch is consistent between the two scenarios. This suggests that the deviations seen here are dominated by local differences in ambient wind conditions.

To correct for those, a wind farm dependent correction factor has been applied (similar for all scenarios) using the observed mismatch of $Sc5$ (i.e. the orange bars of Fig. 4.5).

The consistency of the full year to 50 day discrepancies between $Sc1$ and $Sc5$ is further highlighted in Fig. 4.6. It uses data from 100 preselected 50-day samples with low wind and power biases and a reasonable distribution of wind speed, direction and stability (see Sect. 2.5.2). For the 7 wind farms that are present in both considered scenarios this yields 700 data points. Clearly, when one scenario over or underestimates the production of a wind farm, the same will be the case for the other scenario. The spread of the data can be used as a proxy for the error margin in the correction from the 50-day data to the full year. Expressed in a standard deviation this becomes 0.5%.

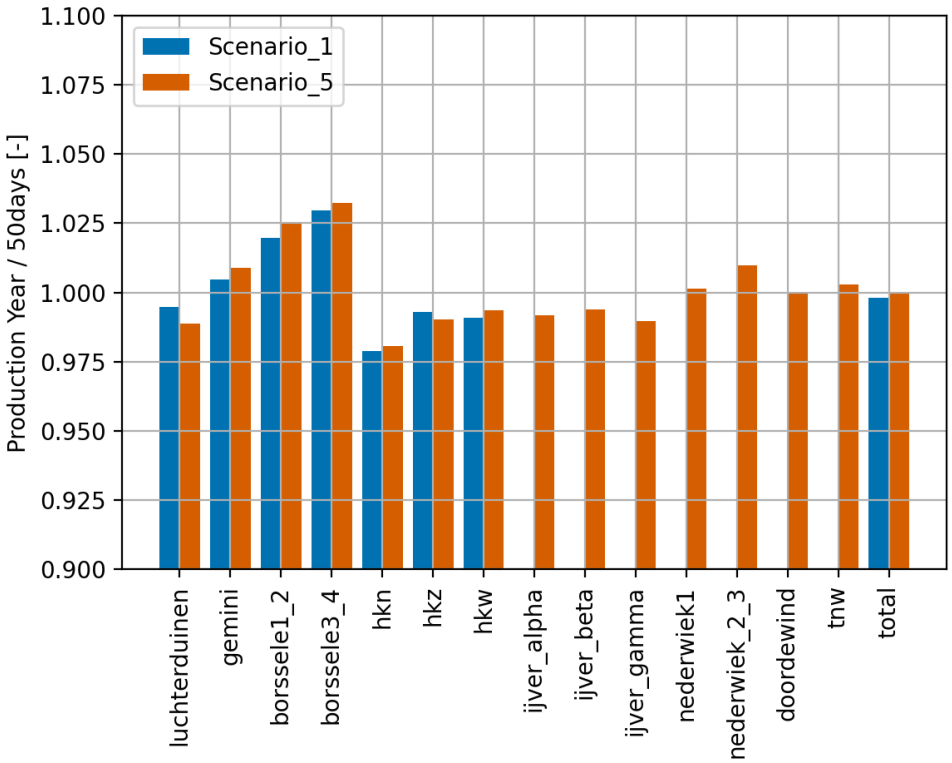

Figure 4.5. Ratio of power production of the full year over the selected 50 days for the 21 GW Roadmap wind farms. Data for $Sc1$ and $Sc5$ are presented.

Summary

Based on data from $Sc5$, a wind farm dependent correction is proposed (similar for all scenarios) to correct for local differences in ambient conditions between the full year and the 50 representative days (indicated by the orange bars in Fig. 4.5). An associated standard deviation on the energy production of 0.5% is assigned that will be included in the overall error margin estimation (Sect. 4.7.2).

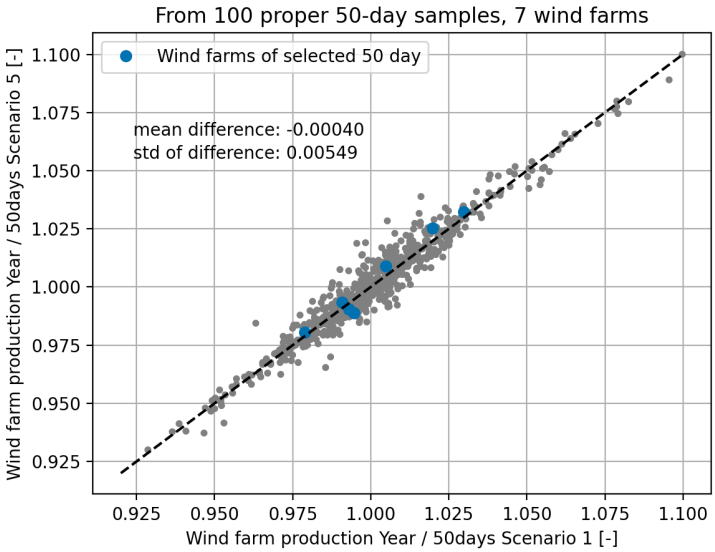

Figure 4.6. Ratio of power production of the full year over the selected 50 days for the 21 GW Roadmap wind farms. Data for $Sc1$ and $Sc5$ are presented.

4.4 Sampling error in the wake effects of the 50 representative days

Although in general the full-year to 50-day discrepancies vary consistently between $Sc1$ and $Sc5$ (Sect. 4.3), small differences exist between the scenarios. These variations will be different for other sets of 50 days and can be considered sampling uncertainty in the wake effects.

Again, we use the data from the 100 preselected set of 50 representative days to estimate the associated uncertainty in power production. For each wind farm, Fig. 4.7 shows the standard deviation of the difference in power production between the scenarios (so 100 data points per wind farm). Only for wind farms present in both scenarios data are available.

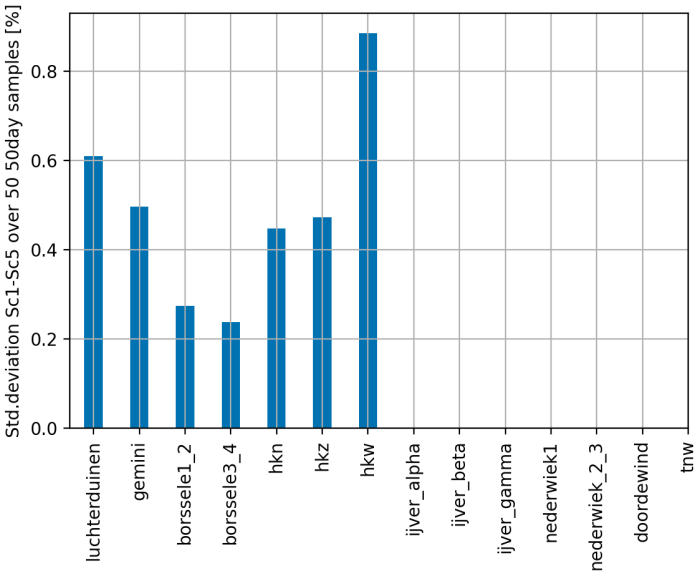

Figure 4.7. Standard deviation of the difference in production between $Sc1$ and $Sc5$ over 100 preselected sets of 50 representative days for the wind farms available in $Sc1$.

Based on these data, a standard deviation of 1% (conservative estimate) on the production is assigned to account for uncertainties in wake effects for the selected 50 days (equal for all wind farms and scenarios) which will be included in the overall uncertainty estimation (Sect. 4.7.2). No corrections to the mean values are applied here.

4.5 Wind farm specific long-term correction

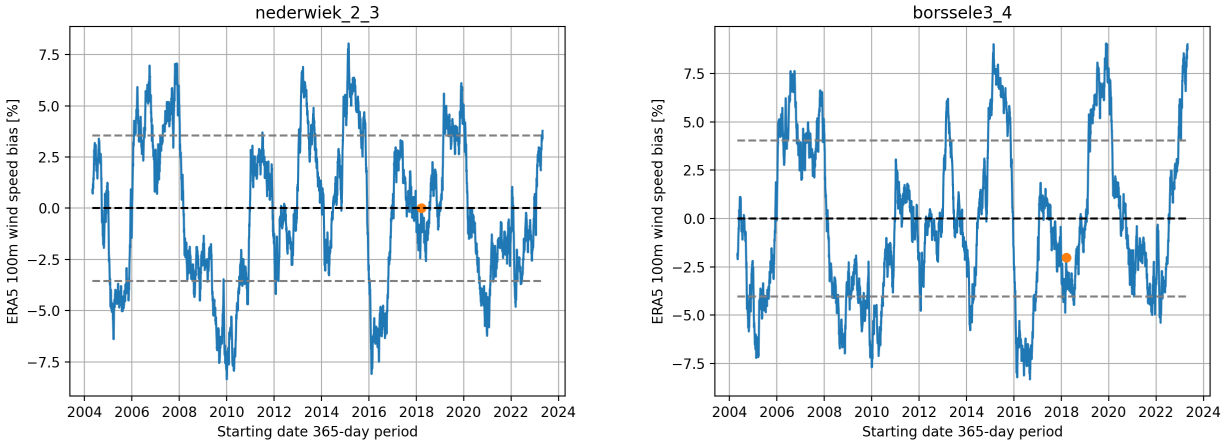

Figure 4.8. ERA5 100m wind speed bias for consecutive 365-day periods between May 2004 and May 2024. Grey dashed lines indicate the inter-annual variability. The orange dot indicates the selected year.

As outlined in Sect. 2.5.1 the selected simulation year closely resembles the long-term wind climate over the North Sea. However, given the significant size of the target area, local discrepancies between the selected year and the long-term (20 year) wind climate as derived from ERA5 exist. This is shown in Fig. 4.8, which shows the mean 100m wind speed obtained from ERA5 for consecutive 365-day periods for two wind farms of the 21 GW Roadmap.

Clearly, while for Nederwiek 2&3 the selected year, indicated by the orange dot, has a negligible bias with respect to the 20-year reference period, for Borssele 3&4 a significant deviation occurs. Figure 4.9 summarized the differences between the selected year and the 20-year reference period per wind farm. Discrepancies in wind speed are transformed to a correction factor in power by making used of the simulated (waked) wind farm power curve. The associated error margin in the power production taken similar to those of the bias correction method, i.e. 0.8% (see Sect. 4.1).

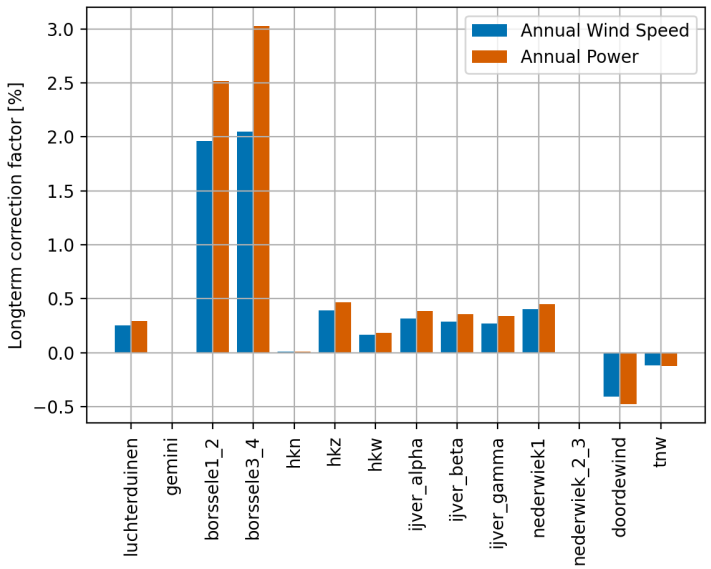

Figure 4.9. Long-term correction factor per wind farm (positive values indicate and underestimation of the selected year: the correction factor is larger than 1).

Summary

It was observed that the selected year spatial variations in the long-term representativeness occur. For this, a wind farm dependent correction is proposed (similar for all scenarios). An associated standard deviation on the energy

production of 0.8% is assigned (chosen similar to that applied for the bias correction method, Sect. 4.1) that will be included in the overall error margin estimation (Sect. 4.7.2).

4.6 Error margin of the wake modeling

Whiffle continuously monitors the quality of their wake modeling with available production data. Results of a recent validation study that was performed independently from the 21 GW Roadmap study are presented here to serve as an indication of model accuracy.

An accurate assessment of the uncertainty of a wake model is complex. Ideally, the uncertainty is estimated from a comparison of modeled versus observed production numbers for a large number of wind farms. However, high quality, publicly available production data are scarce. Moreover, for a proper model validation production data at wind farm level does not suffice (see e.g. Whiffle (2024)). Instead, to account for e.g. turbine stops and curtailment event, production data at turbine level is required for cleaning to enable a one-to-one comparison between model and observations.

A comparison has been made between modeled and observed production data for 10 anonymized offshore wind farms in a separate modeling study. First, for each wind farm the SCADA data has been cleaned by using per-turbine wind speed and power time series to remove e.g. curtailment and maintenance events. Then, all time steps for which less than 90% of the turbines available are discarded. For each of the 10 wind farms, model simulations have been performed for the 365 days with the highest data availability. Domain sizes are tailored to extent of the individual wind farms (much smaller than applied in the present study). The applied model settings are close to the ones used in the 21 GW Roadmap study. Settings of the turbine module are similar. Finally, modeled power production is compared to observed values.

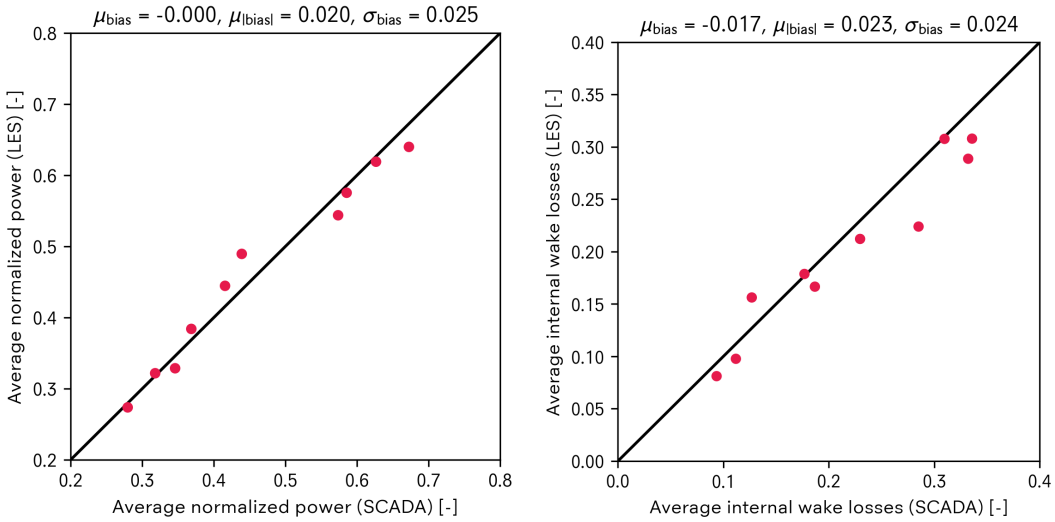

Figure 4.10. Left: Simulated versus observed normalized power for ten offshore wind farms (normalization with respect to wind farm rated power). Right: modeled versus observed internal wake losses. Each dot represent a single wind farm. Results are from a separate modeling study.

Results are shown in Fig. 4.10. Variations between wind farms are well-represented by the model. The standard deviation of the bias in the mean production for the considered 10 wind farms is 2.4% (this number includes uncertainties in power curve modeling and ambient wind speed). To circumvent possible impact of a model wind bias, also internal wake losses are compared. These are defined as the difference in wind farm mean production and the production of the first-row turbines, normalized with the production of the first-row turbines. Also here, the model represents the variations between wind farms reasonably well.

The model validation of wind farm power above provides valuable insight in the quality of the wake model. However, a direct translation to an uncertainty of the power production of the 21 GW Roadmap simulation remains difficult. Guided by these validation results, an uncertainty (expressed in a standard deviation) of 3% on the annual production is assumed. Based on the presented results this is considered reasonable estimate. This number will be included in the overall error margin estimation (Sect. 4.7.2).

4.7 Error propagation

4.7.1 Raw production numbers versus corrected production numbers

In this section raw production numbers are compared with corrected production numbers. Corrections have been applied for model bias, sampling errors resulting from the 50 representative day approach, and long-term representivity as discussed in Sect. 4.1, 4.3, and 4.5, respectively.

Figure 4.11 presents raw and corrected production numbers for each scenario. Corresponding capacity factors are presented in Fig. 4.12. The underlying numbers are given in Table 4.1, with the numbers in brackets indicating the differences in % with respect to $Sc5$.

Although small differences exist, the applied corrections have a uniform impact on the different scenarios; the corrections change the production numbers and capacity factors in a consistent way. When comparing raw and corrected production numbers, the differences with respect to $Sc5$ remain intact within reasonable margins.

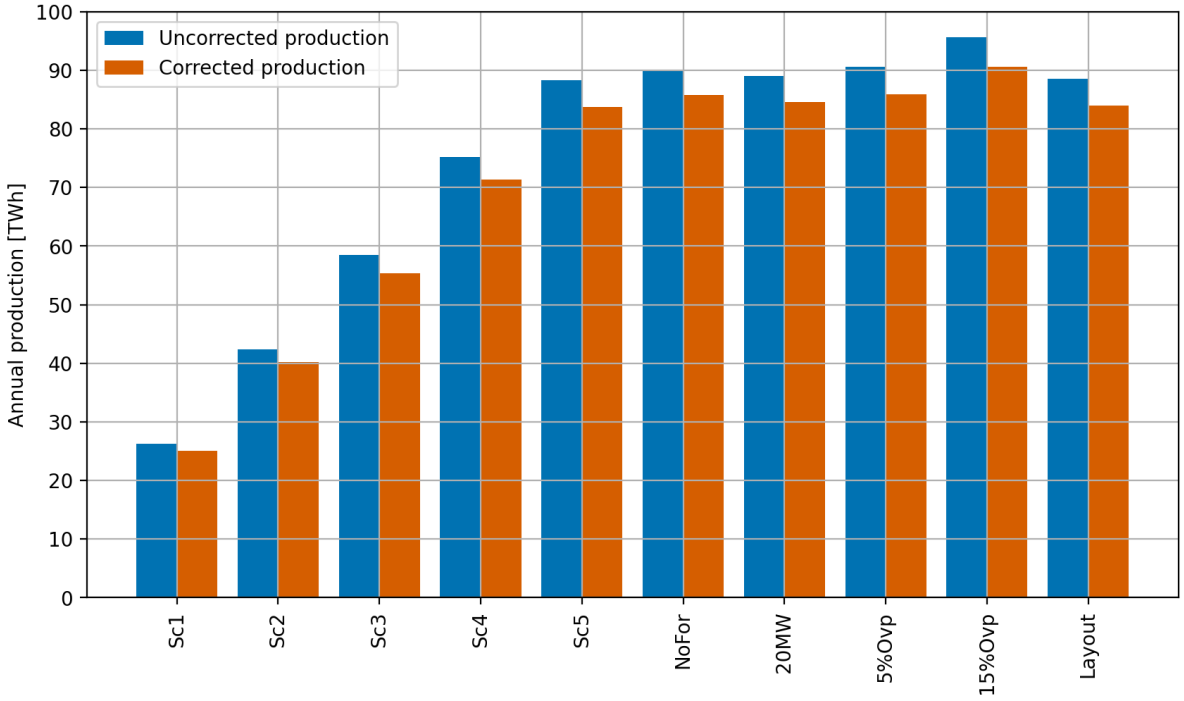

Figure 4.11. Aggregated production numbers (in TWh) per scenario.

Scenario	Raw Prod. [TWh] (w.r.t Sc5)	Corr. Prod [TWh] (w.r.t Sc5)	Raw c.f. [-] (w.r.t Sc5)	Corr c.f. [-] (w.r.t Sc5)
$Sc1$	26.25 (-70.2%)	25.08 (-70.0%)	0.498 (3.1%)	0.476 (3.9%)
$Sc2$	42.35 (-52.0%)	40.20 (-52.0%)	0.481 (-0.2%)	0.457 (-0.1%)
$Sc3$	58.45 (-33.8%)	55.32 (-33.9%)	0.475 (-1.7%)	0.449 (-1.9%)
$Sc4$	75.15 (-14.8%)	71.31 (-14.8%)	0.475 (-1.6%)	0.451 (-1.6%)
$Sc5$	88.24 (0.0%)	83.68 (0.0%)	0.483 (0.0%)	0.458 (0.0%)
$NoFor$	90.08 (2.1%)	85.68 (2.4%)	0.493 (2.1%)	0.469 (2.4%)
$20MW$	89.00 (0.9%)	84.56 (1.0%)	0.488 (1.1%)	0.464 (1.3%)
$5\%Ovp$	90.57 (2.6%)	85.87 (2.6%)	0.478 (-1.0%)	0.453 (-1.0%)
$15\%Ovp$	95.54 (8.3%)	90.52 (8.2%)	0.468 (-3.1%)	0.443 (-3.2%)
$Layout$	88.44 (0.2%)	83.89 (0.2%)	0.484 (0.2%)	0.459 (0.2%)
$Gross$	111.55 (26.4%)	106.97 (27.8%)	0.610 (26.4%)	0.585 (27.8%)

Table 4.1. Overview of AEP numbers for each scenario. Columns indicate Scenario name, raw model production, corrected production, capacity factor based on raw model production, and capacity factor based on corrected production, respectively. In brackets the differences with respect to $Sc5$ are given.

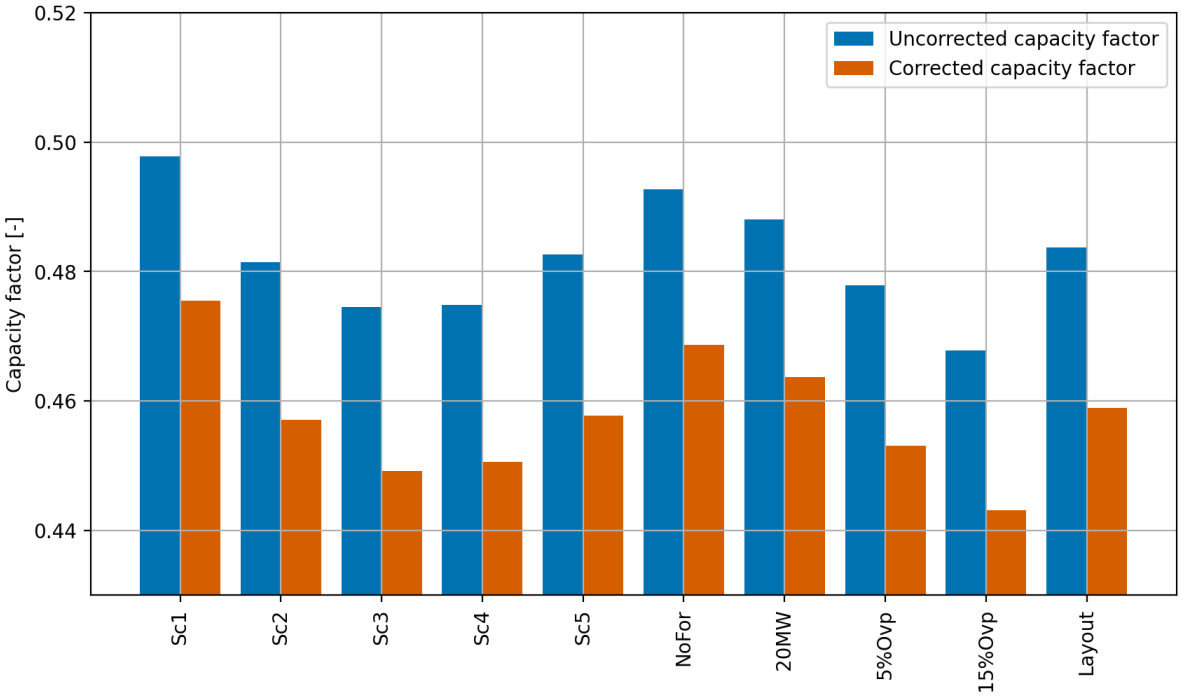

Figure 4.12. Capacity factor per scenario.

4.7.2 Error margin estimation

For practical application of the 21 GW Roadmap wake study results, the error margins arising from different sources as discussed in Sect. 4.1 to Sect. 4.6 need to be combined to a single number.

Source	Standard deviation
Bias correction method	0.8%
Uncertainty in model bias	3.2%
Sampling of 50 repr. days (ambient conditions)	0.5%
Sampling of 50 repr. days (wakes)	1%
Long-term representivity	0.8%
Wake model	3%

Table 4.2. Overview of error sources and the assigned associated standard deviations on simulated production numbers.

Table 4.2 lists the standard deviations of the individual components. When assuming that the different sources are independent, standard deviations can be combined according to

$$\sigma_t^2 = \sigma_1^2 + \sigma_2^2 + \ldots + \sigma_n^2. \tag{4.7}$$

Applied to the standard deviations identified above, this would yield a combined standard deviation of 4.6%. Although the individual error margins are considered largely independent, this number represents a lower-bound for overall uncertainty. To account for this, a rounded-up value of 5% is adopted as a generic standard deviation to the simulated production numbers.

Adding + or - 1 standard deviation indicates a 68% confidence interval around the mean. Applied to the total energy production of the full buildout scenario (mean value of 83.7 TWh), this corresponds to a range of 79.5 - 87.8 TWh. Although the relation between standard deviation and confidence intervals assumes a normal distribution of the errors, which is not necessarily the case, these numbers provide a valuable insight in the accuracy of the presented production numbers.

5

Conclusions and recommendations

The Dutch Roadmap for offshore wind energy aims for an installed capacity of 21 GW in 2032. However, the anticipated large-scale roll-out of offshore wind energy may lead to an increased importance of wind farm wake effects. To date, a systematic assessment of the associated annual energy production had not been conducted.

To reduce uncertainties in the anticipated annual energy production and to offer insights in the potential impact of cluster wake effects, Whiffle was granted an extensive modeling study to the energy production and wake effects of the operational and planned wind farms of the 21 GW offshore energy Roadmap.

Model simulations with Whiffle's high-resolution large-eddy simulation (LES) model were performed for a wide range of wind farm scenarios. A first set of simulation scenarios includes the gradual buildout of the 21 GW Roadmap in five incremental steps. All scenarios include a fixed configuration of wind farms of neighboring countries, representing the most likely situation in the year 2032. In addition, a suite of sensitivity scenarios was run with, for instance, a different turbine type (20 MW turbines instead of the default 15 MW), leaving out all non-Dutch wind farms and applying a basic layout optimization. Also two scenarios with overplanting were considered (5 and 15% respectively). A scenario with thrust-free turbines provided gross ('unwaked') production numbers and free-stream wind field.

The simulation domain had a horizontal extent of 307 x 384 km with a grid spacing of 120 m (2560 x 3200 grid cells) and covered the period 17 March 2018 to 17 March 2019. The wind speed and direction direction distributions of this specific period are close to the long-term wind climate.

For the initial buildout (Scenario 1) and the full buildout scenario (Scenario 5) a full year simulation was performed. For the other scenarios a set of 50 representative days were simulated.

The simulated annual energy production of the full buildout scenario of the 21 GW Roadmap is estimated to be 83.7 TWh with an error margin, expressed in a standard deviation, of 5%. This corresponds to a 68% confidence interval of 79.5 to 87.3 TWh. These numbers are obtained after correcting the raw model output for model bias and sampling errors, and long-term representativeness.

The corresponding aggregated capacity factor is 46%. Overall losses with respect to free-stream conditions (i.e. the sum of internal and external wake and blockage losses) amount to 21.7%. Although a direct comparison with other modeling studies is not possible, the numbers found in the present study are in line with values reported in literature.

The presented production numbers include losses due to wake and blockage effects. Not included are electrical, power curve hysteresis, curtailment and other operational losses.

Simulation of the incremental build out of the 21 GW Roadmap shows significant farm-to-farm wake effects. Inspection of the simulated yearly-averaged wind field at 150 m show mean wake lengths of tens of kilometers downstream of the major wind farm clusters. The addition of the IJmuiden Ver wind farms has a negative impact on the production of HKW in the order of 5%. Similar reductions in production are observed for IJmuiden Ver Beta due to the addition of IJmuiden Ver Gamma and Nederwiek 1, as well as for the production of Gemini due to the addition of Doordewind and TNW. For the production of an individual wind farm, the distance to and the size of neighboring wind farms are as important as its installed capacity density.

Leaving out all wind farms of neighboring countries has a major impact on the Borssele wind farms, Nederwiek 1, Gemini, and Doordewind. The impact on the total production on the 21 GW Roadmap is 2.1%. Wind farms for which the default 15 MW turbines were replaced by 20 MW turbines, while leaving the installed capacity the same,

showed an increase in production between 0.7 to 1.7%. Replacing default layouts that were based on a maximum repulsion algorithm by a boundary-grid layout (more turbines along the wind farm boundaries and an inner grid with a turbine spacing dependent on the dominant wind direction) had less than 1% impact on all of the wind farms.

The scenarios considering overplanting show mixed results. On the one hand, production increases significantly (around 10% in the case of 15% overplanting), but, on the other hand, most of the additional production is realized in the rated power regime. When the wind farm capacity is capped to original rated power the increase in production is reduced to roughly 3% (15% overplanting case). As such, the extent to which overplanting is a beneficial strategy may depend on the ability to store energy locally.

To facilitate the accessibility of the simulation results, a web-based GIS Viewer has been developed, which can be found at https://21gw.whiffle.cloud. The GIS Viewer allows for a straightforward and visual inspection of power production and capacity factors of the different scenarios per wind farm.

The current study has explored given buildout scenarios as well as a number of variations to those scenarios. As expected, significant farm-to-farm wake effects were found. Generalizable lessons and implications for policy makers are however difficult to distill from the current study and would require further studies with a different scope. A number of recommendations along these lines are:

- An energy system study that looks at spatial-temporal production patterns (rather than just TWh or capacity factors) in conjunction with electricity demand and flows though electricity networks can provide additional insights
- Systematic wind farm planning and layout optimization studies can be performed to establish, for instance, optimal sizes, spacings, and energy densities. The results from the current study could serve as input to those studies, for example to calibrate analytical wake models. The results from the present study suggest to focus more on optimizing the configuration of wind farms and wind farm clusters as a whole, rather then on optimization the layout of individual wind farms.

In summary, a high-fidelity atmospheric model was used to calculate the production numbers of the Dutch 21 GW Roadmap. The extensive modeling study presented here provides detailed insight in the effects of an incremental buildout of the Roadmap. With sensitivity experiments the impact of possible design choices was explored. As such, the present study contributes to a better understanding cluster wake effects and the relation between installed capacity and energy production.

A

Overview of wind farms

Table A.1 gives an overview of the wind farms that are included in the simulation. For each wind farm, characteristics like the central location, the capacity, and properties of the applied turbine type are given. The 'In LES' column indicates whether the wind farm is included in the (inner domain) LES simulation (when 'yes') or only in the (outer domain) mesoscale simulation (when 'no').

Also the source of the utilized power curves is indicated. The different entries in this column refer to the following:

- 1: Power and thrust curves obtained from the WindPRO database
- 2: Power curves obtained from https://www.thewindpower.net/
- 3: Power and thrust curve obtained from Desmond et al. (2016)
- 4: Power curve obtained from Grothe et al. (2022)
- 5: Reference-15.0MW turbine
- When another turbine type is mentioned, power and thrust curves from that particular turbine type were used to obtain scaled curves matching the specifications of the target turbine.

For turbine types for which only power curve data were available (entries 2 and 4), thrust coefficients have been estimates by utilizing the relation between power and thrust coefficients from turbines for which both were known.

Wind farm	In LES	Lat, Lon	Turbine type	Number of turbines	Capacity [MW]	Rotor diameter [m]	Hub-height [m]	Power curve source indicator
Albatros	yes	54.49, 6.24	SWT-7.0-154	16	112	154	105	4
AlphaVentus	yes	54.01, 6.61	Senvion-REpower5M	12	60	126	90	1
BardOffshore	yes	54.36, 5.98	Bard-5.0-122	80	400	122	110	Senvion-REpower5M
Belwind	yes	51.67, 2.80	V90-3.0MW	55	165	90	72	1
BorkumRiffgrund1	yes	53.97, 6.55	SWT-4.0-120	78	312	120	83	1
BorkumRiffgrund2	yes	53.95, 6.50	V164-8.0MW	56	448	164	105	3
Borkumriffgrund3	yes	54.05, 6.20	SG 11.0-200 DD	83	913	100	125	3

Table A.1. List of wind farms and their properties that are included in the model simulation. The respective columns indicate the name of the wind farm, whether the wind farm is fully included in the LES domain ('yes'), only partly ('partly'), or is only included in the mesoscale domain ('no'), the central latitude and longitude (taken as the mean value of the wind farm's turbines), the turbine type, the number of turbines, the installed capacity, the rotor diameter, the hub height, and an indicator of the source of the utilized power curve (see text).

Wind farm	In LES	Lat, Lon	Turbine type	Number of turbines	Capacity	Rotor diameter	Hub-height	Power curve source indicator
Borssele_1&2	yes	51.69, 3.07	SG 8.0-167DD	94	752	167	109	2
Borssele_3&4	yes	51.71, 2.93	V164-9.5MW	79	750	164	109	2
DeutscheBucht	yes	54.30, 5.79	V164-8.4MW	31	248	164	105	3
Doordewind	yes	54.27, 5.65	Reference-15.0MW	134	2010	118	150	5
EastAnglia1	yes	52.24, 2.50	SWT-7.0-154	102	714	154	120	4
Eastanglia1North	yes	52.38, 2.43	Scaled-14.0MW	58	812	114	146	Reference-15.0MW
Eastanglia2	partly	52.16, 2.20	Scaled-14.0MW	65	910	114	146	Reference-15.0MW
Eastanglia3	yes	52.66, 2.86	Scaled-14.0MW	100	1400	114	146	Reference-15.0MW
Gemini	yes	54.04, 5.96	SWT-4.0-130	150	600	130	89	1
GlobalTech	yes	54.51, 6.36	Areva M5000-116	80	400	116	90	2
HeDreiht	yes	54.37, 6.19	Reference-15.0MW	64	960	118	143	5
HKN	yes	52.71, 4.26	SG 11.0-200 DD	69	759	200	125	3
HKW	yes	52.68, 3.76	Reference-15.0MW	100	1500	118	150	5
HKZ	yes	52.31, 4.05	SG 11.0-200 DD	140	1540	200	125	3
HoheSee	yes	54.44, 6.33	SWT-7.0-154	71	497	154	105	4
Hornsea3	partly	53.87, 2.54	Scaled-14.0MW	204	2856	114	146	Reference-15.0MW
IJV-Alpha	yes	52.82, 3.49	Reference-15.0MW	134	2010	118	150	5
IJV-Beta	yes	52.91, 3.58	Reference-15.0MW	134	2010	118	150	5
IJV-Gamma	yes	53.03, 3.72	Reference-15.0MW	134	2010	118	150	5
Luchterduinen	yes	52.41, 4.16	V112-3.0MW	43	129	112	81	1
Merkur	yes	54.04, 6.56	Haliade_150-6MW	66	396	150	100	SWT-6.0-154
Mermaid	yes	51.72, 2.74	SG 8.0-167 DD	28	224	167	109	2
N-10-2	yes	54.60, 6.07	Scaled-20.0MW	25	500	136	169	Reference-15.0MW
N-3-5	partly	54.03, 6.85	Reference-15.0MW	28	420	118	150	5
N-3-6	yes	54.05, 6.77	Reference-15.0MW	32	480	118	150	5
N-3-8	partly	54.07, 6.89	Reference-15.0MW	29	435	118	150	5
N-6-6	yes	54.27, 5.95	Reference-15.0MW	42	630	118	150	5
N-6-7	yes	54.36, 5.85	Reference-15.0MW	18	270	118	150	5
N-7-2	yes	54.29, 6.22	Reference-15.0MW	65	975	118	150	5
N-9-1	yes	54.44, 5.76	Reference-15.0MW	134	2010	118	150	5
N-9-2	yes	54.49, 5.68	Reference-15.0MW	134	2010	118	150	5
N-9-3	yes	54.55, 5.88	Reference-15.0MW	100	1500	118	150	5
N-10-1	partly	54.66, 6.05	Scaled-20.0MW	100	2000	136	169	Reference-15.0MW
Nederwiek1	yes	53.10, 3.18	Reference-15.0MW	134	2010	118	150	5
Nederwiek_2&3	yes	53.41, 3.26	Reference-15.0MW	267	4005	118	150	5
Nobelwind	yes	51.66, 2.82	V112-3.3MW	50	165	112	79	1
NordseeOne	partly	53.98, 6.82	Senvion-6.2M126	54	332	126	100	2
NorfolkBoreas	yes	53.04, 2.94	Scaled-14.0MW	100	1400	114	146	Reference-15.0MW
NorfolkVanguard	yes	52.87, 2.70	Scaled-14.0MW	200	2800	114	146	Reference-15.0MW
Norther	yes	51.53, 3.01	V164-8.4MW	44	369	164	98	V164-8.0MW
Northwester2	yes	51.69, 2.75	V164-9.5MW	23	218	164	105	2
Northwind	yes	51.62, 2.90	V112-3.0MW	72	216	112	71	1
PrElizZone1	yes	51.62, 2.56	Reference-15.0MW	47	705	118	150	5
PrElizZone2	yes	51.46, 2.47	Scaled-20.0MW	70	1400	136	169	Reference-15.0MW
PrElizZone3	yes	51.48, 2.40	Scaled-20.0MW	70	1400	136	169	Reference-15.0MW
Rentel	yes	51.59, 2.95	SWT-7.0-154	42	294	154	106	4
Riffgat	yes	53.69, 6.48	SWT-3.6-120	30	108	120	90	1
Seastar	yes	51.63, 2.86	SG 8.0-167 DD	30	240	167	109	2
ThorntonBank1	yes	51.54, 2.94	Senvion-REpower5M	6	30	126	94	1
ThorntonBank23	yes	51.55, 2.95	Senvion-6.2M126	48	295	126	95	2
TNW	yes	54.02, 5.68	Reference-15.0MW	53	795	118	150	5
TrianelBorkum1	yes	54.05, 6.46	Areva M5000-116	40	200	116	90	2
TrianelBorkum2	yes	54.05, 6.47	Senvion-6.2M152	32	196	152	104	2
VejaMate	yes	54.32, 5.87	SWT-6.0-154	67	402	154	103	2

Table A.2. Continuation of Table A.1

Wind farm	In LES	Lat, Lon	Turbine type	Number of turbines	Capacity	Rotor diameter	Hub-height	Power curve source indicator
AmrumbankWest	no	54.52, 7.71	SWT-3.6-120	80	288	120	90	1
Butendiek	no	55.02, 7.77	SWT-3.6-120	80	288	120	91	1
Dantysk	no	55.14, 7.20	SWT-3.6-120	80	288	120	95	1
DoggerbankA	no	54.76, 1.91	Scaled-13.0MW	95	1235	110	150	Reference-15.0MW
DoggerbankB	no	54.98, 1.68	Scaled-13.0MW	95	1235	110	142	Reference-15.0MW
DoggerbankC	no	55.04, 2.82	Scaled-14.0MW	86	1204	114	146	Reference-15.0MW
Dudgeon	no	53.27, 1.38	SWT-6.0-154	67	402	154	110	2
DudgeonExt	no	53.28, 1.37	Reference-15.0MW	27	405	118	150	5
Dunkerque	no	51.17, 2.38	Scaled-13.0MW	46	598	110	142	Reference-15.0MW
FiveEstuaries	no	51.91, 2.16	Scaled-20.0MW	18	360	136	169	Reference-15.0MW
Galloper	no	51.90, 2.04	SWT-6.0-154	56	336	154	103	2
Godewind1_2	no	54.04, 6.99	SWT-6.0-154	97	582	154	110	2
Godewind3	no	54.04, 7.10	SG 11.0-200 DD	23	253	100	125	3
GreaterGabbard	no	51.88, 1.94	SWT-3.6-107	140	504	107	80	1
GunfleetSands	no	51.73, 1.23	SWT-3.6-107	48	172	107	70	1
Hornsea1	no	55.49, 7.84	SWT-7.0-154	174	1218	154	111	4
Hornsea2	no	55.60, 7.58	SG 8.0-167 DD	165	1320	167	200	2
Hornsea4	no	54.04, 1.27	Reference-15.0MW	174	2610	118	150	5
HornsRev1	no	55.70, 7.65	V80-2.0MW	80	160	80	70	1
HornsRev2	no	53.88, 1.92	SWT-2.3-93	91	209	93	68	1
HornsRev3	no	53.94, 1.66	V164-8.3MW	45	374	164	105	V164-8.0MW
HumberGateway	no	53.64, 0.29	V112-3.0MW	73	219	112	80	1
InnerDowsing	no	53.19, 0.45	SWT-3.6-107	30	108	107	85	1
Kaskasi	no	54.49, 7.69	SG 8.0-167 DD	38	304	167	107	2
KentishFlats	no	51.45, 1.08	V90-3.0MW	15	49	90	70	1
KentishFlatsExt	no	51.46, 1.20	V112-3.3MW	38	114	112	70	1
Lincs	no	53.18, 0.49	SWT-3.6-120	63	226	120	100	1
LondonArray	no	51.63, 1.50	SWT-3.6-120	175	630	120	87	1
Lynn	no	53.14, 0.45	SWT-3.6-107	27	97	107	85	1
MeerwindSudost	no	54.39, 7.70	SWT-3.6-120	80	288	120	95	1
N-11-1	no	54.73, 6.37	Scaled-20.0MW	100	2000	136	169	Reference-15.0MW
N-11-2	no	54.86, 6.37	Scaled-20.0MW	75	1500	136	169	Reference-15.0MW
N-12-1	no	54.77, 6.17	Scaled-20.0MW	100	2000	136	169	Reference-15.0MW
N-12-2	no	54.87, 6.12	Scaled-20.0MW	100	2000	136	169	Reference-15.0MW
N-12-3	no	54.99, 6.18	Reference-15.0MW	67	1005	118	150	5
N-13-1	no	54.99, 6.32	Reference-15.0MW	34	510	118	150	5
N-13-2	no	55.07, 6.33	Reference-15.0MW	67	1005	118	150	5
N-13-3	no	55.11, 6.45	Scaled-20.0MW	100	2000	136	169	Reference-15.0MW
N-14-1	no	54.78, 5.08	Scaled-20.0MW	100	2000	136	169	Reference-15.0MW
N-3-7	no	54.05, 7.06	Reference-15.0MW	15	225	118	150	5
Nordergrunde	no	53.84, 8.17	Senvion-6.2M126	18	110	126	84	2
NordseeOst	no	54.44, 7.68	Senvion-6.2M126	48	295	126	92	2
Nordsoen	no	55.83, 6.30	Scaled-20.0MW	50	1000	136	169	Reference-15.0MW
Northfalls	no	51.75, 1.89	Reference-15.0MW	34	510	118	150	5
Racebank	no	53.28, 0.84	SWT-6.0-154	93	558	154	110	2
Round4-Project1	no	54.63, 1.47	Scaled-10.0MW	150	1500	96	129	Reference-15.0MW
Round4-Project2	no	54.50, 1.91	Scaled-10.0MW	150	1500	96	129	Reference-15.0MW
Round4-Project3	no	53.57, 1.29	Reference-15.0MW	100	1500	118	150	nan
Sandbank	no	55.20, 6.85	SWT-4.0-130	72	288	130	95	1
ScrobySands	no	52.65, 1.79	V80-2.0MW	30	60	80	60	1
SheringhamShoal	no	53.14, 1.15	SWT-3.6-107	88	316	107	80	1
SheringhamshoalExt	no	53.16, 1.17	Scaled-12.0MW	27	324	106	138	Reference-15.0MW
Sofia	no	54.99, 2.23	Scaled-14.0MW	100	1400	114	146	Reference-15.0MW
Thanet	no	51.43, 1.63	V90-3.0MW	100	300	90	70	1
TritonKnoll	no	53.48, 0.84	V164-9.5MW	90	720	164	140	2
WesternmostRough	no	53.81, 0.15	SWT-6.0-154	35	210	154	102	2

Table A.3. Continuation of Table A.1

B

Tables with production data per wind farm per scenario

Several Figures in the main text present simulated production numbers for the different wind farms of the 21 GW Roadmap for the different scenarios (e.g. Figs. 3.6 - 3.9). For completeness, the Tables below provide the data underlying these Figures.

The Tables include the following data:

- Annual mean production production in MW per wind farm for each scenario (Table B.1)
- Annual production per wind farm for each scenario relative to Sc5 (Table B.2)
- Overview of capacity factors per wind farm for each scenario (Table B.3)
- Overview of annual mean gross production in MW per wind farm for each scenario (Table B.4)
- Overview of total aerodynamic losses in % per wind farm for each scenario. This indicates the difference between waked and gross production (Table B.5)

Wind farm	Sc1	Sc2	Sc3	Sc4	Sc5	NoFor	20MW	5%Ovp	15%Ovp	Layout
Luchterduinen	59.6	59.6	59.4	59.4	59.4	58.7	59.5	59.5	59.4	59.3
Gemini	320.1	320.8	321.9	321.9	304.3	328.8	306.1	302.8	302.3	304.7
Borssele I&II	320.6	319.0	318.0	317.8	318.0	360.9	318.0	317.5	317.5	317.8
Borssele III&IV	279.4	279.1	278.5	278.4	278.6	346.9	278.5	278.1	278.2	278.7
HKN	388.8	386.5	383.1	384.0	384.4	376.9	384.5	383.5	383.1	384.2
HKZ	737.5	736.7	735.1	736.2	737.6	725.3	737.7	737.3	736.8	736.4
HKW	756.5	728.2	718.9	718.2	719.1	706.6	724.4	748.4	802.4	721.8
IJVer-Alpha	nan	889.9	870.5	867.3	868.4	865.4	877.4	893.7	945.8	871.4
IJVer-Beta	nan	869.6	824.8	818.5	819.3	809.7	831.1	840.0	888.4	819.6
IJVer-Gamma	nan	nan	881.1	872.2	873.0	868.1	886.5	897.3	953.7	871.2
Nederwiek I	nan	nan	924.4	893.1	893.7	961.7	906.8	923.6	995.4	893.2
Nederwiek II&III	nan	nan	nan	1873.6	1872.8	1878.9	1906.1	1943.6	2079.5	1890.4
Doordewind	nan	nan	nan	nan	979.6	1048.1	986.0	1011.5	1088.7	981.6
TNW	nan	nan	nan	nan	444.8	444.5	450.6	465.6	501.6	446.7

Table B.1. Annual mean production in MW per wind farm for each scenario.

Wind farm	Sc1	Sc2	Sc3	Sc4	Sc5	NoFor	20MW	5%Ovp	15%Ovp	Layout
Luchterduinen	0.3%	0.3%	-0.1%	-0.0%	-0.0%	-1.3%	0.2%	0.1%	-0.0%	-0.1%
Gemini	5.2%	5.4%	5.8%	5.8%	0.0%	8.1%	0.6%	-0.5%	-0.6%	0.1%
Borssele I&II	0.8%	0.3%	0.0%	-0.1%	0.0%	13.5%	-0.0%	-0.1%	-0.2%	-0.1%
Borssele III&IV	0.3%	0.2%	-0.1%	-0.1%	0.0%	24.5%	-0.1%	-0.2%	-0.2%	0.0%
HKN	1.1%	0.6%	-0.3%	-0.1%	0.0%	-1.9%	0.0%	-0.2%	-0.3%	-0.0%
HKZ	-0.0%	-0.1%	-0.3%	-0.2%	0.0%	-1.7%	0.0%	-0.0%	-0.1%	-0.2%
HKW	5.2%	1.3%	-0.0%	-0.1%	0.0%	-1.7%	0.7%	4.1%	11.6%	0.4%
IJVer-Alpha	nan%	2.5%	0.2%	-0.1%	-0.0%	-0.3%	1.0%	2.9%	8.9%	0.4%
IJVer-Beta	nan%	6.1%	0.7%	-0.1%	0.0%	-1.2%	1.4%	2.5%	8.4%	0.0%
IJVer-Gamma	nan%	nan%	0.9%	-0.1%	0.0%	-0.6%	1.5%	2.8%	9.2%	-0.2%
Nederwiek I	nan%	nan%	3.4%	-0.1%	0.0%	7.6%	1.5%	3.3%	11.4%	-0.1%
Nederwiek II&III	nan%	nan%	nan%	0.0%	0.0%	0.3%	1.8%	3.8%	11.0%	0.9%
Doordewind	nan%	nan%	nan%	nan%	0.0%	7.0%	0.6%	3.3%	11.1%	0.2%
TNW	nan%	nan%	nan%	nan%	0.0%	-0.1%	1.3%	4.7%	12.8%	0.4%

Table B.2. Annual production per wind farm for each scenario relative to Sc5.

Wind farm	Sc1	Sc2	Sc3	Sc4	Sc5	NoFor	20MW	5%Ovp	15%Ovp	Layout
Luchterduinen	0.462	0.462	0.460	0.460	0.461	0.455	0.461	0.461	0.461	0.460
Gemini	0.534	0.535	0.536	0.536	0.507	0.548	0.510	0.505	0.504	0.508
Borssele I&II	0.426	0.424	0.423	0.423	0.423	0.480	0.423	0.422	0.422	0.423
Borssele III&IV	0.372	0.372	0.371	0.371	0.371	0.462	0.371	0.370	0.370	0.371
HKN	0.512	0.509	0.505	0.506	0.506	0.497	0.507	0.505	0.505	0.506
HKZ	0.482	0.482	0.481	0.482	0.482	0.474	0.482	0.482	0.482	0.482
HKW	0.504	0.485	0.479	0.479	0.479	0.471	0.483	0.475	0.465	0.481
IJVer-Alpha	nan	0.443	0.433	0.431	0.432	0.431	0.439	0.426	0.409	0.434
IJVer-Beta	nan	0.433	0.410	0.407	0.408	0.403	0.416	0.400	0.385	0.408
IJVer-Gamma	nan	nan	0.438	0.434	0.434	0.432	0.443	0.427	0.413	0.433
Nederwiek I	nan	nan	0.460	0.444	0.445	0.478	0.453	0.440	0.431	0.444
Nederwiek II&III	nan	nan	nan	0.468	0.468	0.469	0.477	0.463	0.452	0.472
Doordewind	nan	nan	nan	nan	0.487	0.521	0.493	0.482	0.471	0.488
TNW	nan	nan	nan	nan	0.559	0.559	0.563	0.554	0.548	0.562

Table B.3. Overview of capacity factors per wind farm for each scenario.

Wind farm	Sc1	Sc2	Sc3	Sc4	Sc5	NoFor	20MW	5%Ovp	15%Ovp	Layout
Luchterduinen	78.1	78.1	78.1	78.1	78.1	78.1	78.1	78.1	78.1	78.1
Gemini	411.5	411.5	411.5	411.5	411.5	411.5	411.5	411.5	411.5	411.5
Borssele I&II	425.4	425.4	425.4	425.4	425.4	425.4	425.4	425.4	425.4	425.4
Borssele III&IV	383.7	383.7	383.7	383.7	383.7	383.7	383.7	383.7	383.7	383.7
HKN	455.6	455.6	455.6	455.6	455.6	455.6	455.6	455.6	455.6	455.6
HKZ	885.7	885.7	885.7	885.7	885.7	885.7	885.7	885.7	885.7	885.7
HKW	908.7	908.7	908.7	908.7	908.7	908.7	907.7	954.2	1044.9	908.7
IJVer-Alpha	1224.1	1224.1	1224.1	1224.1	1224.1	1224.1	1216.9	1278.9	1406.9	1224.1
IJVer-Beta	1226.7	1226.7	1226.7	1226.7	1226.7	1226.7	1219.1	1281.7	1409.9	1226.6
IJVer-Gamma	1230.2	1230.2	1230.2	1230.2	1230.2	1230.2	1222.8	1285.3	1414.1	1230.5
Nederwiek I	1212.8	1212.8	1212.8	1212.8	1212.8	1212.8	1205.2	1267.1	1394.1	1213.0
Nederwiek II&III	2425.1	2425.1	2425.1	2425.1	2425.1	2425.1	2419.3	2543.1	2788.3	2425.0
Doordewind	1338.8	1338.8	1338.8	1338.8	1338.8	1338.8	1332.1	1398.8	1538.7	1338.8
TNW	527.3	527.3	527.3	527.3	527.3	527.3	530.6	557.2	606.9	527.2

Table B.4. Overview of annual mean gross production in MW per wind farm for each scenario.

Wind farm	Sc1	Sc2	Sc3	Sc4	Sc5	NoFor	20MW	5%Ovp	15%Ovp	Layout
Luchterduinen	23.7%	23.7%	24.0%	24.0%	23.9%	24.9%	23.8%	23.9%	24.0%	24.0%
Gemini	22.2%	22.0%	21.8%	21.8%	26.1%	20.1%	25.6%	26.4%	26.5%	26.0%
Borssele I&II	24.6%	25.0%	25.2%	25.3%	25.3%	15.2%	25.3%	25.4%	25.4%	25.3%
Borssele III&IV	27.2%	27.3%	27.4%	27.4%	27.4%	9.6%	27.4%	27.5%	27.5%	27.4%
HKN	14.7%	15.2%	15.9%	15.7%	15.6%	17.3%	15.6%	15.8%	15.9%	15.7%
HKZ	16.7%	16.8%	17.0%	16.9%	16.7%	18.1%	16.7%	16.8%	16.8%	16.9%
HKW	16.7%	19.9%	20.9%	21.0%	20.9%	22.2%	20.2%	21.6%	23.2%	20.6%
IJVer-Alpha	nan%	27.3%	28.9%	29.2%	29.1%	29.3%	27.9%	30.1%	32.8%	28.8%
IJVer-Beta	nan%	29.1%	32.8%	33.3%	33.2%	34.0%	31.8%	34.5%	37.0%	33.2%
IJVer-Gamma	nan%	nan%	28.4%	29.1%	29.0%	29.4%	27.5%	30.2%	32.6%	29.2%
Nederwiek I	nan%	nan%	23.8%	26.4%	26.3%	20.7%	24.8%	27.1%	28.6%	26.4%
Nederwiek II&III	nan%	nan%	nan%	22.7%	22.8%	22.5%	21.2%	23.6%	25.4%	22.0%
Doordewind	nan%	nan%	nan%	nan%	26.8%	21.7%	26.0%	27.7%	29.2%	26.7%
TNW	nan%	nan%	nan%	nan%	15.6%	15.7%	15.1%	16.4%	17.4%	15.3%

Table B.5. Overview of total aerodynamic losses in % per wind farm for each scenario. This indicates the difference between waked and gross production.

Bibliography

Akhtar, N., Geyer, B., Rockel, B., Sommer, P., S., and Schrum, C. (2021). Accelerating deployment of offshore wind energy alter wind climate and reduce future power generation potentials. *Nature Scientific Reports*, page 11826.

Baas, P. (2024). Winds of the North Sea in 2050 - Public Final Report. https://wins50.nl/downloads/wins50_endreport_final_20240403.pdf. Accessed: March 2025.

Baas, P., Verzijlbergh, R., van Dorp, P., and Jonker, H. (2023). Investigating energy production and wake losses of multi-gigawatt offshore wind farms with atmospheric large-eddy simulation. *Wind Energy Science*, 8(5):787–805.

Bardal, L. M., Onstad, A. E., and Lund, J. A. (2018). Evaluation of methods for estimating atmospheric stability at two coastal sites. *Wind Engineering*, pages 561–575.

Borgers, R., Dirksen, M., Wijnant, I. L., Stepek, A., Stoffelen, A., Akhtar, N., Neirynck, J., Walle, J. v. d., Meyers, J., and Lipzip, N. P. M. v. (2024). Mesoscale modelling of north sea wind resources with cosmo-clm: model evaluation and impact assessment of future wind farm characteristics on cluster-scale wake losses. *Wind Energy Science*, pages 697–719.

Cañadillas, B., Beckenbauer, M., Trujillo, J. J., Dörenkämper, M., Foreman, R., Neumann, T., and Lampert, A. (2022). Offshore wind farm cluster wakes as observed by long-range-scanning wind lidar measurements and mesoscale modeling. *Wind Energy Science*, pages 1241–1262.

Cantero, E., Sanz, J., Borbón, F., Paredes, D., and García, A. (2022). On the measurement of stability parameter over complex mountainous terrain. *Wind Energy Science*, pages 221–235.

Charnock, H. (1955). Wind stress on a water surface. *Quarterly Journal of the Royal Meteorological Society*, 81:639–640.

Cheneka, B. R., Watson, S. J., and Basu, S. (2023). Quantifying the impacts of synoptic weather patterns on north sea wind power production and ramp events under a changing climate. *Energy and Climate Change*, page 100113.

Desmond, C., Murphy, J., Blonk, L., and Haans, W. (2016). Description of an 8 MW reference wind turbine . *Journal of Physics: Conference Series*, 753:092013.

DNV GL (2016). A study on UK offshore wind variability. DNV GL Report nr L2C124303-UKBR-R-01, Issue B Issue B, 67 pp. Technical report, DNVGL.

ECMWF (2017). IFS Manual Part IV: Physical Processes. IFS Documentation Cy43R3. Technical report, ECMWF.

Energiewende, Agora Verkehrswende, Technical University of Denmark and Max-Planck-Institute for Biogeochemistry (2020). Making the Most of Offshore Wind: Re-Evaluating the Potential of Offshore Wind in the German North Sea, 84 pp. Technical report, Agora.

Fitch, A. C., Olsen, J. B., Lundquist, J. K., D. J., Gupta, A. K., Michalakes, J., and Barstad, I. (2012). Local and mesoscale impacts of wind farms as parameterized in a mesoscale nwp model. *Monthly Weather Review*, pages 3017–3038.

Gandoin, R. and Garza, J. (2024). Underestimation of strong wind speeds offshore in ERA5: evidence, discussion and correction. *Wind Energy Science*, 9:1727–1745.

Geyer, B., Weisse, R., Bisling, P., and Winterfeldt, J. (2012). Climatology of north sea wind energy derived from a model hindcast for 1958–2012. *Journal of Wind Engineering and Industrial Aerodynamics*, pages 18–29.

Grothe, O., Kächele, F., and Watermeyer, M. (2022). Analyzing Europe's Biggest Offshore Wind Farms: A Data Set with 40 Years of Hourly Wind Speeds and Electricity Production. *Energies*, 15:1700.

Gualtieri, G. (2022). Analysing the uncertainties of reanalysis data used for wind resource assessment: A critical review. *Renewable and Sustainable Energy Reviews*, page 112741.

Hersbach, H., Bell, B., P., B., Hirahara, S., Horányi, A., Muñoz-Sabater, J., Nicolas, J., Peubey, C., Radu, R., Schepers, D., Simmons, A., Soo ci, C., Abdalla, S., Abellan, X., Balsamo, G., Bechtold, P., Biavati, G., Bidlot, J., Bonavita, De Chiara, G., Dahlgren, P., Dee, D., Diamantakis, M., Dragani, R., Flemming, J., Forbes, R., Fuentes, M., Geer, A., Haimberger, L., Healy, S., Hogan, R. J., Hólm, E., Janisková, M., Keeley, S., Laloyaux, P., Lopez, P. ann d Lupu, C., Radnoti, G., De Rosnay, P., Rozum, I., Vamborg, F., Villaume, S., and Thépaut, J. N. (2020). The ERA5 global reanalysis. *Quarterly Journal of the Royal Meteorological Society*, 146:1999–2049.

Heus, T., van Heerwaarden, C., Jonker, H., Siebesma, A., Axelsen, S., Dries, K., Geoffroy, O., Moene, A., Pino Gonzalez, D., Roode, S., and Arellano, J. (2010). Formulation of the dutch atmospheric large-eddy simulation (dales) and overview of its applications. *Geoscientific Model Development, v.3, 415-444 (2010)*, 3.

Holthuijzen, M. F., Beckage, B., Clemins, P. J., Higdon, D., and Winter, J. (2021). Constructing high-resolution, bias-corrected climate products: A comparison of methods. *Journal of the Atmospheric Sciences*, pages 455–475.

Holtslag, A. A. M. and Boville, B. A. (1993). Local Versus Nonlocal Boundary-Layer Diffusion in a Global Climate Model . *Journal of Climate*, 6:1825–1842.

Holtslag, M., Bierbooms, W. A. A. M., and Brussel, G. J. W. v. (2014). Estimating atmospheric stability from observations and correcting wind shear models accordingly. *Journal of Physics: Conference Series*, page 012052.

Hooijdonk, I. G. S., Donda, J. M. M., C. H. J. H. B. F. C., and Wiel, B. J. H. v. d. (2015). Shear capacity as prognostic for nocturnal boundary layer regimes. *Journal of the Atmospheric Sciences*, pages 1518–1532.

Jourdier, B. (2020). Evaluation of era5, merra-2, cosmo-rea6, newa and arome to simulate wind power production over france. *Advances in Science and Research*, pages 63–77.

KEC 5.0 (2024). https://www.noordzeeloket.nl/functies-gebruik/windenergie/ecologie/wind-zee-ecologisch-programma-wozep/newsletter-wozep/wozep-nieuwsflits-april-2024/kec-5-0-start/. Accessed: March 2025.

Meijer, J., Steinfeld, G., Vollmer, L., and Dörenkämper, M. (2024). The global blockage effect of a wind farm cluster - an les study. *Journal of Physics: Conference Series*, page 092093.

Meyers, J. and Meneveau, C. (2010). Large eddy simulations of large wind-turbine arrays in the atmospheric boundary layer.

Netherlands Enterprise Agency (2024). Offshore Wind Energy Roadmap 21 GW. https://english.rvo.nl/sites/default/files/2024-10/Offshore-Wind-Energy-Roadmap-July-2024.pdf. Accessed: April 2025.

Olauson, J. (2018). Era5: The new champion of wind power modelling? *Renewable Energy*, pages 322–331.

Perkins, S. E., Pitman, A. J., Holbrook, N. J., and McAneney, J. (2007). Evaluation of the AR4 Climate Models' Simulated Daily Maximum Temperature, Minimum Temperature, and Precipitation over Australia Using Probability Density Functions. *Journal of Climate*, 20:4356–4376.

Porchetta, S., Howland, M. F., Borgeres, R., Buckingham, S., and Munters, W. (2024). Annual wake impacts in and between wind farm clusters modelled by a mesoscale numerical weather prediction model and fast-running engineering models. *Wind Energy Science Discussions*.

Postema, B., Verzijlbergh, R., Van Dorp, P., Baas, P., and Jonker, H. (2024). Estimating long-term annual energy production of a large offshore wind farm from large-eddy simulations: Methods and validation with a 10-year simulation. *Wind Energy Science Discussions*.

Pryor, S. C. and Barthelmie, R. J. (2024). Wind shadows impact planning of large offshore wind farms. *Applied Energy*, page 122755.

Pryor, S. C., Barthelmie, R. J., and Sheperd, T. J. (2021). Wind power production from very large offshore wind farms. *Joule*, pages 2663–2686.

Ramon, J., Lledó, L., Torralba, V., Soret, A., and Doblas-Reyes, F. J. (2019). What global reanalysis best represents near-surface winds? *Quarterly Journal of the Royal Meteorological Society*, pages 3236–3251.

Ronda, R., Wijnant, I. L., and Stepek, A. (2017). Inter-annual wind speed variability on the North Sea. KNMI Technical Report: TR-360, 17 pp. Technical report, KNMI.

Schalkwijk, J., Jonker, H., Siebesma, A., and Bosveld, F. (2015). A year-long large-eddy simulation of the weather over cabauw: An overview. *Monthly Weather Review*, 143:828–844.

Schneemann, J., Rott, A., Dörenkämper, M., Steinfeld, G., and Kühn, M. (2020). Cluster wakes impact on a far-distant offshore wind farm's power. *Wind Energy Science*, pages 29–49.

Stanley, A. P. J. and Ning, A. (2019). Massive simplification of the wind farm layout optimization problem. *Wind Energy Science*, 4:663–676.

Sterl, A., B. A. M. R., Brink, H. W. v. d., Haarsma, R., Stepek, A., Wijnant, I. L., and Winter, R. C. d. (2015). Large-scale winds in the southern north sea region: the wind part of the knmi'14 climate change scenarios. *Environmental Research Letters*, page 035004.

Stratum, B., Theeuwes, N., Ulft, B. v., and Wijnant, I. (2022). A One-Year-Long Evaluation of a Wind-Farm Parameterization in HARMONIE-AROME. *Journal of Advances in Modeling Earth Systems*, 14:e2021MS002947.

TNO (2019a). Verification of Leosphere Windcube WLS7-577 at ECN part of TNO LiDAR Calibration Facility, for offshore measurements at Lichteiland Goeree, Tech. rep., TNO 2019 R10398, ECN. Technical report, TNO.

TNO (2019b). Verification of ZephIR 300 unit 315 at ECN part of TNO LiDAR Calibration Facility, for offshore measurements at Euro Platform, Tech. rep., TNO 2018 R10762, ECN. Technical report, TNO.

TNO (2019c). Verification of ZephIR 300 unit 563 at ECN part of TNO LiDAR Calibration Facility, for off- shore measurements at K13-A production platform, Tech. rep., TNO 2018 R10850, ECN. Technical report, TNO.

TNO (2024). Offshore wind resource at the North Sea, TNO 2024 R11678, 33pp. Technical report, TNO.

Volker, P. J. H., Badger, J., Hahmann, A. N., and Ott, S. (2015). The explicit wake parametrisation v1.0: a wind farm parametrisation in the mesoscale model wrf. *Geoscientific Model Development*, pages 3481–3522.

Whiffle (2024). 21GW Roadmap Wake Study Model Validation Report, 34 pp. Technical report, Whiffle.